Wissenschaftszentrum Weihenstephan für Ernährung, Landnutzung und Umwelt

Lehrstuhl für Ernährungsmedizin

From GWAS to functionality: association of rs2014355 in the ACADS gene locus with acylcarnitine ratio and postprandial metabolic and inflammatory activation of human PBMC

Kerstin Christina Ehlers

Vollständiger Abdruck der von der Fakultät Wissenschaftszentrum Weihenstephan für Ernährung, Landnutzung und Umwelt der Technischen Universität München zur Erlangung des akademischen Grades eines

Doktors der Naturwissenschaften

genehmigten Dissertation.

Vorsitzende:	Univ.-Prof. Dr. H. Daniel
Prüfer der Dissertation:	1. Univ.-Prof. Dr. J. J. Hauner
	2. Univ.-Prof. Dr. M. Klingenspor

Die Dissertation wurde am 26.06.2013 bei der Technischen Universität München eingereicht und durch die Fakultät Wissenschaftszentrum Weihenstephan für Ernährung, Landnutzung und Umwelt am 25.11.2013 angenommen.

„Man muss noch Chaos in sich haben,
um einen tanzenden Stern zu gebären.“

Friedrich Nietzsche

Acknowledgement

Meinen herzlichsten Dank möchte ich gern all denen aussprechen, die mich auf dem Weg zur Entstehung dieser Doktorarbeit begleitet haben.

Herrn Prof. Dr. Hans Hauner möchte ich danken für die Überlassung des Themas und die Unterstützung während der Durchführung und Erstellung dieser Arbeit. Die außerordentlich guten Bedingungen in diesem Institut, die freundliche Atmosphäre, die exzellenten Mitarbeiter und die wohlwollende Unterstützung haben die Arbeit dort sehr fruchtbar und angenehm gestaltet.

Ganz besonders bedanke ich mich bei meinem Betreuer Dr. Helmut Laumen für seine vielfältigen und kreativen Ideen, seinen unerschöpflichen Optimismus, für die Korrekturen an Manuskripten und dieser Arbeit, sowie die zahlreichen Diskussionen die sehr zu meinen Vorankommen beigetragen haben.

Ich danke meinen Kooperationspartnern Dr. Regina Ensenauer für die Hilfe bei der Etablierung des Metaboliten Assays; Dr. Christian Thirion und Dr. Michael Salomon von Sirion Biotech für die Bereitstellung der Plasmide und die Hilfe bei der Klonierung; Alexander Haag für die Acylcarnitin Messungen und Dr. Gabi Kastenmüller und Max Hastreiter für die statistische Auswertung der Metaboliten Assays.

Nicht zuletzt danken möchte ich Syli, der guten Fee des Lehrstuhls, ALLEN ehemaligen und jetzigen MitarbeiterInnen der AGs Laumen und Skurk, vor allem Caro, Lissy und Manu die mir bei so vielen Experimenten geholfen haben und den vielen DoktorandInnen, Bachelor- und Masterstudenten, die ich in der Zeit meiner Doktorarbeit erleben durfte. Besonderer Dank geht an Tina und Kathrin, die so viel mehr für mich sind als Arbeitskollegen.

Großer Dank gilt auch meiner Familie die immer für mich da war, und so am Ende tatkräftig zum Zustandekommen dieser Arbeit beigetragen hat. Besonders Steve danke ich für seine Geduld und Unterstützung, in guten wie in schlechten Zeiten. Danke!

Table of contents

Summary

This thesis is divided into two major topics:

1) From GWAS to functionality: association of rs2014355 in the ACADS gene locus with acylcarnitine ratio

Genome-wide association studies (GWASs) revealed an association of rs2014355 in the acyl-CoA dehydrogenase short-chain (ACADS) locus with the plasma C3/C4-acylcarnitine ratio. To confirm the hypothesized impaired ACADS activity, *in situ* mitochondrial metabolite flux assays in genotyped Epstein-Barr virus immortalized lymphoblastoid cell lines (EBV-LCLs) were used. A decreased metabolic rate of C4:0-acylcarnitine in cells homozygous for the minor C allele was found, which may be in part explained by the observed allele-dependent decrease of ACADS gene and protein expression in EBV-LCLs. Moreover, reporter-gene assays of bioinformatically predicted *cis*-regulatory variants in high linkage disequilibrium (LD) with rs2014355 in Huh7- and 3T3L1-cells revealed an allelic *cis*-regulatory effect of four associated SNPs, but not for the GWASs lead SNP rs2014355. Besides these *cis*-regulatory effects the decreased ACADS activity associated with rs2014355 may be caused by a non-synonymous coding variant (rs1799958) in perfect LD with rs2014355. Thus, repressing *cis*-regulatory variants might contribute to the decreased ACADS activity by reducing ACADS mRNA expression while several activating *cis*-regulatory variants might act compensatory to the impaired enzyme function by increasing gene expression.

To further address the influence of reduced ACADS gene expression in a cell type where fatty acid oxidation (FAO) serves as substantive energy source for the peripheral energy metabolism gradual knock-downs of endogenous ACADS protein level in a human liver cell line (Huh7) were used. The residual protein amount determined the extent of intracellular C4:0-acylcarnitine accumulation, modelling the SNP associated phenotype found in population studies and genotype-dependent cell models. Notably, palmitic acid loading and short-term time-resolved measurement of acylcarnitines revealed novel, dynamic regulatory events on long- and medium-chain acylcarnitines in knock-down cells. Further, the mitochondrial respiration was decelerated probably caused by a decreased amount of reducing equivalents or inhibitory effects of arising metabolites. Both, the *in situ*

mitochondrial metabolite flux assay and the partial knock-down approach provide valuable tools to investigate biological effects of lipid metabolism-associated GWASs SNPs. Here, unexpected, possibly regulatory processes influencing acylcarnitine profiles were found after short-term fatty acid loading.

2) Postprandial metabolic and inflammatory activation of human PBMC

High-fat, high-carbohydrate (HFHC) meals have been reported to induce an inflammatory response in peripheral blood mononuclear cells (PBMC). Here, the interaction between metabolic and inflammatory signalling by measurement of postprandial effects of three different test meals on intracellular Akt, S6K (mTOR) and NF-κB signalling in human PBMC was studied. For this purpose, six healthy, lean individuals were recruited. Each individual ingested three different meals in the morning separated by at least three days: (a) a HFHC meal, (b) an oral lipid tolerance test (OLTT) and (c) a healthy breakfast (HB). Blood samples were obtained before and 1, 2, 4, 6 and 8h after ingestion. Plasma insulin was measured and intracellular metabolic and inflammatory signalling was assessed by measuring phosphorylation of Akt kinase, S6 kinase (S6K), inhibitor κB-α (IκB-α) protein degradation and nuclear factor-κB (NF-κB) DNA binding activity in PBMC. The mRNA expression levels of the Akt and NF-κB target genes manganese superoxid dismutase (MnSOD), CC-chemokine-receptor 5 (CCR5), intercellular adhesion molecule-1 (ICAM-1) and plasminogen activator inhibitor-1 (PAI-1) were measured by qRT-PCR. A significant positive correlation was found for postprandial Akt and NF-κB activation and, moreover, a significant positive correlation of S6K activation with plasma insulin levels. The activation of Akt and proinflammatory NF-κB signalling was supported by up-regulation of the respective target genes MnSOD and CCR5. In conclusion, these data suggests an interaction of the metabolic and inflammatory signalling pathways Akt and NF-κB in PBMC after meal ingestion, contributing to deeper understanding of immune system-metabolism interaction.

Zusammenfassung

Diese Doktorarbeit ist in zwei Hauptforschungsziele gegliedert:

1) Von GWAS zu Funktionalität: die Assoziation von rs2014355 im ACADS Genlocus mit dem Verhältnis von Acylcarnitinen

Genomweite Assoziationsstudien (GWASs) haben eine Assoziation zwischen rs2014355 im Kurzketten-Acyl-CoA-Dehydrogenase (ACADS) Locus mit dem Plasma C3/C4-Acylcarnitin Verhältnis aufgedeckt. Um die daraus resultierende Hypothese einer gestörten ACADS Aktivität zu bestätigen, wurde der *in situ* mitochondriale Metaboliten Fluss-Assay in genotypisierten, mit dem Epstein-Barr Virus immortalisierten lymphoblastoiden Zelllinien (EBV-LCLs) angewendet. Entdeckt wurde eine verminderte Stoffwechselrate von C4:0-Acylcarnitin in Zellen, die homozygot für das seltene C Allel sind, welche zum Teil auf die niedrigere ACADS Gen- und Proteinexpression in EBV-LCLs zurückgeführt werden könnte. Darüber hinaus wurden bioinformatisch vorhergesagte *cis*-regulatorische Varianten in hohem Linkage Disequilibrium (LD) mit rs2014355 mithilfe von Reportergen Assays untersucht. Dabei wurden allelische, *cis*-regulatorische Effekte von vier assoziierten SNPs aufgedeckt, jedoch zeigte der GWASs lead SNP rs2014355 keinen Effekt. Allerdings besteht die Möglichkeit, dass neben den *cis*-regulatorischen Effekten auch eine nicht-synonym kodierende Variante (rs1799958) im perfekten LD mit rs2014355 kausal für die verringerte ACADS Aktivität sein könnte. Folglich könnten unterdrückende *cis*-regulatorische Varianten durch eine reduzierte ACADS mRNA Expression zu der verringerten ACADS Aktivität beitragen, während mehrere aktivierende *cis*-regulatorische Varianten durch eine erhöhte Genexpression der gestörten Enzymfunktion entgegenwirken könnten.

Um dem Einfluss der verminderten ACADS Genexpression in einem Zelltyp, der in erheblichem Maß durch Fettsäureoxidation zum peripheren Energiemetabolismus beiträgt, weiter nachzugehen, wurde eine humanen Leberzelllinie (Huh7) mit abgestuften Knockdowns des endogenen ACADS Proteins verwendet. Die verbleibende Porteinmenge bestimmte das Ausmaß der intrazellulären C4:0-Acylcarnitin Akkumulation und ist somit ein Modell für den Phänotyp, der in populationsbasierten Studien und genotypabhängigen Zellmodellen mit dem SNP assoziiert wurde. Insbesondere die Beladung der Knockdown Zelllinien mit Palmitat und die darauffolgende kurzzeitige, zeitaufgelöste Acylcarnitin-

Messung zeigten neue, dynamische, regulatorische Vorgänge bezüglich lang- und mittelkettiger Acylcarnitine. Außerdem wurde die mitochondriale Respiration, vermutlich durch eine geringe Menge an Reduktionsäquivalenten oder durch inhibitorische Effekte entstehender Metabolite, verringert. Sowohl der *in situ* mitochondriale Metabolien Fluss-Assay, als auch die graduelle Knockdown Methode sind wertvolle Werkzeuge bei der Erforschung von biologischen Funktionen Lipidmetabolismus-assoziierter SNPs aus GWASs. Unerwarteter Weise wurden hier nach kurzfristiger Fettsäurebeladung potentielle Regulationsvorgänge mit Einfluss auf die Acylcarnitin-Profile gemessenen.

2) Postprandiale metabolische und inflammatorische Aktivierung von humanen PBMC

Es ist bekannt, dass Fett- und Kohlenhydratreiche (HFHC) Mahlzeiten eine inflammatorische Antwort in peripheren mononukleären Zellen (PBMC) hervorrufen. In dieser Doktorarbeit wurde die Interaktion metabolischer und inflammatorischer Signalübertragung in humanen PBMC durch die Messung der postprandialen Wirkung von drei verschiedenen Testmahlzeiten auf die intrazelluläre Akt, S6K (mTOR) und NF-κB Signalübertragung untersucht. Zu diesem Zweck wurden sechs gesunde, normalgewichtige Probanden rekrutiert. Jeder Proband nahm im Abstand von mindestens drei Tagen jeweils morgens eine von drei verschiedene Mahlzeiten ein: (a) eine HFHC Mahlzeit, (b) einen oralen Lipid-Toleranztest (OLTT) und (c) ein gesundes Frühstück (HB). Blutproben wurden jeweils vor und 1, 2, 4, 6 und 8h nach Nahrungsaufnahme abgenommen. Es wurden die Plasmainsulinspiegel gemessen und die intrazelluläre metabolische und inflammatorische Signalübertragung wurde durch die Messung der Akt Kinase-, S6 Kinase (S6K) Phosphorylierung, der IκB-α Degradierung und der NF-κB Bindungsaktivität in PBMC erfasst. mRNA Expressionslevel der Akt- und NF-κB-Zielgene Mangan Superoxiddismutase (MnSOD), CC-Chemokinrezeptor 5 (CCR-5), intrazelluläres Adhesionsmolekül-1 (ICAM-1) und Plasminogen-Aktivator-Inhibitor 1 (PAI-1) wurden mithilfe von qRT-PCR gemessen. Eine signifikante positive Korrelation wurde für die postprandiale Akt und NF-κB Aktivierung gefunden und darüber hinaus eine positive Korrelation der S6K Aktivierung mit dem Plasmainsulinspiegel. Die Aktivierung der Akt- und der proinflammatorischen NF-κB Signalübertragung wurde durch die Hochregulierung der jeweiligen Zielgene MnSOD und CCR5 gestützt. Schlussendlich deuten die erhobenen Daten

nach Nahrungsaufnahmen eine Interaktion der metabolischen und inflammatorischen Signalübertragungswege von Akt und NF-κB in PBMC an. Diese Beobachtung trägt zu einem tieferen Verständnis der Interaktion von Immunsystem und Stoffwechsel bei.

Abbreviations

ACADL	Acyl-CoA dehydrogenase long-chain
ACADM	Acyl-CoA dehydrogenase medium-chain
ACADS	Acyl-CoA dehydrogenase short-chain
ACADs	Acyl-CoA dehydrogenases
ACSL1	Long-chain-fatty-acid-CoA ligase 1
Acyl-CoA	Acyl-coenzyme A
ADP	Adenosine diphosphate
ANOVA	Analysis of variance
ATP	Adenosine triphosphate
BCA	Bicinchoninic acid
BMI	Body mass index
BSA	Bovine serum albumin
CACT	Mitochondrial carnitine acylcarnitine translocase
CCR5	CC-chemokine-receptor 5
CIP	Calf intestinal phosphatase
CPT I	Carnitine palmitoyltansferase I
CPT II	Carnitine palmitoyltransferase II
CS	Citrate synthase
DMSO	Dimethylsulfoxid
DTNB	5,5-dithiobis-(2-nitrobenzoic acid)
EBV-LCLs	Epstein-Barr virus immortalized lymphoblastoid cell lines
EMA	Ethylmalonic acid
EMSA	Electrophoretic mobility shift assay
eQTL	Expression quantitative trait loci
ESI	Electron spray ionization
ETF	Electron transfer flavoprotein
ETFDH	Electron transfer flavoprotein dehydrogenase
FAO	Fatty acid oxidation
FAD	Flavin adenine dinucleotide
FATPs	Fatty acid transporters

FCCP	Trifluorocarbonylcyanide phenylhydrazone
FCS	Fetal calf serum
GAPDH	Glyceraldehyde 3-phosphate dehydrogenase
GWASs	Genome-wide association studies
HB	Healthy breakfast
HFHC	High-fat, high-carbohydrate
HOMA-B	Homeostatic model assessment-B
ICAM-1	Intercellular adhesion molecule-1
IκB-α	Inhibitor κB-α
IKK2	Inhibitor NF-κB kinase 2
KORA	Kooperative Gesundheitsforschung in der Region Augsburg
IR	Insulin-receptor
LD	Linkage disequilibrium
LDH	Lactate dehydrogenase
MAF	Minor allele frequency
MnSOD	Manganese superoxid dismutase
mTOR	Mammalian target of rapamycin
NAD	Nicotinamide adenine dinucleotide
NF-κB	Nuclear factor-κB
NTC	Non-target control
OCR	Oxygen consumption rate
OGTT	Oral glucose tolerance test
OLTT	Oral lipid tolerance test
PAI-1	Plasminogen activator inhibitor-1
PBMC	Peripheral blood mononuclear cells
PBS	Phosphate buffered saline
PGK1	Phosphoglycerate kinase 1
PMCA	Phylogenetic module complexity analysis
PNK	Polynucleotide kinase
PPIA	Peptidyl-prolyl cis-transisomerase A
RGI	Reference gene index
ROS	Reactive oxygen species

SCD	Stearoyl-CoA desaturase
SD	Standard deviation
SDS-PAGE	Sodium dodecyl sulfate-polyacrylamide gel electrophoresis
SEM	Standard error of the mean
SNPs	Single nucleotide polymorphisms
S6K	S6 kinase
TCA	Tricarboxylic acid cycle
TFBSs	Transcription factor binding sites
TK	Thymidine kinase
TNB	Thionitrobenzoic acid
UTR	Untranslated region
YWHAZ	Tyrosine 3-monooxygenase/tryptophan 5-monooxygenase activation protein, zeta polypeptide

1 From GWAS to functionality: association of rs2014355 in the ACADS gene locus with acylcarnitine ratio

1.1 Introduction

1.1.1 Genetics meets Metabolomics

Recent advances in genome-wide association studies (GWASs) have been successful in the identification of thousands of single nucleotide polymorphisms (SNPs) associated with a large number of phenotypes (Hindorff et al. 2009). However, GWASs have shown that the majority of common SNPs are located in non-coding regions (Hindorff et al. 2009) and in most cases GWASs do not offer any direct evidence about the biological processes that link either the associated variant or the affected gene to the associated phenotype (Califano et al. 2012). Metabolomics, a rapid evolving field of measuring endogenous metabolites in a cell or body fluid, may contribute to solving this problem by providing more specific phenotypes which may be directly linked to the affected gene. Serum metabolite concentrations provide a direct readout of biological processes in the human body and, therefore, might provide more insight into disease-related metabolic deregulation. GWASs have shown that common genetic variations can have a profound impact on the homeostatic concentrations of specific metabolites (Montoliu et al. 2013; Illig et al. 2010; Gieger et al. 2008).

1.1.2 Association of rs2014355 with acylcarnitine ratio

In GWASs of human metabolites, where metabolite concentration ratios were used as proxies for enzymatic reaction rates, several genetic loci were found to be highly associated with observed variance of the respective metabolite pairs (Gieger et al. 2008; Illig et al. 2010). In a recent GWAS, Illig et al. measured 163 metabolic traits in human serum from 1,809 participants from the KORA population, with replication in 422 participants of the TwinsUK cohort, and found a strong association for the SNP rs2014355, in the acyl-CoA dehydrogenase short-chain (ACADS) gene locus, with the C3/C4-acylcarnitine ratio ($p = 5.10 \times 10^{-96}$) (Figure 1.1-1a). The observed genetic variance explained 21.5% of the inter-individual variance of this ratio (Illig et al. 2010). The same association was reported by Gieger et al. who showed that the measurement of 363 metabolites in human serum of 284 participants

of the KORA study revealed an association of rs2014355 with the C3/C4-acylcarnitine ratio ($p = 9.30 \times 10^{-17}$, explained variance: 21.8%) (Gieger et al. 2008). Hong et al. also found a strong association of rs2014355 with a molecular feature (m/z 232.122), corresponding to C4-acylcarnitine with a p-value of 4.3×10^{-6} by employing a non-targeted metabolite profiling approach (^{1}H NMR) (Hong et al. 2013). The finding of Illig et al. was replicated by Nicholson et al. in a study with longitudinal twin design. This study design allowed detailed variance-components analysis of the sources of population variation in metabolite levels. The SNP rs2014355 explained 26% of biological population variation in the C3/C4-acylcarnitine levels. They further discovered a previously uncharacterized, yet substantial, familial component of variation (51%) in metabolite levels in addition to the heritability contribution from the rs2014355 effect (Nicholson et al. 2011).

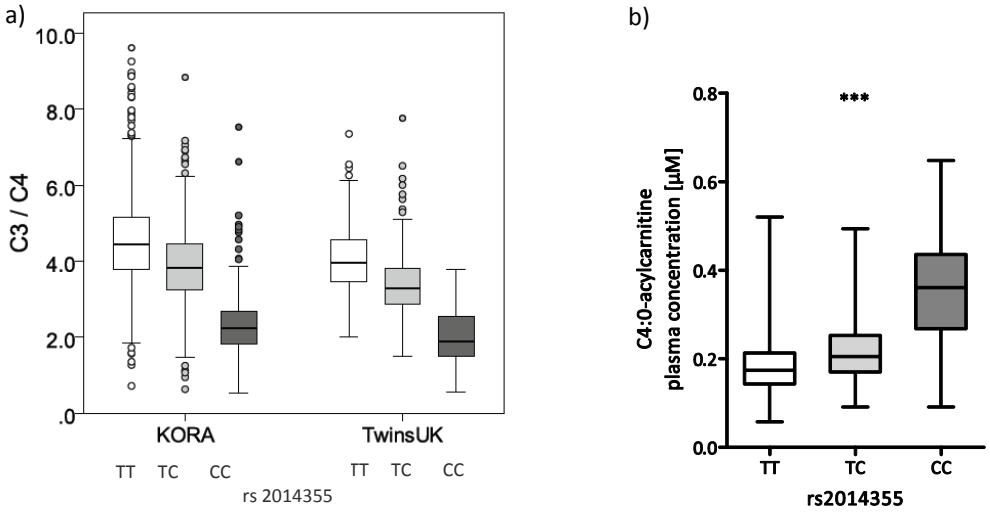

Figure 1.1-1: Box plots of plasma C3/C4-acylcarnitine ratio and plasma C4:0-acylcarnitine concentrations associated with rs2014355
a) Plotted as a function of genotype (white: major allele homozygotes (TT), light grey: heterozygotes (TC), dark grey: minor allele homozygotes (CC)) and study (KORA, n=1809; TwinsUK, n=422); boxes extend from 1st quartile (Q1) to 3rd quartile (Q3); median is indicated as a horizontal line; whiskers are drawn to the observation that is closest to, but not more than, a distance of 1.5 (Q3-Q1) from the end of the box; observations that are more distant than this are shown individually on the plots (Illig et al. 2010). b) Box plots show the differentiation of the population that is induced by genetically determined metabotypes. Boxes extend from 1st quartile (Q1) to 3rd quartile (Q3); median is indicated as a horizontal line; whiskers are drawn from minimum to maximum. Data is extracted from KORA F4 (http://www.helmholtz-muenchen.de/cmb/research/metabolomics/ggms-on-metabolomics-data/index.htm). One-way ANOA was calculated; *** = $p < 0.001$.

Acylcarnitine profiles in serum or plasma reflect the intra-mitochondrially accumulating acyl-CoAs which are exported out of the mitochondria as their corresponding carnitine esters (Noland et al. 2009; Ventura et al. 1999; ter Veld et al. 2009). Of note, some newborn

screening programs determine C4-acylcarnitine based ratios (McHugh et al. 2011). Therefore, a reduced C3/C4-acylcarnitine ratio implies a reduced activity of the enzyme ACADS in particular in view of the fact that butyryl (C4)-CoA is the major substrate for ACADS (Ghisla and Thorpe 2004) and its surrogate C4-acylcarnitine is accumulating in the serum of KORA participants (Figure 1.1-1b). Consequently, minor allele homozygotes have the lowest enzymatic turnover of the reaction catalysed by ACADS (Figure 1.1-1a, b).

1.1.3 ACADS and its role in energy metabolism

The *ACADS* gene (OMIM: 606885) has been localized to the terminal region of the long arm of chromosome 12, spans approximately 13 kb and consists of 10 exons (Corydon et al. 1997). Its transcription product is an enzyme involved in energy metabolism in humans. ACADS participates in the mitochondrial fatty acid oxidation (FAO). The FAO occurs at the level of the β-carbon (β-oxidation) and is the major energy source of the organism in the absence of sufficient glucose supply (Houten and Wanders 2010).

Lipid mobilization of FAO substrate and transport into tissues

The substrates for FAO, fatty acids, are stored in the adipose tissue as triacylglycerols and are released during lipolysis. This is initiated by the activation of the hormone-sensitive lipase under fasting conditions or exercise, induced by the hormones adrenalin, noradrenaline, glucagon and adrenocorticotropic hormone. Fatty acids which are released from triacylglycerols during lipolysis, in particular long-chain fatty acids, are imported into various tissues by fatty acid transporters (FATPs) (Figure 1.1-2). Inside the cytosol fatty acids are esterified by acyl-coenzyme A (acyl-CoA) synthethase resulting in fatty acyl-CoAs. After binding to acyl-CoA binding proteins, acyl-CoA esters are delivered to carnitine palmitoyltansferase I (CPT I) which is located in the outer mitochondrial membrane and is a key enzyme of the FAO (Houten and Wanders 2010; Nelson et al. 2008; Eaton et al. 1996).

Transport of fatty acyl-CoAs into mitochondria

Medium- and short-chain fatty acids can enter the mitochondria passively. Long-chain acyl-CoAs cannot cross the mitochondrial inner membrane; they need to be converted into the corresponding acylcarnitine esters by the enzyme CPT I. The mitochondrial carnitine-acylcarnitine translocase (CACT) mediates the transfer of the acylcarnitine into the

mitochondrion followed by the regeneration of long-chain acyl-CoAs and thereby releasing free carnitine by carnitine palmitoyltransferase II (CPT II). Free carnitine is transported back into the cytosol by the acylcarnitine translocase completing the carnitine shuttle (Houten and Wanders 2010; Nelson et al. 2008; Eaton et al. 1996) (Figure 1.1-2).

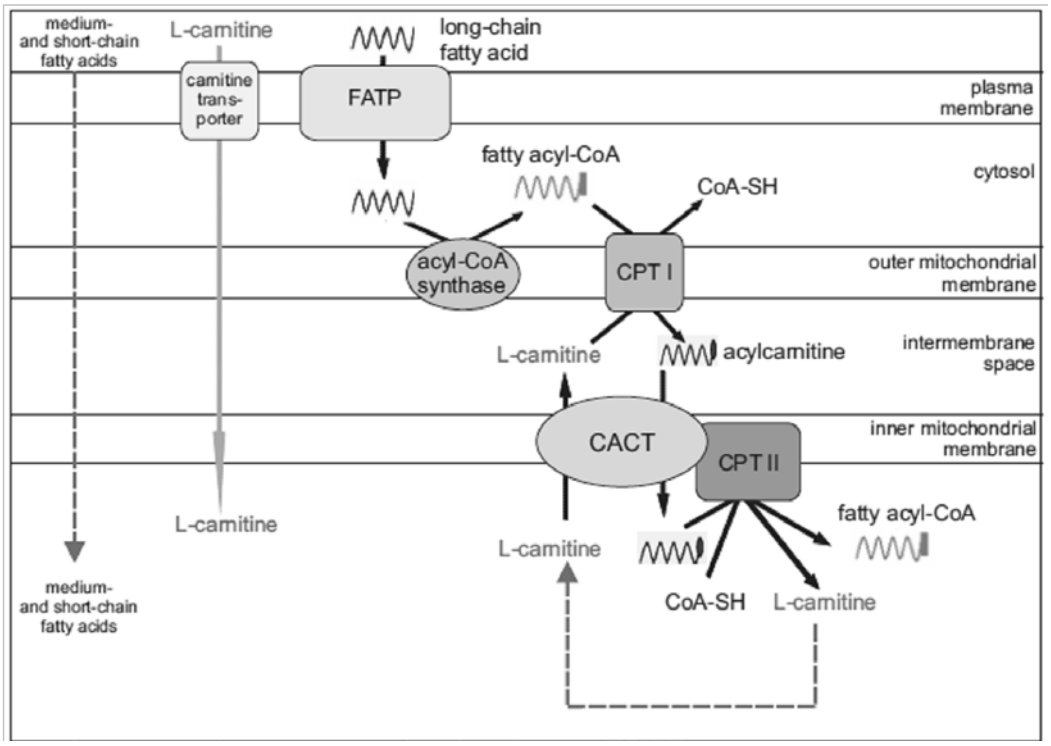

Figure 1.1-2: Transport of long-chain fatty acids into mitochondrial matrix
CACT = carnitine-acylcarnitine translocase, CPT I = carnitine palmitoyltransferase I, CPT II = carnitine palmitoyltransferase II, FATP = fatty acid transport protein. (Created by A. Matthey based on the model of Dokoupil and Ensenauer, 2008).

Oxidation of fatty acyl-CoAs

Inside the mitochondrion the acyl-CoAs can be degraded by mitochondrial FAO. This involves the process of chain-shortening by repetitive β-oxidation cycles (Figure 1.1-3). An acyl-CoA is shortened by two carbons at the end of one full β-oxidation cycle by a series of four consecutive enzymatic reactions, which results in the release of an acetyl-CoA unit. The action of four enzymes is required for each chain-shortening step. Each group of enzymes has chain length specific isoforms. The first step is catalysed by acyl-CoA dehydrogenases (ACADs), which are flavin adenine dinukleotide (FAD)-dependent oxidoreductases. In this reaction two hydrogen atoms in the 2- and 3-position of the fatty acid acyl-CoAs are removed. FAD is reduced to $FADH_2$ and a double bond is formed between these positions. The resulting 2-trans-enoyl-CoA esters are hydrated by enoyl-CoA hydratases, resulting in a

hydration of the double bond and forming L-3-hydoxyacyl-CoA esters. L-3-hydroxy-acyl-CoA dehydrogenases convert L-3-hydroxyacyl-CoAs to the corresponding 3-ketoacyl-CoAs, including the reduction of nicotinamide adenine dinucleotide (NAD^+) to $NADH+H^+$. The last part of the FAO is the thiolytical cleavage of the 3-ketoacyl-CoA by 3-oxoacyl-CoA thiolases releasing an acetyl-CoA. The ACADS enzyme is one of these acyl-CoA dehydrogenases and catalyses the initial and committing step of the final reaction cycles resulting in the production of another 2 molecules of acetyl-CoA. The acetyl-CoA molecules produced during FAO can be used by tricarboxylic acid cycle (TCA) and respiratory chain for adenosine triphosphate (ATP) production (Houten and Wanders 2010; Nelson et al. 2008; Eaton et al. 1996).

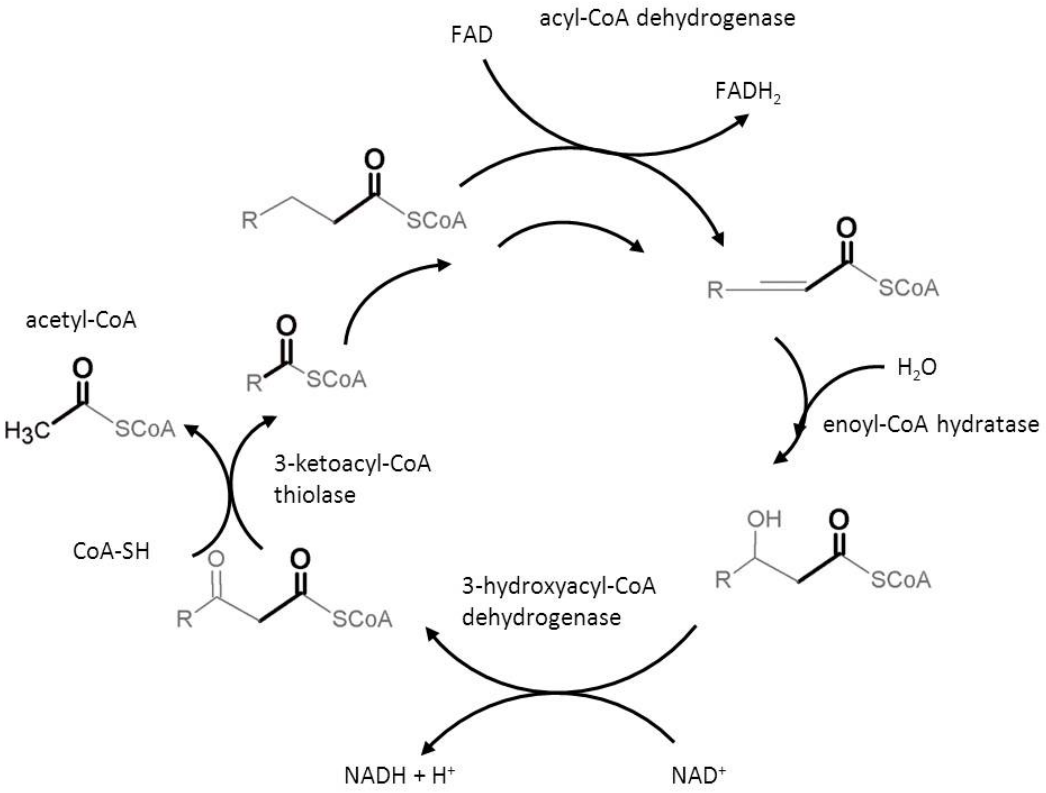

Figure 1.1-3: Four chain-shortening steps of FAO
FAD = flavin adenine dinucleotide.

1.1.4 ACADS deficiency

ACADS deficiency is an autosomal recessive inborn error of mitochondrial FAO with highly variable biochemical, genetic, and clinical characteristics (van Maldegem et al. 2006). C4:0-CoA is the primary substrate of ACADS (compare paragraph 1.1.2), therefore a deficiency of

this enzyme is biochemically characterized by increased C4:0-CoA by-products including C4:0-acylcarnitine, butyrylglycine, ethylmalonic acid (EMA), and methylsuccinic acid in blood, urine and cells (Corydon et al. 1996). The largest published series of ACADS deficiency patients, identified by biochemical markers, in the California newborn screening revealed a birth prevalence for ACADS deficiency of approximately 1/35,000 (Gallant et al. 2012). The diagnosis of ACADS deficiency is confirmed by DNA analysis showing ACADS gene mutations and/or variants. More than 40 inactivating mutations and two common missense variants, c.511C>T (rs1800556; R147W) and c.625 G>A (rs1799958; G185S) have been reported to be associated with ACADS deficiency (Gallant et al. 2012). These two missense variants have a remarkably high prevalence; approximately 7% of the population were found to be either homozygous for one of the variants or compound heterozygous for each (Corydon et al. 1996). Both the common variants and most of the reported deleterious mutation, cause single amino acid substitutions leading to protein misfolding and aggregation (Pedersen et al. 2003; Pedersen et al. 2008). The clinical relevance of several mutations and polymorphisms has been reported in previous studies, however the presentation of clinical symptoms is variable, but the phenotype commonly includes developmental delay, hypotonia, hypoglycaemia, epilepsy and behavioural disorders. However, often these symptoms ameliorate or disappear spontaneously and were found to be unrelated to the ACADS genotype. Moreover, many ACADS deficiency diagnosed individuals remain asymptomatic (van Maldegem et al. 2010).

1.1.5 Association of rs2014355 and metabolic disease

The rs2014355 variant has been suggested to cause a mild biochemical phenotype (Gieger et al. 2008; Illig et al. 2010; Nicholson et al. 2011) characterized by altered levels of plasma FAO metabolites in comparison to the average population. Although this phenotype does not lead to clinical symptoms, it might well be that carriers are more sensitive to periods of metabolic stress (e.g. fasting) and thus potentially more susceptible to the development of metabolic diseases during their lifetime (Illig et al. 2010). Moreover, it was shown, that the minor allele (C) of the SNP rs2014355 associates with reduced measures of glucose-stimulated insulin release during an oral glucose tolerance test (OGTT) in glucose-tolerant individuals. The authors hypothesized that reduced FAO induced by rs2014355 CC initiates accumulation of fatty acids. This might initially stimulate insulin secretion leading to hyperinsulinaemia. In the

chronic state, this induced hyperinsulinaemia might exhaust the β-cell leading to reduced insulin release. The reduced β-cell function could in turn predispose some individuals to type 2 diabetes mellitus (Hornbak et al. 2011). However, the study of Hornbak et al. (Hornbak et al. 2011), as well as previous published meta-analyses (Zeggini et al. 2008; Morris et al. 2012) showed that the analysed ACADS variant (rs2014355 CC) did not associate directly with an increased risk to develop type 2 diabetes. Moreover, no significant association was found between fasting glucose, fasting insulin (Manning et al. 2012), as well as 2h glucose (adjusted for BMI) in response to an oral glucose tolerance test (Saxena et al. 2010) and a variety of SNPs in high linkage disequilibrium (LD) with rs2014355. However, there was a significant association ($p = 3.70 \times 10^{-3}$) of rs2066938 (LD: $r^2 = 0.91$ with rs2014355, European population, 1,000 Genome Phase 1) and homeostatic model assessment-B (HOMA-B) (Scott et al. 2012; Dupuis et al. 2010) (Data on glycaemic traits have been contributed by MAGIC investigators and have been downloaded from www.magicinvestigators.org). In summary, the association of rs2014355 with impaired insulin secretion and type 2 diabetes remains controversial and needs further investigation.

1.1.6 Identification of causal variants

A major challenge in the interpretation of GWASs results is caused by the fact that an associated SNP is likely linked to a larger set of correlated variants (Califano et al. 2012). SNPs that are in close proximity in the genome tend to be in LD with each other (The International HapMap Consortium 2005). Only one or a few SNPs per LD region are measured on a given genomic platform. Thus, the fact that causal variants in a LD region remain elusive from GWASs results, and the consequent identification of SNPs that have a biological link with the phenotype, remains a major challenge in human genetics.

Nagan et al. reported plasma C4:0-acylcarnitine concentrations of two common missense variants associated with ACADS deficiency (Nagan et al. 2003), c.511C>T (rs1800556, minor allele frequency (MAF) = 6% in European population, 1,000 Genome Phase 1) and c.625 G>A (rs1799958, MAF = 26% in European population, 1,000 Genome Phase 1) which are similar to the plasma C4:0-acylcarnitine concentrations observed for rs2014355 (compare Figure 1.1-1b). The variant rs1799958 is in strong LD with rs2014355 (LD: $r^2 = 1.0$, European population, 1,000 Genome Phase 1), whereas rs1800556 is not associated with rs2014355 (European

population, 1,000 Genome Phase 1). Interestingly, there is a substantial body of literature stating that the rs1799958 minor A allele encodes proteins with reduced catalytic activity and/or thermostability (Corydon et al. 2001; Gregersen et al. 1998; Corydon et al. 1996). Thus, the coding variant rs1799958 may be one of the functional SNPs accountable for the association with the C3/C4-acylcarnitine ratio found by Illig et al. (Illig et al. 2010). Noteworthy, the association of rs1799958 and rs2014355 was not covered in HapMap release 22 (Table 1.1-1) that was used in the beginning of this thesis and became apparent not until the release of Genome 1,000 Pilot 1 (Table 1.1-1). Furthermore, a statistically significant *cis*-eQTL was found in the *ACADS* gene in strong LD with rs2014355. The variant rs10431384 (in LD: r^2 = 0.64 with rs2014355, European population, 1,000 Genome Phase 1) was associated with increased mRNA expression of *ACADS* in the liver (Table 1.1.2) (Mirkov et al. 2012). The *cis*-regulatory variants underlying this expression quantitative trait loci (eQTL) observation may additionally contribute to the associated C3/C4-acylcarnitine ratio. Thus, possibly one or more SNPs in LD with rs2014355 might have a causal biological link with the phenotype in addition or instead of rs2014355.

Table 1.1-1: LD blocks (r^2 = 1.0) of lead SNP rs2014355 according to different public data bases
HapMap release 22 and 1,000 Genome Pilot 1: CEU (Utah residents with ancestry from northern and western Europe) population, data obtained from SNAP (Broad institute) (Johnson et al. 2008). 1,000 Genome Phase 1: European population, data obtained from HaploReg (Broad institute) (Ward and Kellis 2011).

	tag SNP	proxy SNP	Chr	Position	MAF	type of SNP	Nearest Gene(s)
HapMap release 22	rs2014355	rs3916	12	119661655 [GRCh36/hg18]	0.25	3'-UTR	ACADS
CEU data		rs3999408	12	119651770 [GRCh36/hg18]	0.25	INTRONIC	ACADS
		rs2066938	12	119644998 [GRCh36/hg18]	0.25	INTRONIC	UNC119B
		rs7306541	12	119614429 [GRCh36/hg18]	0.25	INTRONIC	KIAA0152
1,000 Genome Pilot 1	rs2014355	rs1799958	12	119660466 [GRCh36/hg18]	0.242	MISSENSE	ACADS
CEU data		rs3916	12	119661655 [GRCh36/hg18]	0.242	3'-UTR	ACADS
		rs34708625	12	119664402 [GRCh36/hg18]	0.242	DOWNSTREAM	N/A
1,000 Genome Phase 1	rs2014355	rs1799958	12	121176083 [GRCh37/hg19]	0.26	MISSENSE	ACADS
European population		rs3916	12	121177272 [GRCh37/hg19]	0.26	3'-UTR	ACADS
		rs34708625	12	121180019 [GRCh37/hg19]	0.26	N/A	N/A

Chr = chromosome, MAF = minor allele frequency, UTR = untranslated region

LD block analysis comes with an additional challenge: up to now full knowledge of DNA sequence variation across the entire spectrum of allele frequencies and types of DNA differences has not been obtained in association studies. There has been substantial progress by the release of public databases like genome 1,000 (Abecasis et al. 2010) and the availability of data sets generated by the ENCODE project (Birney et al. 2007; Dunham et al.

2012). However, the incomplete knowledge exacerbates the identification of causal SNPs for phenotypic traits and functional research, e.g. LD block analysis using different databases result in variable proxy SNPs (Table 1.1-1).

Table: 1.1-2: Relationship between metabolite associated SNPs and eQTL data in the liver
Measures of pair-wise LD (r^2 and D') between the GWASs tag SNP (rs2014355) and the proxy SNP (rs10431384) are derived from European population, 1,000 Genome Phase 1. The p-value is derived from unpaired t-test and was likewise the distance adopted from Mirkov et al. (Mirkov et al. 2012).

Gene	SNP	eQTL	Distance (bp)	r^2	D'	p value
ACADS	rs2014355	rs10431384	48177	0.64	0.91	1.01×10^{-7}
eQTL = expression quantitative trait loci, SNP = single nucleotide polymorphism						

DNAse I hypersensitivity site-, DNAse I footprint- (Thurman et al. 2012; Neph et al. 2012) and ChIP-seq (Dunham et al. 2012) data have been published and are useful to search for *cis*-regulatory variants in LD blocks. Also bioinformatics approaches, assuming functionality for a candidate variant when located in gene regulatory regions can be used. One of them is the phylogenetic module complexity analysis (PMCA) which integrates evolutionary conservation with a complexity assessment of co-occurring transcription factor binding sites (TFBSs) (Claussnitzer M, personal communication).

1.1.7 Hypotheses and aim

The integrated genomics and metabolomics approach is an important step towards the understanding of key pathways involved in the regulation of human metabolism and the pathogenesis of polygenic complex diseases like cancer and type 2 diabetes. However, this approach usually does not offer any direct evidence if the GWASs-identified variants and the respective nearby genes are causative for the biochemical phenotype. One example is the association of the SNP rs2014355 in the ACADS locus with the C3/C4-acylcarnitine ratio.

This part of the work addresses the investigation of the biological effect of rs2014355 by establishing a method (*in situ* mitochondrial metabolite flux assay) to measure the mitochondrial FAO in EBV-LCLs carrying various rs2014355 alleles. The *in situ* mitochondrial metabolite flux assay is used for indirect measurement of ACADS activity which was hypothesised to be responsible for the associated phenotype. Moreover, this method will be a valuable tool to investigate further SNPs associated with FAO since EBV-LCLs are readily available from several GWASs-cohorts.

In most cases it remains elusive which genes are regulated by trait-associated variants (Califano et al. 2012). Even in cases where associated SNPs were found to regulate certain genes which have well-known functions, nailing down how these genes confer metabolic alterations or disease susceptibility can be time consuming and requires access to appropriate human tissue or cell culture models. Therefore, a further aim of this thesis was to generate and test a system that allows a partial down-regulation of a target protein and thereby represents an *in vitro* genotype-phenotype model for moderate genetic effects from common variants, with subsequent use in functional assays. In this thesis, the system is applied for gradual knock-downs of ACADS in a liver cell line (Huh7) with subsequent measurements of induced acylcarnitine flux and mitochondrial respiration both reflecting FAO. It is expected that the gradual ACADS knock-downs are reflected in the *in vitro* measured biochemical phenotypes, which should reflect and help to explain the *in vivo* phenotypes observed in association studies. Further, the question is addressed if an ACADS knock-down affects the acylcarnitine flux, reflecting FAO and the mitochondrial respiration during induced FAO. The compiled data will be provided to bioinformatics modelling approaches with the aim to further improve a recently published FAO model based on human plasma metabolite data (Krug et al. 2012). Such systems biology modelling approaches might confirm and or even reveal new explanations, which can hardly be obtained from experimental data alone (the bioinformatics model is not part of the present thesis). The here presented approach enables the study of down-regulated genes/proteins, the subsequent effect on cellular pathway, and their involvement in metabolic alterations and disease susceptibility.

The majority of SNPs found to be associated with metabolic or disease traits from the recent wave of GWASs are non-coding. These non-coding SNPs either regulate gene activity at the transcript level directly, or they are linked to other DNA variations which are involved in this type of *cis*-regulatory role. As stated above, rs2014355 links to both, a coding, protein sequence varying SNP (rs1799958) and several non-coding SNPs. To explore if rs2014355 or a non-coding SNP in LD have *cis*-regulatory effects on *ACADS* gene expression qPCR analysis is carried out complemented by western blots of the ACADS protein levels in genotyped EBV-LCLs, human preadipocytes and human adipocytes. Additionally, PMCA is applied to identify potential causal *cis*-regulatory SNPs in LD (r^2 = 0.6) of rs2014355. The effect on regulatory

activity of these identified variants is tested in reporter-gene assays in a human liver cell line (Huh7) and a mouse preadipocyte cell line (3T3L1) differentiated until day 6.

1.2 Materials

Eukaryote cells and cell lines

Primary human preadipocytes

Cell type: Primary human adipocyte precursor cells

Source: Isolated stromal cell fraction from human adipose tissue specimens obtained from elective surgery

Characterization: Stromal cells have the ability to proliferate and adipocyte conversion is induced by adding hormone-supplemented medium which results in the expression of genes required for adipose differentiation. The average differentiation rate is 40-50%.

EBV-LCLs (Helmholtz Zentrum München)

Cell type: Epstein-Barr virus immortalized lymphoblastoid cell lines

Source: Obtained from *in vitro* transfection of human B-lymphocytes with the Epstein-Barr virus

Characterization: *In vitro* infection of human B-lymphocytes with Epstein-Barr virus induces metabolic activation, morphological transformation, cell proliferation and eventual immortalization. Genotype discrepancy analysis between PBMC and EBV-LCLs revealed no considerable genotypic errors due to the EBV-transformation process (Yenamandra et al. 2009). Gene expression in EBV-LCLs encompasses a wide range of metabolic pathways that are specific to the genotype of their donors and are therefore suitable for molecular and functional studies (Amoli et al. 2008).

Table 1.2-1: Genetic background of EBV-LCLs used in this thesis
EBV-LCLs obtained from the Helmholtz Zentrum München were resequenced for rs2014355 and rs1799958 (Sanger sequencing performed by L. Pfeiffer, Helmholtz Zentrum München). Additionally, EBV-LCLs were genotyped (performed by H. Grallert, Helmholtz Zentrum München) for further SNPs affecting acylcarnitine ratios as reported in the study by Illig et al. (Illig et al. 2010) (rs211718, rs2286963, rs8396, rs2046813 and rs603424). Unfortunately, the attempt to select exclusively homozygous carriers of the major allele of the potential confounding SNPs failed because of limited availability of cell lines. However, alternative selection solely included heterozygous genotypes.

EBV-LCL ID	Group	ACADS rs2014355	ACADS rs1799958	ACADM rs211718	ACADL rs2286963	ETFDH rs8396	ACSL1 rs2046813	SCD rs603424
310001441	rs2014355 TT	T/T	G/G	C/C	T/T	T/T	T/T	G/G
310000438	rs2014355 TT	T/T	G/G	C/C	T/T	T/T	T/T	G/G
310001205	rs2014355 TT	T/T	G/G	C/C	T/T	T/T	T/T	G/G
310001525	rs2014355 TT	T/T	G/G	C/C	T/T	T/T	T/T	G/G
310001468	rs2014355 CC	C/C	A/A	C/C	T/T	T/C	T/T	G/G
310001142	rs2014355 CC	C/C	A/A	C/C	T/T	T/C	T/T	G/A
310001214	rs2014355 CC	C/C	A/A	C/C	T/T	T/C	T/T	G/G
310000379	rs2014355 CC	C/C	A/A	C/C	T/T	T/C	T/T	G/G
310000077	rs2014355 CC	C/C	A/A	C/C	T/T	T/T	T/T	G/G
310001359	rs2014355 TC	T/C	G/A	C/C	T/T	T/C	T/C	G/A
310001093	rs2014355 TC	T/C	G/A	C/C	T/T	T/T	T/C	G/G

ACADL = acyl-CoA dehydrogenase long-chain, ACADM = acyl-CoA dehydrogenase medium-chain, ACSL1 = long-chain-fatty-acid-CoA ligase 1, ETFDH = electron transferring-flavoprotein dehydrogenase, SCD = stearoyl-CoA desaturase

3T3L1

Cell type: Mouse, embryonic, fibroblast cell line

Source: 3T3L1 a continuous subclone of 3T3 (Swiss albino) parental line developed through clonal isolation

Characterization: The cells undergo a pre-adipose to adipose like conversion as they progress from a rapidly dividing to a confluent and contact inhibited state. High serum content in the medium enhances fat accumulation (Green and Meuth 1974). The average differentiation rate is 80-95%.

Huh7

Cell type: Human hepatoma cell line

Source: Obtained from a hepatocellular carcinoma from a 57-year old Japanese in 1982

Characterization: Huh7 is an immortal cell line of epithelial-like tumorigenic cells. It usually grows in 2D monolayers. They are well differentiated and are often used for hepatitis research (Nakabayashi et al. 1984).

Plasmids

pGL4.22 (Promega, Mannheim, Germany)

The pGL4.22 Vector encodes the luciferase reporter gene luc2CP (Photinus pyralis) and is designed for high expression and reduced anomalous transcription. The pGL4.22 Vector is a basic vector with no promoter. Therefore, a 752 bp thymidine kinase (TK) promoter was cloned upstream of the firefly luciferase gene into the EcoRV and BglII sites.

pJet (Thermo Scientific, Dreieich, Germany)

pJET1.2/blunt is a linearized cloning vector, which accepts inserts from 6 bp to 10 kb. The vector contains a lethal gene which is disrupted by ligation of a DNA insert into the cloning site. As a result, only cells with recombinant plasmids are able to propagate.

pENTR1B-U6-Puro (generous gift from Sirion Biotech, Martinsried, Germany)

pENTR1B-U6-Puro is an entry vector designed to clone DNA sequences using restriction endonucleases and ligase to create an entry clone. The shRNA-sequences are cloned into the entry vector pENTR1B. The shRNA expression cassettes are cloned via LR recombination in the destination vector pTER-EGFP-PL-Dest to create an expression clone.

pTER-EGFP-PL-Dest (generous gift from Sirion Biotech, Martinsried, Germany)

The use of the pTER-EGFP-PL-Dest vector enables the specific inhibition of gene expression and shRNA-sequences can be tested on their functionality in cell culture experiments.

pLVI-shmir-Puro (generous gift from Sirion Biotech, Martinsried, Germany)

pLVI-shmir-Puro is a modified pTRIPZ plasmid (Thermo Scientific, Dreieich, Germany). The pTRIPZ vector is engineered to be tet-On and thereby enables induced expression of a shRNA in the presence of doxycycline.

1.3 Methods

1.3.1 Cell culture methods

Cultivation of EBV-LCLs

EBV-LCLs were cultured in uncoated 75 cm^2 flasks (BD Falcon TM, Greiner Bio-One, Kremsmünster, Austria) at 37°C and 5% CO_2. Every 2-4 days they were passaged (about 1:10) according to their growth celerity. Attention was paid that cell concentrations never exceeded 1.2 x 10^6 cells/ml. For cryopreservation cells were counted and centrifuged with 500 g for 10 min at RT (Centrifuge 5810, Eppendorf, Hamburg, Germany). The supernatant was discarded and cells were resuspended in ice cold freezing medium (Table 1.3-1) resulting in 3 million cells/ml medium. One ml was transferred in each cryogenic tube (Roth GmbH, Karlsruhe, Germany). The tubes were embedded for 3 days in a cryogenic freezing container (Nalgene, Rochester, NY, USA) containing isopropanol and were slowly cooled down to -80°C and subsequently stored in liquid nitrogen.

Table 1.3-1: Media for EBV-LCLs culture

	Principal component	Additives
Proliferation medium	RPMI 1640 (11 mM glucose, 2 mM L-glutamine, 25 mM Hepes) (Gibco, Invitrogen, Karlsruhe, Germany)	10% heat-inactivated (30 min; 56°C) FCS (PAA Laboratories GmbH, Pasching, Austria) 1% penicillin-streptomycin (PAA Laboratories GmbH, Pasching, Austria) 50 µg/ml gentamycine (Roth, Karlsruhe, Germany) 50 µM ß-mercaptoethanol (Sigma-Aldrich, Steinheim, Germany)
Freezing medium	Proliferation medium	10% DMSO (Roth, Karlsruhe, Germany)

Cells were defrosted in a 37°C water bath (Julabo, Seelbach, Germany) and gently suspended in 10 ml proliferation medium (Table 1.3-1). Cells were centrifuged with 500 g for 10 min at RT (Centrifuge 5810, Eppendorf, Hamburg, Germany). The medium was discarded and replaced by fresh proliferation medium in order to remove dimethylsulfoxid (DMSO) (Roth, Karlsruhe, Germany).

Cultivation of Huh7 and 3T3L1 cells

The human hepatoma cell line Huh7 and the mouse fibroblast cell line 3T3L1 were cultured in DMEM medium (Gibco, Invitrogen, Karlsruhe, Germany) containing 10% fetal calf serum

(FCS) (PAA Laboratories GmbH, Pasching, Germany) and 1% penicillin-streptomycin (PAA Laboratories GmbH, Pasching, Germany) at 37°C in a humidified atmosphere at 5% CO_2. Cells were passaged twice a week (in the case of 3T3L1 cells at pre-confluence (80%)). Therefore, cells were washed twice with phosphate buffered saline (PBS) (Biochrome AG, Berlin, Germany) and then detached from the flask by adding 1 ml trypsin (PAA Laboratories GmbH, Pasching, Germany). After 5-10 min incubation at 37°C the reaction was stopped with medium and cells were seeded in the desired density. For cryopreservation cells were counted and centrifuged with 500 g for 10 min at RT (Centrifuge 5810, Eppendorf, Hamburg, Germany). The supernatant was discarded and cells were resuspended in ice cold freezing medium (DMEM medium, 10% FCS, 1% penicillin-streptomycin, 10% DMSO) resulting in 1 million cells/ml medium. One ml was transferred in each cryogenic tube. The tubes were embedded for 3 days in cryogenic freezing containers containing isopropanol and were slowly cooled down to -80°C and subsequently stored in liquid nitrogen.

For transfection experiments Huh7 and 3T3L1 cells were seeded in 48 well culture plates (Falcon, BD Bioscience, NJ, USA) and cultured until 80% confluence. To promote adipose differentiation of 3T3L1 cells, medium was supplemented with 250 nM dexamethasone (Sigma-Aldrich, Steinheim, Germany) and 0.5 mM isobutylmethylxanthine (Serva, Heidelberg, Germany) for the first 3 days and 66 nM insulin (Sigma-Aldrich, Steinheim, Germany) throughout the entire differentiation period. 3T3L1 cells were transfected at day 6 of differentiation.

1.3.2 Adaptation of the mitochondrial metabolite flux assay protocol

Ensenauer et al. developed the *in situ* mitochondrial metabolite flux assay, a specific model to monitor FAO. It is established for human and murine fibroblasts, 3T3L1 cells and primary human adipocytes (Ensenauer et al. 2012). To investigate alterations in FAO associated with rs2014355 the *in situ* mitochondrial metabolite flux assay protocol was adjusted for EBV-LCLs because a multitude of EBV-LCLs was created at the Helmholtz Zentrum München, from genotyped donors of the KORA-cohort, which are available for functional assays. The same EBV-LCL was used for all experiments that served the adaptation of the assay protocol.

Digitonin purification

Commercially available digitonin (purity 50-80%) (Sigma-Aldrich, Steinheim, Germany) was dissolved in 100% ethanol at 75°C followed by precipitation on ice for 20 min and subsequent separation by centrifugation (10 min, 2,000 g, 4°C) (Centrifuge 5424 R, Eppendorf, Hamburg, Germany). This procedure was repeated twice and the resulting digitonin pellets from each purification cycle were collected. Additionally, supernatants from each cycle were combined and heated to 75°C followed by precipitation and subsequent centrifugation. Purified digitonin was then vacuum dried (Concentrator 5301, Eppendorf, Hamburg, Germany) and re-dissolved in 100% DMSO (Roth, Karlsruhe, Germany) at 50 mg/ml (Ensenauer et al. 2012).

Digitonin permeabilization

In situ permeabilization of cell membranes with digitonin decreases incubation and assay turnaround time compared to whole-cell incubation assays (Ensenauer et al. 2012). However, digitonin exhibits cytotoxic properties and, therefore, it is necessary to optimize the permeabilization conditions to avoid damage. Digitonin titration experiments in EBV-LCLs analysing lactate dehydrogenase (LDH) and citrate synthase (CS) activities as markers for the cytosolic and mitochondrial compartments, respectively, were carried out. An optimal concentration would render the plasma membrane permeable whilst keeping the mitochondrial membrane intact.

For digitonin titration experiments, 5 x 10^5 EBV-LCL cells were incubated with 0, 5, 10, 20, 30, 50 µg/ml purified digitonin (Sigma-Aldrich, Steinheim, Germany) in 500 µl acylcarnitine basic-buffer (Table 1.3-2) for 5 min at RT. Cell suspension was centrifuged for 5 min at 500 g. Supernatant was collected for LDH and CS activity measurements.

Table 1.3-2: Acylcarnitine-basic-buffer

ACN-basic-buffer	Concentration
KCl (Roth, Karlsruhe, Germany)	110 mM
EGTA (Calbiochem, San Diego, CA, USA)	1 mM
Hepes (Roth, Karlsruhe, Germany)	10 mM
$MgCl_2$ (Roth, Karlsruhe, Germany)	5 mM
K_3PO_4 (Merck KGaA, Darmstadt, Germany)	10 mM
target pH = 7.2	

LDH activity measurement

LDH activity was measured by adding 12.5 µl of the cell supernatant to 625 µl Tris (80 mM)/NaCl (200 mM)/NADH (0.3 mM) (Applichem GmbH, Darmstadt, Germany; Roth, Karlsruhe, Germany; Omnilab, Bremen, Germany) solution in a plastic cuvette. The reaction was started by adding 125 µl Tris (80 mM)/NaCl (200 mM)/sodium pyruvate (10 mM) (Sigma-Aldrich, Steinheim, Germany) solution. LDH catalyses the conversion of pyruvate to lactate (Figure 1.3-1) with concomitant conversion of NADH in NAD+. NADH concentration decrease was detected spectrophotometrically at 339 nm for 10 min every 30 sec (DU 800 Spectrophotometer, Beckmann Coulter, Krefeld, Germany).

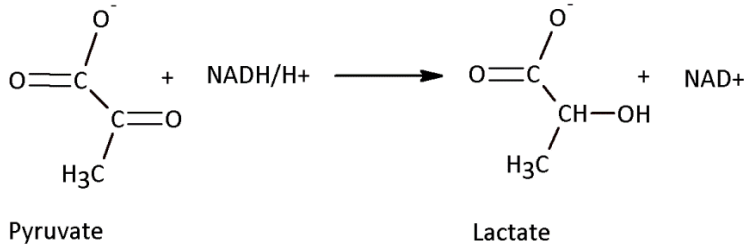

Figure 1.3-1: Chemical reaction of LDH measurement

Samples were measured in duplicates from which mean values were calculated. The LDH activity was calculated according to the following equation:

$$\text{LDH activity}\left[\frac{U}{\text{min}}\right] = \frac{\Delta E \cdot V_{\text{cuvette}} \cdot 1,000}{6.22\ (\text{extinction coefficient}) \cdot 1\ (\text{cuvette diameter}) \cdot 10\,\text{min} \cdot V_{\text{sample}}}$$

Δ E is the measured extinction of the probe

CS activity measurement

CS activity was measured by adding 20 µl 5,5-dithiobis-(2-nitrobenzoic acid) (DTNB) (6 mM dissolved in CS buffer) (Sigma-Aldrich, Steinheim, Germany), 20 µl acetyl-CoA (5 mM dissolved in ddH_2O) (Sigma-Aldrich, Steinheim, Germany), 520 µl CS buffer (1 mM EDTA (Calbiochem, San Diego, CA, USA), 100 mM KCl (Roth, Karlsruhe, Germany), 50 mM Tris/HCl, pH = 8.0) (Applichem GmbH, Darmstadt, Germany) and 20 µl of the sample in a quartz cuvette. After 5 min of incubation at RT, to avoid unspecific reactions, 20 µl oxaloacetic acid (Sigma-Aldrich, Steinheim, Germany) was added to start the reaction. The mitochondrial CS catalyses the condensation reaction of acetyl-CoA, oxaloacetic acid, and water that forms citrate and coenzyme A. The reaction of coenzyme A with DTNB produces thionitrobenzoic

acid (TNB) (Figure 1.3-2). The yellow product TNB is the absorbing substance with an intense absorption at 412 nm. The absorption was spectrophotometrically measured at 412 nm for 5 min every 30 sec to gather linear substrate formation (DU 800 Spectrophotometer, Beckmann Coulter, Krefeld, Germany).

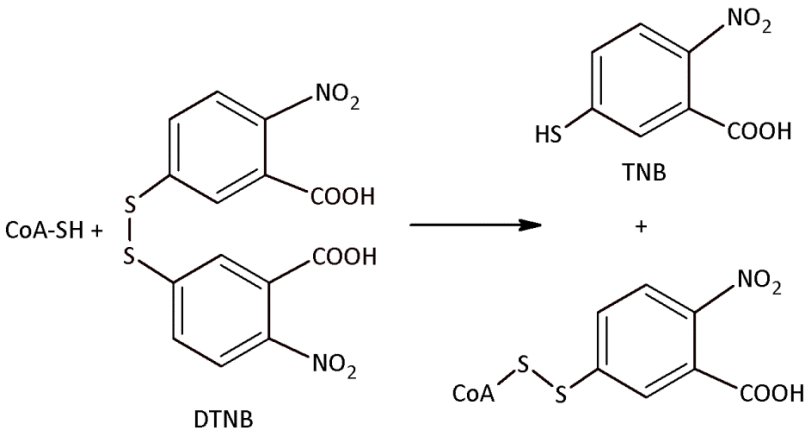

Figure 1.3-2: Chemical reaction of CS measurement
TNB = thionitrobenzoic acid; DTNB = 5,5-dithiobis-(2-nitrobenzoic acid)

Samples were measured in duplicates and mean values were calculated. The CS activity was calculated according to the following equation:

$$\frac{\text{CS activity}}{5 \times 10^5}\,[\text{kat}] = \frac{\text{mean slope} \cdot V_{\text{cuvette}}}{13{,}600\ \text{ml/mmol (extinction coefficient)} \cdot V_{\text{sample}}} \cdot 16.67 \frac{\text{kat}}{\text{U}} \cdot 500\ \mu\text{l}$$

Selection of oleic acid concentration and incubation time

To maximize the assay efficiency incubation buffers with various concentrations of oleic acid (0, 25, 50, 100, 500 µM) were prepared (preparation of the incubation buffer see section 1.3.3). 5 x 10^5 EBV-LCL cells were treated with various incubation buffers in triplicates. After 120 min incubation at 37°C the protocol proceeds as in 1.3.3. The experiment was performed twice.

In order to find the most efficient incubation time for acylcarnitine abundance, an incubation buffer with 100 µM oleic acid was used and the cells were incubated for various time periods (40, 80, 120, 160 min). The assay procedure is described in 1.3.3 and was performed three times.

1.3.3 *In situ* mitochondrial metabolite flux assay

As described in paragraph 1.3.2, the mitochondrial metabolite flux assay is a highly sensitive method to quantify intermediates of FAO. Here it was used to compare the FAO performance of EBV-LCLs with the TT genotype in the locus rs2014355 versus the minor CC genotype and the heterozygous TC genotype.

Incubation with oleic acid

Oleic acid (Sigma-Aldrich, Steinheim, Germany) stock solution was prepared in chloroform. For each experiment, oleic acid stock solution (200 mM) was transferred into a glass tube followed by evaporation to dryness under a stream of nitrogen for 20 min. The dried oleic acid was resuspended in acylcarnitine-basic-buffer (Table 1.3-2) containing fatty acid-free bovine serum albumin (BSA) (Sigma-Aldrich, Steinheim, Germany) in a molar ratio of 5:1 of the dried fatty acid bound to BSA (200 µM fatty acid, BSA 0.04 mM). The oleic acid substrate was then incubated at 37°C in a water bath (GFL 1083, Hilab, Düsseldorf, Germany) for 30 min and subsequently subjected to sonification 3 times for 10 sec (amplitude 10%) (Sonifer Sonopuls, Bandelin electronics, Berlin, Germany). Appropriate cofactors were added to the fatty acid substrate (1 mM ADP, 5 mM ATP, 0.1 mM CoA, 0.2 mg/ml cytochrome *c*, and 0.4 mM L-carnitine (all four: Sigma-Aldrich, Steinheim, Germany)) considering potential losses through membrane permeabilization. The final concentration of oleic acid was 100 µM. In parallel, a control incubation medium consisting of acylcarnitine-basic-buffer (Table 1.3-2) containing all cofactors including 0.4 mM L-carnitine and 0.04 mM fatty acid free BSA was prepared.

EBV-LCLs were counted using an automated cell counter (Countess, Invitrogen, Karlsruhe, Germany). After permeabilization of 5 x 10^5 cells/cell line (triplicates) with digitonin (10 µg/ml) (Sigma-Aldrich, Steinheim, Germany) for five minutes, EBV-LCLs were treated with incubation buffer for 160 min in a water bath at 37°C (GFL 1083, Hilab, Düsseldorf, Germany) while shaking gently. Cells treated with control incubation buffer without oleic acid served as background control.

Extraction of acylcarnitines

Following incubation, both incubation medium and cell lysate were combined and subjected to the extraction of acylcarnitines. EBV-LCLs were centrifuged, 500 g, 5 min (Centrifuge 5415, Eppendorf, Hamburg, Germany) and incubation medium (500 µl) was transferred into a 10 ml polypropylene tube (Sarstedt, Nürmbrecht, Germany). Cell pellets were precipitated in 2.8 ml acetonitrile (Merck KGaA, Darmstadt, Germany)/methanol (Sigma-Aldrich, Steinheim, Germany) (4:1, v/v) and the cell lysate was then transferred into the same sample tube, resulting in a volume ratio of 6.5:1 acetonitrile/methanol to sample). 40 µl internal standard mixture containing 300 pmol D_3-C0, 120 pmol D_3-C4, 60 pmol D_3-C8, and 120 pmol D_3-C16 (Laboratory Becker, Olgemöller and Colleagues, München, Germany) was added to each sample. After vigorous mixing on an orbital shaker (Certomat® BS-1, Sartorius AG, Melsungen, Germany) at 160 rpm for 30 min at room temperature to extract the acylcarnitines, samples were centrifuged at 3,000 g for 20 min (Centrifuge 5810, Eppendorf, Hamburg, Germany).

Purification of acylcarnitines with silica gel columns

One ml of cell-free supernatant of each sample was added to solid-phase extraction columns (Bond Elut® SI-columns, Varian GmbH, Darmstadt, Germany) which were equilibrated with 1 ml of 100% methanol (Sigma-Aldrich, Steinheim, Germany) prior to use. Bound acylcarnitines were stepwise eluted with 2 x 1 ml methanol (100%) and 2 x 1 ml methanol/H_2O 1:2. The volume of 4 ml eluate was collected (polypropylene tubes, Sarstedt, Nürmbrecht, Germany) and vacuum concentrated (ILMVAC Speed-Vac, Ilmvac GmbH, Ilmenau, Germany) before being subjected to derivatization and quantification.

ESI-MS/MS analysis

The purified acylcarnitines were quantified by electron spray ionization (ESI)-MS/MS (Laboratory Becker, Olgemöller and Colleagues, München, Germany). A panel of 43 acylcarnitines was simultaneously measured (Appendix Table A.1). Each measured metabolite was checked against limits of detection defined by Ensenauer et al. (Ensenauer et al. 2012).

Normalization of the acylcarnitine concentrations

To adjust for differences in number and activity of mitochondria in the different EBV-LCLs that might create differences in the FAO, MS/MS data in pmol were expressed relative to CS activity (nkat/5 x 10^5) (compare 1.3.2), resulting in normalized amounts of each metabolite (mmol/kat).

1.3.4 Prediction and verification of *cis*-regulatory variants

Definition of LD block

To identify SNPs with *cis*-regulatory functions in strong LD (r^2 > 0.6) with the GWASs identified lead SNP (rs2014355) a 500-kb genomic region, with the SNP at the central position, based on 1,000 Genome Phase 1 (HaploReg, Broad Institute, Ward and Kellis 2011) was defined. The resulting SNP set was analysed with PMCA (Claussnitzer M., personal communication). The PMCA determines the complexity of TFBS modules as a predictor of SNP-adjacent functional *cis*-regulatory regions. In the end, each SNP of an analysed LD block is classified as a complex region (predicted *cis*-regulatory) or a non-complex region SNP according to the modular complexity of its adjacent region. Four SNPs defined as complex region SNP and the lead SNP (rs2014355) defined as non-complex region SNP were used for luciferase expression experiments.

Luciferase expression construct

To characterise the SNP-adjacent regions for allele-specific transcriptional activity, genomic sequences surrounding the respective SNPs were cloned into a basal pGL4.22 promoter vector. For the promoter construct, a 752 bp thymidine kinase (TK) promoter was cloned upstream of the firefly luciferase gene into the EcoRV and BglII sites of the pGL4.22 firefly luciferase reporter vector (Promega, Mannheim, Germany). SNP regions were extracted from human genome build (NCBI Build 37, hg19). SNP regions were commercially synthesised as double-stranded oligonucleotides (Table 1.3-3). Complementary oligonucleotides were annealed and subcloned upstream of the TK promoter into the KpnI and SacI sites of the pGL4.22-TK vector. The orientation and integrity of each luciferase vector was confirmed by sequencing (MWG Biotech, München, Germany).

Table 1.3-3: Overview of SNP regions cloned in luciferase expression constructs
The respective SNP is shown in bold. r^2 is the correlation coefficient of the frequencies (describes proportion of observations in which the SNP occurs in combination with rs2014355 (European population, Genome 1,000 Phase 1)). MAF = minor allele frequency.

SNP	r^2	MAF	oligo sequence forward (5'-> 3')	oligo sequence reverse (5'-> 3')
			CAGCTTTGGGACCCTCATCTT**T**GGAGCCC	CACCCTATGACTCGGGCTCC**A**AAGATG
rs2014355T			GAGTCATAGGGTGAGCT	AGGGTCCCAAAGCTGGTAC
			CAGCTTTGGGACCCTCATCTT**C**GGAGCCC	CACCCTATGACTCGGGCTCC**G**AAGATG
rs2014355C	1	0.26	GAGTCATAGGGTGAGCT	AGGGTCCCAAAGCTGGTAC
			CGAGCATGGAGGTCCTGGAGC**G**GGCTT	CTGGAGAGCAGAGGCAAGCC**C**GCTCCA
rs35599677G			GCCTCTGCTCTCCAGAGCT	GGACCTCCATGCTCGGTAC
			CGAGCATGGAGGTCCTGGAGC**A**GGCTTG	CTGGAGAGCAGAGGCAAGCC**T**GCTCCA
rs35599677A	0.88	0.29	CCTCTGCTCTCCAGAGCT	GGACCTCCATGCTCGGTAC
			CGCAGGAGAGGGAAGAGACGA**G**ACAG	CGTTTCTCCTTTTTGACTGT**C**TCGTCTCTT
rs3999408G			TCAAAAAGGAGAAACGAGCT	CCCTCTCCTGCGGTAC
			CGCAGGAGAGGGAAGAGACGA**A**ACAG	CGTTTCTCCTTTTTGACTGT**T**TCGTCTCTT
rs3999408A	0.93	0.25	TCAAAAAGGAGAAACGAGCT	CCCTCTCCTGCGGTAC
			CCAGGCTTCTGCTCATTCTGG**C**TTTCCCA	CGAACCACAAGAGTGGGAAA**G**CCAGA
rs10431386C			CTCTTGTGGTTCGAGCT	ATGAGCAGAAGCCTGGGTAC
			CCAGGCTTCTGCTCATTCTGG**T**TTTCCCA	CGAACCACAAGAGTGGGAAA**A**CCAGA
rs10431386T	0.65	0.31	CTCTTGTGGTTCGAGCT	ATGAGCAGAAGCCTGGGTAC
			CCTTGTTGCAACATTGCGCTT**A**CCAGGTT	CGCCTTTCTCAGGAACCTGG**T**AAGCGCA
rs10431384A			CCTGAGAAAGGCGAGCT	ATGTTGCAACAAGGGTAC
			CCTTGTTGCAACATTGCGCTT**G**CCAGGTT	CGCCTTTCTCAGGAACCTGG**C**AAGCGC
rs10431384G	0.64	0.31	CCTGAGAAAGGCGAGCT	AATGTTGCAACAAGGGTAC

Luciferase expression assays

Huh7 cells (48 well plate) were transfected one day after plating with approximately 90% confluence, 3T3L1 cells (48 well plate) were transfected at day six after induction of differentiation with approximately 80% confluence. Huh7 were transfected with 0.2 µg of the respective firefly luciferase reporter vector and 0.4 µl Lipofectamine 2,000 transfection reagent (Invitrogen, Karlsruhe, Germany), and differentiated 3T3L1 adipocytes were transfected with 0.3 µg of the respective pGL4.22-TK construct and 0.4 µl Lipofectamine reagent. The firefly luciferase constructs were co-transfected with 0.04 µg for Huh7 cells and 0.05 µg for 3T3L1 cells of the ubiquitin promoter-driven renilla luciferase reporter vector pRL-CMV (Laumen et al. 2009) to normalise for transfection efficiency. Twenty hours after transfection, the cells were washed with PBS (Biochrome AG, Berlin, Germany) and lysed in 1x passive lysis buffer (Promega, Madison, WI, USA) on a rocking platform (Titramax 100, Heidolph Instruments, Schwabach, Germany) for 30 min at room temperature. Firefly and renilla luciferase (substrates D-luciferin and coelenterazine from PJK, Kleinblittersdorf, Germany) activity were measured using a Luminoscan Ascent microplate luminometer (Thermo, Braunschweig, Germany) in Huh7 cell lysate and a Sirius tube luminometer

(Berthold, Pforzheim, Germany) in 3T3L1 cell lysates. The ratios of firefly luciferase expression to renilla luciferase expression were calculated and normalised to the TK promoter control vector. Each construct was analysed in 5-7 independent experiments for each cell line.

1.3.5 Gene expression analysis

Isolation and quantification of total RNA

Total RNA from EBV-LCLs, primary human preadipocytes and Huh7 was isolated using the isolation kit NucleoSpin RNA II (Macherey-Nagel, Düren, Germany) according to the manufacturer's protocol. RNA concentrations of all samples were measured by absorption at 260 nm using the NanoQuant plate (Tecan, Männedorf, Switzerland). The absence of protein or solvent contaminations were ensured by the 260/280 ratio (2.1 - 1.8).

cDNA synthesis

The reverse transcription of 300 ng (V = 10 µl) EBV-LCL RNA, 500 ng (V = 10 µl) primary preadipocyte RNA, and 1 µg (V = 10 µl) Huh7 RNA into cDNA for each sample was performed using the High capacity cDNA reverse transcription kit (Applied Biosystems, Darmstadt, Germany) according to the manufacturer's protocol. All temperature steps of the reverse transcription took place in the Multicycler® gradient ep from Eppendorf (Hamburg, Germany). The prepared cDNA was stored at -20°C until usage for qPCR.

Quantitative polymerase chain reaction (qPCR)

PCR amplification of the human transcripts was performed using quantitative PCR Maxima SYBR-Green (Fermentas, St. Leon-Rot, Germany) in duplicate using the Mastercycler® ep realplex from Eppendorf (Hamburg, Germany). The 10 µl PCR included 2 µl template cDNA, 5 µl Maxima SYBR PCR Master Mix (Rox adjusted), 0.3 µM forward and 0.3 µM reverse primer (primer sequences: Table 1.3-4). The reactions were incubated at 95°C for 10 min, followed by 40 cycles of 15 sec at 95°C and 40 sec at 61°C. A melting curve from 65°C to 95°C with an increment of 0.5°C/step was performed after each run to confirm primer specificity. The Ct values of candidate genes were normalized by reference genes using the ΔΔCt method:

RGI (reference gene index): arithmetic mean of Ct values from all reference genes
Fold-difference: ΔCt = Ct (target gene) - Ct (RGI)
Fold change normalization: ΔΔCt = ΔCt intervention - ΔCt reference sample
Relative fold change: $2^{(-\Delta\Delta Ct)}$

Table 1.3-4: Primer pairs used for qPCR analysis in EBV-LCLs, preadipocytes and Huh7
Primers were purchased at MWG Biotech (München, Germany).

Primer ID		Sequence (5'-> 3')	Exon	Tm[°C]	Product size (bp)
hACADS	for	AGGGCCTGGCGGCAGTTACA	2	60	271
	rev	CGCAGCCACGGCTGATCTCC	3		
PPIA	for	GGATTTGGTTATAAGGGTTCC	3	60	226
	rev	CAGTCTTGGCAGTGCAGAT	4		
GAPDH	for	GATCATCAGCAATGCCTCCTGC	5	62	109
	rev	ACAGTCTTCTGGGTGGCAGTGA	5		
YWHAZ	for	GCAACCAACACATCCTATCAGAC	8	60	244
	rev	TTCTCCTGCTTCAGCTTCGTC	10		

GAPDH = glyceraldehyde 3-phosphate dehydrogenase, PPIA = peptidyl-prolyl cis-trans isomerase A , YWHAZ = tyrosine 3-monooxygenase/tryptophan 5-monooxygenase activation protein, zeta polypeptide

1.3.6 Protein expression analysis

SDS-PAGE

Sodium dodecyl sulfate-polyacrylamide gel electrophoresis (SDS-PAGE) is a method for separation of protein mixtures by molecular mass under denaturating conditions. Glass plates with polymerized gel (Table 1.3-5) were placed in an electrophoresis chamber (Biometra, Göttingen, Germany) filled with 1x running buffer (10x running buffer: 144 g glycine, 30 g Tris, 10 g SDS, add H_2O to 1 L). Protein content of cells lysed in RIPA buffer (50 mM Tris-HCl (pH=8), 150 mM NaCl, 0.2% SDS, 1% NP-40, 0.5% Deoxycholat) with freshly added PMSF (1mM) and protease- and phosphatase inhibitors (amount according to the manufacturer's protocol) (Roche Diagnostics, Manheim, Germany), was measured by bicinchoninic acid (BCA) assay (Pierce, Thermo Scientific, Dreieich, Germany) according to the manufacturer's protocol. 5x Lämmli buffer (0.375 M TrisCl, pH 6.8, 1.6% SDS, 15.6% glycerol, 1 mM DTT, 0.0125% bromophenol blue) in the ratio protein lysate: Lämmli buffer = 4:1 was added and heated at 95°C for 10 minutes. 5-15 µg protein was loaded per lane. The gel was run in the electrophoresis chamber at 30 mA (120 V) approximately 1.5h until the blue band ran out of the gel.

Table 1.3-5: Reagents for resolving and stacking gel

	Resolving gel (12.5%)	Stacking gel (5%)
30% PAA/BisAA	2.5 ml	330 µl
1.5 M Tris/HCl pH 8.8	1.5 ml	500 µl
10% SDS	60 µl	20 µl
Aqua pur	3 ml	1.2 ml
Temed	2 µl	2 µl
10% (w/v) APS	62 µl	15 µl

PAA = polyacrylamid, BisAA = bisacrylamid, SDS = sodium dodecyl sulfate, Temed = tetramethylethylendiamin, APS = amonium persulfate

Western blot

Proteins were blotted onto nitrocellulose membranes (Whatman, Dassl, Germany) by a semi dry blotting apparatus (Biometra, Göttingen, Germany) using semi-dry blotting buffer (20% MeOH, 5 M glycine, 250 mM Tris base) with 200 mA for 45 min. After blotting, the membranes were blocked for 1h at RT in 3% BSA (Sigma-Aldrich, Steinheim, Germany) solved in TBST (20 mM Tris pH 7.6, 140 mM NaCl, 0.1% Tween 20), to block unspecific binding sites The blots were incubated over night at 4°C with primary antibodies diluted in 3% BSA. Following 4 wash steps in TBST (7 min each) and incubation for 1h at RT with a fluorochrome-conjugated secondary antibody (LI-COR Bioscience, Bad Homburg, Germany) in blocking reagent (1:15,000), infrared fluorescence signals were detected using Odyssey infrared imager (LI-COR Bioscience, Bad Homburg, Germany).

Quantification of band intensities

The intensity of each fluorescently labeled protein band was quantified using the Odyssey Application Software (LI-COR, Bioscience, Bad Homburg, Germany). Background fluorescence was assessed and corrected using Odyssey Software which determined median pixel densities above and below each protein band and normalized these bands of interest accordingly.

1.3.7 Generation of a lentiviral tet-On system and stable integration in Huh7

1.3.7.1 Transformation of competent E. coli

50 µl E. coli DH5α competent cells were thawed on ice, carefully mixed with 2 µl of the ligation mixture, and kept on ice for 20 min. The heat-shock was conducted at 42°C (Thermomixer comfort, Eppendorf, Hamburg, Germany) for 90 sec; afterwards the reactions

were incubated on ice for 10 min. Then, 1 ml antibiotic-free LB medium (Applichem, Darmstadt, Germany) was added, and the suspension was incubated at 37°C for 1h on a shaking platform (180 rpm) (Certomat® BS-1, Sartorius AG, Melsungen, Germany). 100 µl were streaked out on ampicillin (100 mg/L) (Sigma-Aldrich, Steinheim, Germany) containing agar plates, and the plates were incubated overnight at 37°C. On the next day, they were checked for the presence of colonies.

1.3.7.2 Cloning of validation vector (pTER-ACADS-EGFP-PL-Dest)

The use of the pTER-EGFP-PL-Dest (Sirion Biotech, Martinsried, Germany) allows a specific inhibition of gene expression and shRNA-sequences can be tested on their functionality in cell culture experiments.

Preparation of the ACADS-DNA insert

The target DNA (ACADS-clone ordered at ImaGenes, Berlin, Germany) was generated by amplification via PCR from the template DNA with designed primers. The forward primer has an XbaI restriction site (5'-GTCTAGAAGCCTGGGACTGTGTCTGT-3') and the reverse primer (5'-GAAAAGACAGACCCCACCAA-3') was phosphorylated prior to PCR (Table 1.3-6).

Table 1.3-6: Reaction mixture for primer phosphorylation

Component	Concentration	Volume [µl]
Reverse primer	100 µM	10
T4 PNK Buffer	10 x	2
T4 PNK	2.5 mM	1
ATP	10 mM	2
H_20		5

ATP = adenosine triphosphate, PNK = polynucleotide kinase

The reaction (Table 1.3-6) was incubated at 37°C for 30 min. The 20 µl PCR included 0.4 µl template cDNA (8 ng), 4 µl Phusion HF buffer (5x), 2.5 mM dNTPs, 10 µM forward and 10 µM reverse primer and 2 U/µl Phusion polymerase (FINNZYMES, Espoo, Finland). The reactions were incubated at 98°C for 1 min, followed by 20 cycles of 15 sec at 98°C, 20 sec at 60°C and 150 sec at 72°C. All temperature steps took place in the Multicycler® gradient ep from Eppendorf (Hamburg, Germany).

After amplification the ACADS target DNA was inserted in a pJet1.2 linearized cloning vector (Thermo Scientific, Dreieich, Germany).

Table 1.3-7: Ligation reaction of PCR-product ACADS and pJet

Component	Concentration	Volume [µl]
Oligonucleotid for	50 µM	11
Oligonucleotid rev	50 µM	11
Ligase buffer	10x	2.5
T4 PNK	4U/ml	0.5
ATP	10 mM	2

ATP = adenosine triphosphate, PNK = polynucleotide kinase

The ligation mixture (Table 1.3-7) was incubated at 22°C for 30 min and transformed in E.coli according to paragraph 1.3.7.1. Five clones were picked and grown in 5 ml LB-medium containing 100 mg/ml ampicillin overnight on a shaking platform (180 rpm) at 37°C (Certomat® BS-1, Sartorius AG, Melsungen, Germany).

The orientation of the insert in the pJet vector (Thermo Scientific, Dreieich, Germany) was checked by XbaI (Fermentas, St. Leon-Rot, Germany) digest and subsequent agarose gel electrophoresis using 1% agarose gel to find the right restriction sites for excision of the ACADS target gene.

A vector with the adequate orientation was cut with the restriction enzyme XhoI (20 µl reaction containing 1 µg vector DNA, 1x fast digest buffer and 1 µl XhoI FastDigest enzyme) (Fermentas, St. Leon-Rot, Germany) and incubated at 37°C for 5 min. The enzyme was inactivated by incubation for 5 min at 80°C. The big fragment of the DNA-Polymerase I (Klenow) was used to fill in the 5’ overhang and generate a blunt end. In the Klenow reaction the XhoI reaction was mixed with 0.5 µl dNTP (2 mM) and 0.5 µl Klenow-enzyme (10 U/µl) (Fermentas, St. Leon-Rot, Germany). The reaction mixture was incubated at 37°C for 5 min. Afterwards the reaction was stopped by heating at 75°C for 10 min. Subsequently, 1 µl XbaI (Fermentas, St. Leon-Rot, Germany) was added to the Klenow reaction and incubated at 37°C for 5 min to cut the other end of the ACADS insert.

DNA was loaded on a 1% agarose gel. After gel electrophoresis (100 V; 45 min), (Biometra, Göttingen, Germany) the desired band was excised under UV illumination. Isolation of DNA from the agarose fragment was accomplished by the SV Clean-up kit (Promega, Mannheim, Germany) according to the manufacturer’s protocol. DNA concentration of samples was measured by absorption at 260 nm using the NanoQuant plate (Tecan, Männedorf,

Switzerland). The absence of protein or solvent contaminations were ensured by the 260/280 ratio.

Cloning of the ACADS cDNA insert into pTER-EGFP-PL-Dest

The pTER-EGFP-PL-Dest (Sirion Biotech, Martinsried, Germany) was double-digested with XbaI and PmeI (Fermentas, St. Leon-Rot, Germany). The 50 µl reaction contained 12 µg pTER-EGFP-PL-Dest, 1x NEB buffer 4 (New England BioLabs, Frankfurt, Germany), 1x BSA (New England BioLabs, Frankfurt, Germany), and 40 U of each restriction enzyme. After incubation at 37°C for 2h alkaline phosphatase (CIP) (New England BioLabs, Frankfurt, Germany) was added, to dephosphorylate the vector to prevent a religation of the blunt-end vector in the ligation reaction, and incubated at 37°C for 30 min. The reaction product was purified by the use of the SV clean-up kit (Promega, Mannheim, Germany) according to the manufacturer's protocol. The digested ACADS target DNA and the digested vector backbone were ligated. Based on 80 ng vector DNA, a 3-fold molecular excess of insert DNA was used for the ligation reaction. The corresponding amount of insert was calculated with the equation:

$$ng_{insert} = ng_{vector} \times length_{insert}\,(bp)/length_{vector}\,(bp) \times (insert/vector)$$

80 ng of vector DNA and the corresponding amount of insert DNA (55 ng) were supplemented with 1 µl 10x concentrated ligation buffer and 0.5 µl T4-ligase (5 U/µl) (Fermentas, St. Leon-Rot, Germany). The reaction mixture was filled up to a total volume of 10 µl with ddH2O. The ligation reaction was incubated overnight at 4°C.

Transformation of One Shot® *ccdB* Survival™ competent *E. coli*

ccdB-encoded toxin, which has been incorporated into plasmid vectors, can be used to positively select for only those cells that have taken up a plasmid containing the inserted gene of interest, screening out those that lack the inserted gene.

To propagate plasmids containing the ccdB-gene before the insert is integrated one Shot® ccdB Survival™ chemically competent E. coli (Invitrogen, Karlsruhe, Germany) are used. For each transformation 20 µl competent ccdB E. coli were thawed on ice. 2.5 µl ligation reaction was added, briefly mixed and incubated for 30 min on ice. Heat shock of the cells was done by placing the tubes for 30 sec in a 42°C heat block. 200 µl of SOC medium (supplied with the bacteria) was added and the transformation reaction was shaken for 1h at 200 rpm on a

shaking platform. The complete sample was plated onto LB-plates with ampicillin and incubated overnight at 37°C.

Digestion control and sequencing of generated vector

Four colonies were picked and inoculated in 10 ml LB-medium with 100 mg/L ampicillin and grown overnight at 37°C with shaking (200 rpm). Mini-scale plasmid DNA was prepared from 4 ml culture using Promega Miniprep System (Promega, Mannheim, Germany) according to the manufacturer's recommendations. The inclusion of the target DNA into the destination vector was verified by a control digest. Therefore, a 20 µl reaction was set up including 2 µl fast digest buffer, 1 µl XbaI and KpnI FastDigest restriction enzymes (Fermentas, St. Leon-Rot, Germany) and 500 ng destination vector. The reaction was incubated at 37°C for 5 min. The expected bands (7484 bp and 1398 bp) were monitored in a 1% agarose gel. The destination vector pTER-ACADS-cDNA-EGFP-PL-Dest showing the expected band pattern was commercially sequenced by the MWG Biotech sequencing service (München, Germany).

Cloning of shRNA cassette into pENTR1B-U6-shRNA

Ten different shRNA-sequences, designed by Sirion Biotech (Martinsried, Germany), (Table 1.3-8) were cloned as double-stranded DNA-oligonucleotides into the Entry vector pENTR1B-U6-shRNA (Sirion Biotech, Martinsried, Germany). The sense and antisense oligonucleotides were phosphorylated by setting up the following master mix (Table 1.3-9).

Table 1.3-8: Sequences of shRNA constructs designed by Sirion Biotech (Martinsried, Germany)

Construct No.	shRNA sequence (5' -> 3')
368_F	5'- ACCGCGGAGTCATCATGAGTGTCAAATCAAGAGTTTGACACTCATGATGACTCCGTTTTTTG -3'
368_R	5'- AATTCAAAAAACGGAGTCATCATGAGTGTCAAACTCTTGATTTGACACTCATGATGACTCCG -3'
561_F	5'- ACCGTGGGTTCTGAATGGAACCAAAATCAAGAGTTTTGGTTCCATTCAGAACCCATTTTTTG -3'
561_R	5'- AATTCAAAAAATGGGTTCTGAATGGAACCAAAACTCTTGATTTTGGTTCCATTCAGAACCCA -3'
179_F	5'- ACCGCGAGAAGGAGTTGTTTCCCATATCAAGAGTATGGGAAACAACTCCTTCTCGTTTTTTG -3'
179_R	5'- AARTCAAAAAACGAGAAGGAGTTGTTTCCCATACTCTTGATATGGGAAACAACTCCTTCTCG -3'
888_F	5'- ACCGCAGGGATGGGCTTCAAGATAGATCAAGAGTCTATCTTGAAGCCCATCCCTGTTTTTTG -3'
888_R	5'- AATTCAAAAAACAGGGATGGGCTTCAAGATAGACTCTTGATCTATCTTGAAGCCCATCCCTG -3'
292_F	5'- ACCGCCAGGTGGATAAGGAACATCTATCAAGAGTAGATGTTCCTTATCCACCTGGTTTTTTG -3'
292_R	5'- AATTCAAAAAACCAGGTGGATAAGGAACATCTACTCTTGATAGATGTTCCTTATCCACCTGG -3'
466_F	5'- ACCGGAGTGTCAACAACTCTCTCTAATCAAGAGTTAGAGAGAGTTGTTGACACTCTTTTTG -3'
466_R	5'- AATTCAAAAAAGAGTGTCAACAACTCTCTCTAACTCTTGATTAGAGAGAGTTGTTGACACTC -3'
1040_F	5'- ACCGCAGGTCATCCAGTTCAAGTTGATCAAGAGTCAACTTGAACTGGATGACCTGTTTTTTG -3'
1040_R	5'- AATTCAAAAAACAGGTCATCCAGTTCAAGTTGACTCTTGATCAACTTGAACTGGATGACCTG -3'
1114_F	5'- ACCGCATGCTGAAGGATAACAAGAAATCAAGAGTTTCTTGTTATCCTTCAGCATGTTTTTTG -3'
1114_R	5'- AATTCAAAAAACATGCTGAAGGATAACAAGAAACTCTTGATTTCTTGTTATCCTTCAGCATG -3'
268_F	5'- ACCGGAAGGAGTTGTTTCCCATTGCATCAAGAGTGCAATGGGAAACAACTCCTTCTTTTTTG -3'
268_R	5'- AATTCAAAAAAGAAGGAGTTGTTTCCCATTGCACTCTTGATGCAATGGGAAACAACTCCTTC -3'
643_F	5'- ACCGCTCATGGGTTCTGAATGGAACATCAAGAGTGTTCCATTCAGAACCCATGAGTTTTTTG -3'
643_R	5'- AATTCAAAAAACTCATGGGTTCTGAATGGAACACTCTTGATGTTCCATTCAGAACCCATGAG -3'

The reaction mixture was incubated at 37°C for 30 min. T4 polynucleotide kinase (T4 PNK) (Fermentas, St. Leon-Rot, Germany) was heat inactivated by incubation at 95°C in a block heater (Thermoleader, UniEquip, Planegg, Germany) for 5 min. Oligonucleotide annealing was achieved by slowly cooling down the reaction from 95°C to RT.

Table 1.3-9: Phosphorylation of single-stranded oligonucleotides

Component	Volume [µl]
2x reaction buffer	5
Non-purified PCR-product (200 ng/µl)	0.5
pJet (50 ng/µl)	0.5
H_20	3.5
T4 DNA ligase (5 U/µl)	0.5

The pENTR1B-U6-shRNA vector was digested with BpiI and EcoRI (Fermentas, St. Leon-Rot, Germany) in a 60 µl reaction containing 12 µg vector, 1x NEB buffer 4, 1x BSA (New England BioLabs, Frankfurt, Germany) and 40 U of each restriction enzyme. After incubation at 37°C of 1.5h CIP was added and incubated at 37°C for 30 min. The reaction product was purified by the use of the SV clean-up kit according to the manufacturer's protocol. The digested pENTR1B-U6-shRNA vector and the prepared shRNA inserts were ligated. Based on 80 ng

vector DNA, a 10-fold molecular excess of insert DNA (20 ng) was used for the ligation reaction. The 10 µl reaction was supplemented with 1 µl 10x concentrated ligation buffer and 0.5 µl T4-ligase (5 U/µl) and H_2O. The ligation reaction was incubated overnight at 4°C. The ligation reaction was chemically transformed into dH5α cells (paragraph 1.3.7.1), except that kanamycin (50 mg/L) (Sigma-Aldrich, Steinheim, Germany) was used instead of ampicillin. The generated vectors were prepared by plasmid DNA preparation over columns using Promega Miniprep System (Promega, Mannheim, Germany) according to the manufacturer's recommendations and controlled by commercial sequencing by the MWG Biotech sequencing service.

***In vitro* recombination with clonase enzyme mix**

The shRNA expression cassettes were cloned via LR recombination in the validation vector by using Gateway® LR Clonase® II enzyme mix (Invitrogen, Karlsruhe, Germany) according to the manufacturer's instructions. It catalyses the *in vitro* recombination between an entry clone (shRNA cassettes flanked by attL sites) and the destination vector (pTER-ACADS-cDNA-EGFP-PL-Dest containing attR sites) to generate an expression clone. The recombination reactions were transformed in E. coli DH5α (paragraph 1.3.7.1). One colony was picked and inoculated in 200 ml LB medium with ampicillin and grown overnight with shaking (200 rpm). Maxi-scale plasmid DNA was prepared using Maxiprep System (Promega, Mannheim, Germany).

1.3.7.3 Validation of shRNA knock-down efficacy and generation of LVi-sh-hACAD-puro

pTER-ACADS-cDNA-EGFP-PL-Dest vectors with 11 different integrated shRNAs (including one non-target shRNA control (ACCGCAACAAGATGAAGAGCACCAA)) were transferred to Sirion Biotech (Martinsried, Germany). Transfections of the validation vectors into NIH-3T3L1 were performed and relative quantification of ACADS gene expression was measured by RT-qPCR. The most efficient shRNA (knock-down efficiency of 9% on mRNA level) and a non-target shRNA were each cloned into a lentiviral vector tet-inducible platform. Stable Huh7 cell pools (shACADS Huh7 and shNTC Huh7) were generated by packaging, transduction and stable integration of the tet-On expression vector and subsequent antibiotic selection.

1.3.8 FAO measurement in knock-down shACADS Huh7 cells

ACADS is a major player in the FAO pathway. Therefore, the effect of the induced ACADS knock-downs on mitochondrial acylcarnitine flux and mitochondrial respiration was measured after palmitic acid loading (Figure 1.3-3).

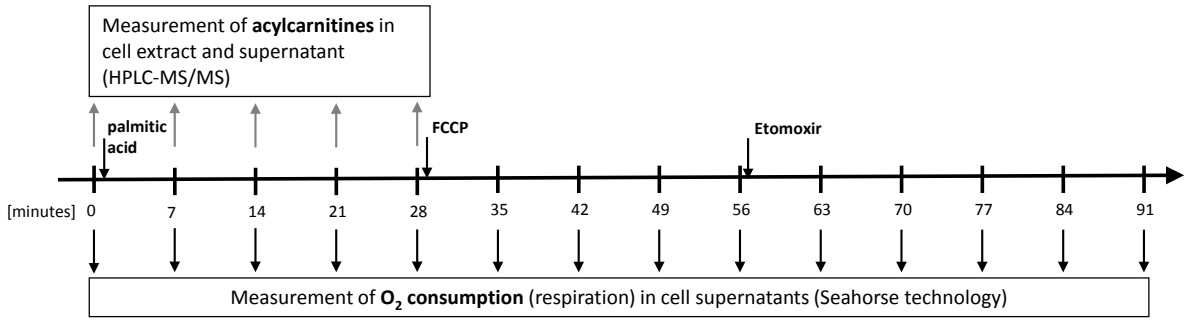

Figure 1.3-3: Experimental setup of time course experiments in shACADS and shNTC Huh7 cells
Experimental set up using shACADS knock-down - and shNTC Huh7 cells. Grey arrows pointing away from time line indicate time points of intra- and extracellular acylcarnitine measurements. Black arrows pointing away from the time line indicate measurement of oxygen consumption rate. Black arrows pointing towards the time line indicate injection of palmitic acid, FCCP and etomoxir. FCCP = trifluorocarbonylcyanide phenylhydrazone, HPLC = high-performance liquid chromatography, MS = mass spectrometry.

1.3.8.1 Doxycycline treatment

Stable Huh7 cells transduced with a tet-inducible shRNA for down-regulation of ACADS (Figure 1.3-4) were incubated with doxycycline (Sigma-Aldrich, Steinheim, Germany), a tetracycline antibiotic, concentrations ranging from 0 - 50 ng/ml for 3 or 5 days. Medium was changed after 3 days. Knock-down efficiency was examined on RNA- (paragraph 1.3.5) and protein level (paragraph 1.3.6).

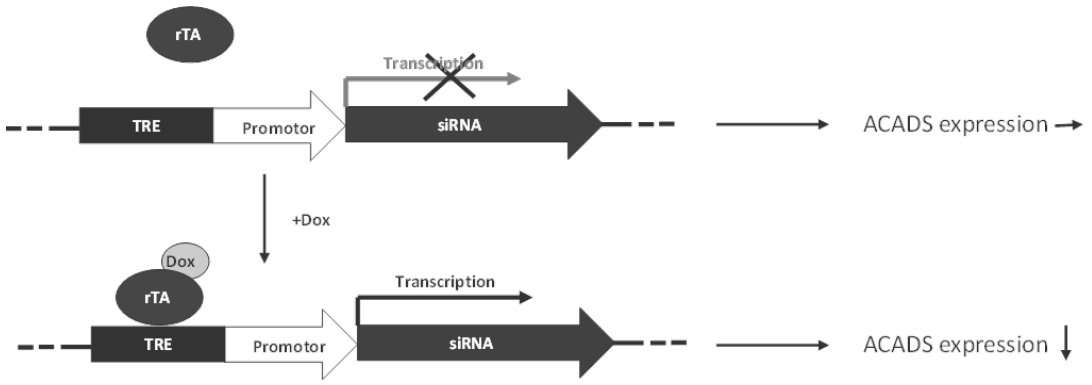

Figure 1.3-4: The tet-On systems allows inducible shRNA expression
Only if doxycycline binds, the transactivator (rTA) undergoes a conformational change allowing it to bind to the operator within the tetracycline response element (TRE). Thus the introduction of doxycycline to the system initiates the transcription of the genetic product, and here the down-regulation of ACADS by shRNA.

1.3.8.2 Preparation of palmitic acid-BSA conjugates

Palmitic acid was conjugated to fatty acid free BSA (molar ratio palmitic acid:BSA = 6:1) when both components were solubilized. Briefly, sodium palmitic acid (Sigma-Aldrich, Steinheim, Germany) was solubilized in 150 mM sodium chloride by heating up to 70°C in a water bath. BSA (Sigma-Aldrich, Steinheim, Germany) was dissolved in 150 mM sodium chloride and warmed up to 37°C with continuous stirring. Solubilized palmitic acid was added to BSA at 37°C with continuous stirring. The pH was adjusted to 7.4 with 1N NaOH. The conjugated palmitic acid-BSA was aliquoted and stored at -20°C.

1.3.8.3 Seahorse measurement

The Seahorse Extracellular Flux Analyzer XF96 (Seahorse Bioscience, North Billerica, MA, USA) measures oxygen consumption rate (OCR) in a 96 well format by sensing changes in oxygen content in a < 3 µl volume above the plated cells with a fluorescence biosensor. The measurements are noninvasive and made in short and repeated intervals. An assay medium composed of 111 mM NaCl, 4.7 mM KCl, 2 mM $MgSO_4$, 1.2 mM Na_2HPO_4, 0.5 mM carnitine (Sigma-Aldrich, Steinheim, Germany) and pH 7.4 was used in the XF analysis.

The cells were seeded in a collagen pre-treated XF96 96 well cell culture microplate (Seahorse Bioscience, North Billerica, MA, USA) at 10,000 cells/well in 80 µl of growth medium (paragraph 1.3.1) supplemented with different doxycycline concentrations and incubated 2 days at 37°C in a humidified atmosphere of 5% CO_2. Prior to assay, growth medium was removed and replaced by 140 µl of assay medium. The cells were preincubated under these conditions for 1h at 37°C in air. The experiments were designed to determine respiration in response to palmitic acid loading after one hour of fasting (Figure 1.3-3). After four consecutive baseline OCR measurements palmitic acid was injected as a BSA-palmitic acid conjugate in a final concentration of 200 µM. To determine maximal respiratory capacity of the cells trifluorocarbonylcyanide phenylhydrazone (FCCP) (Sigma-Aldrich, Steinheim, Germany) was added after 28 min in a final concentration of 100 µM. To ensure that palmitic acid was metabolised in FAO and its products were used for respiration, the inhibitory effect of etomoxir on CPT-I was used which blocks the intake of palmitic acid into the mitochondrial matrix. Etomoxir (Sigma-Aldrich, Steinheim, Germany) was injected after a further 28 minutes at a final concentration of 100 µM. Optimal cell number, drug concentrations and starvation conditions were determined in preliminary experiments (Portius 2012).

1.3.9 Acylcarnitine measurement after palmitic acid loading

Incubation with BSA-palmitic acid

Corresponding to the Seahorse measurement cells treated with doxycycline (paragraph 1.3.8.1) were seeded in 6 well plates at 250,000 cells/well and grown in 37°C, 5% CO_2 incubator. After two days, growth medium was changed to 1.8 ml assay medium. After 1h, 0.2 ml 2 mM palmitic acid-BSA was added. At baseline and after 7, 14, 21 and 28 min 20 µl supernatant was given on a 6 mm filter paper punch. Cells were washed with PBS (Biochrome AG, Berlin, Germany) and harvested by scraping in 300 µl ice-cold 100% methanol. Both, supernatant and cells were shock frozen in liquid nitrogen.

Extraction of acylcarnitines from cells and supernatant

Cells harvested in 300 µl 100% methanol were broken up in an ultrasonic bath for 10 sec (SONOREX SUPER RK 106 Bandelin, Berlin, Germany). After shaking for 20 min at full speed (Thermomixer comfort, Eppendorf, Hamburg, Germany) and 4°C, cell debris was spun down by full speed (10 min, 4°C) centrifugation (Eppendorf 5417 R, Hamburg, Germany). Supernatant was collected and vacuum dried in a speed vac (Savant SPD 111V SpeedVac® Concentrator, Thermo Scientific, Dreieich, Germany) for approximately 2h. Dried pellets were resuspended in 100 µl 5 mM NH_4Ac in LC-MS MeOH, containing internal standard (Chromsystems, Gräfeling, Germany), and filtered through a Millipore filter plate (Billerica, MA, USA) by centrifugation at 1,500 g for 20 min. Flow-through was collected in glass vials (Chromacol, Herts, UK) and stored at -80°C until measurement.

Filter paper punches soaked with 20 µl supernatant were vacuum dried in a speed vac (Savant SPD 111V SpeedVac® Concentrator, Thermo Scientific, Dreieich, Germany) for approximately 45 min. 100 µl 5 mM NH_4Ac in LC-MS MeOH containing internal standard was added to the dried filter paper punches which were shaken for 30 min at full speed and RT (Thermomixer comfort, Eppendorf, Hamburg, Germany). Supernatant was transferred into a Millipore filter plate and filtered by centrifugation at 1,500 g for 20 min. Flow-through was collected in glass vials and stored at -80°C until measurement.

Acylcarnitine measurement in supernatant and cell extracts

Chromatographic separations of metabolites in supernatant and cell extracts were conducted on a ZIC®-HILIC column (150 x 4.6 mm, 5 µm). A QTRAP 5500 (AB Sciex, Framingham, MA, USA) triple-quadrupole tandem mass spectrometer with Turbo V spray electron spray interface was used in positive ion mode for detection. Analyst and MultiQuant software (AB Sciex, Framingham, MA, USA) were used for data acquisition and data processing. Quantification of each acylcarnitine was performed by comparison of its peak area with the appropriate internal standard. Limit of quantification was defined as signal/noise ratio > 9.

1.3.10 Statistical analysis

All data are expressed as mean and standard deviation (SD) except for the time course experiments after palmitic acid loading in shACADS and shNTC Huh7 cells which are expressed as mean ± standard error of the mean (SEM). In the digitonin titration experiment a paired, two-tailed t-test for CS activity and Wilcoxon matched paired test were calculated for LDH activity to compare measurements against baseline. Kruskal-Wallis one-way ANOVA with Dunn's post hoc test was used to compare CS activity of EBV-LCLs by genotype and C4:0-acylcarnitine accumulation in shACADS and shNTC Huh7 cells. Acylcarnitines measured after palmitic acid loading in shACADS and shNTC Huh7 cells were normalized to the protein amount/well. Data was analysed by two-way ANOVA with Bonferroni post hoc test for multiple comparisons against control to study effects of different knock-downs over time. One-way ANOVA with Dunnett's post hoc test for multiple comparisons between groups was used to analyse baseline OCR and protein amounts/per well. The baseline OCR values were normalized to one for baseline and the following values were expressed as fold change of basal level. Statistical analysis was performed with repeated measures one-way ANOVA comparing wild type, intermediate- and maximal knock-down shACADS and control shNTC Huh7 cells. Additionally, two-tailed one sample t-tests were used to compare each value to baseline separately for each knock-down shACADS and shNTC Huh7 cell line. Spearman correlation was calculated between intra- and extracellular acylcarnitine amounts in shACADS and shNTC Huh7 cells. mRNA expression of EBV-LCLs, primary human preadipocytes and Huh7 cells were normalized to the reference gene index (compare paragraph 1.3.5). Fold changes were calculated using the ΔΔ Ct method (compare paragraph 1.3.5). Differences of gene expression in EBV-LCLs, human primary preadipocytes and Huh7

cells were assessed by two-tailed, one sample t-test. Luciferase activity of each single construct was normalized to the TK-promoter construct and allele-dependent differences were calculated using unpaired, two-tailed t-test or Mann Whitney U tests for non-parametric data sets. All statistical analysis described so far was performed using GraphPad Prism5 (GraphPad software, La Jola, USA).

Acylcarnitines measured in the metabolite flux assay were normalized to the corresponding CS activity. Statistical data analysis of the *in situ* metabolite flux assay data was performed using the metaP server at Helmholtz Zentrum München (http://metabolomics.helmholtz-muenchen.de/metap2/) providing automated and standardized data analysis for quantitative metabolomics data (Kastenmüller et al. 2011). For testing the association of metabolite amounts with multiclass categorical phenotypes, the nonparametric Kruskal-Wallis one-way ANOVA was used. P-values were Bonferroni corrected for multiple testing. The linear regression assuming an additive genetic model was calculated using R statistical software by M. Hastreiter and G. Kastenmüller (Helmholtz Zentrum, München).

1.4 Results

1.4.1 Adaptation of the *in situ* mitochondrial metabolite flux assay protocol for EBV-LCLs

1.4.1.1 Optimization of digitonin concentration

The permeabilization of cell membranes with digitonin shortens incubation and assay turnaround time without damaging the organelle environment. To master the balancing act between cell damage by cytotoxic properties of digitonin and sufficient permeabilization of the cell membrane, a variety of digitonin concentrations were tested. LDH and CS activity as markers for the cytosolic and mitochondrial compartments, respectively, were analysed. An optimal concentration would render the plasma membrane permeable while keeping the mitochondrial membrane intact.

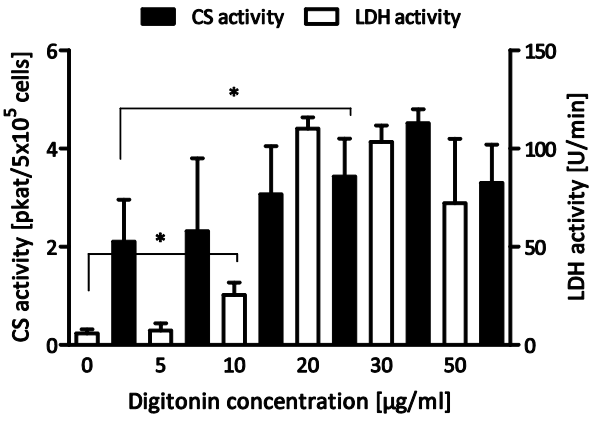

Figure 1.4-1 Permeabilization with digitonin
Increase of LDH- and CS activity in supernatant of one EBV-LCL incubated with several digitonin concentrations for five minutes at RT. The values are means + SD (n = 6, n = 3 for LDH- and CS activity, respectively). * = $p < 0.05$, paired, two-tailed t-test for CS activity and Wilcoxon matched paired test for LDH activity.

LDH activity in the supernatant increased significantly after incubation of the EBV-LCL with 10 µg/ml digitonin for five minutes compared to 0 µg/ml (Figure 1.4-1). By contrast, the CS activity in the supernatant of the EBV-LCLs showed a significant increase after incubation with the next higher concentration (20 µg/ml) compared to 0 µg/ml digitonin (Figure 1.4-1). Consequently, incubation with 10 µg/ml digitonin for five minutes is considered to be optimal to achieve sufficient leakage of the cytosolic enzyme LDH in the supernatant and without disintegration of mitochondrial physiology.

1.4.1.2 Optimization of oleic acid concentration

In order to ensure a saturated state of the mitochondrial metabolite flux assay, oleic acid concentration was titrated. The majority of measured metabolites did not show a consistent effect triggered by various oleic acid concentrations. Solely, C18:1-acylcarnitine levels, C18:2-acylcarnitine levels and C14:1-acylcarnitine levels increased significantly with rising oleic acid concentrations (Figure 1.4-2). However, 100 µM oleic acid seems to initiate the highest acylcarnitine abundance in most cases (Figure 1.4-2). Therefore, for all further experiments an oleic acid concentration of 100 µM was used.

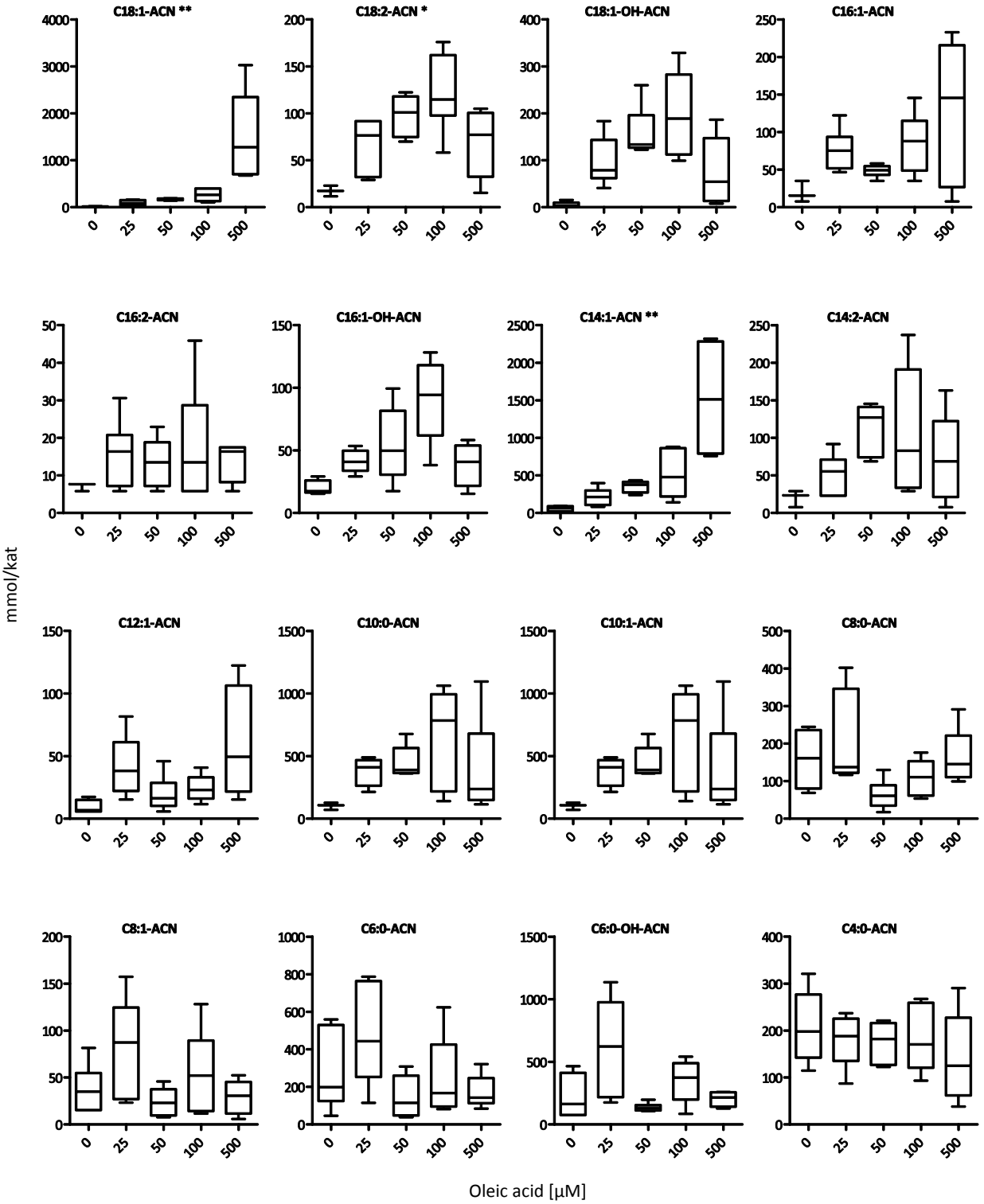

Figure 1.4-2 Titrations of oleic acid concentrations
Depicted are levels of 16 acylcarnitines with various chain lengths extracted from EBV-LCL cells and supernatants after 120 min incubation with different oleic acid concentrations. Acylcarnitine levels were normalized to the CS activity. The results of two independent experiments in triplicates are shown as box plots. Boxes extend from 1st quartile to 3rd quartile, median is indicated as a horizontal line, whiskers are drawn equal to 1.5 times the interquartile distance. * = $p < 0.001$, **= $p < 2.20 \times 10^{-4}$ (Bonferroni corrected significance levels) by Kruskal-Wallis one-way ANOVA. ACN = acylcarnitine.

1.4.1.3 Optimization of incubation time

The optimal incubation time for the elected oleic acid concentration (100 µM; compare Figure 1.4-2) was determined by using various periods of incubation (40 - 160 min). The results are shown as metabolite abundance in [mmol/kat] (Figure 1.4-3). Comparison of the various incubation times revealed that all long-chain acylcarnitine levels (C18:1-C12:1) significantly increased over time. In contrast, short- and middle-chain acylcarnitine levels did not increase significantly over time. Incubation with oleic acid for 160 min showed the highest acylcarnitine yields. Therefore, an incubation time for 160 min was selected for all further assays.

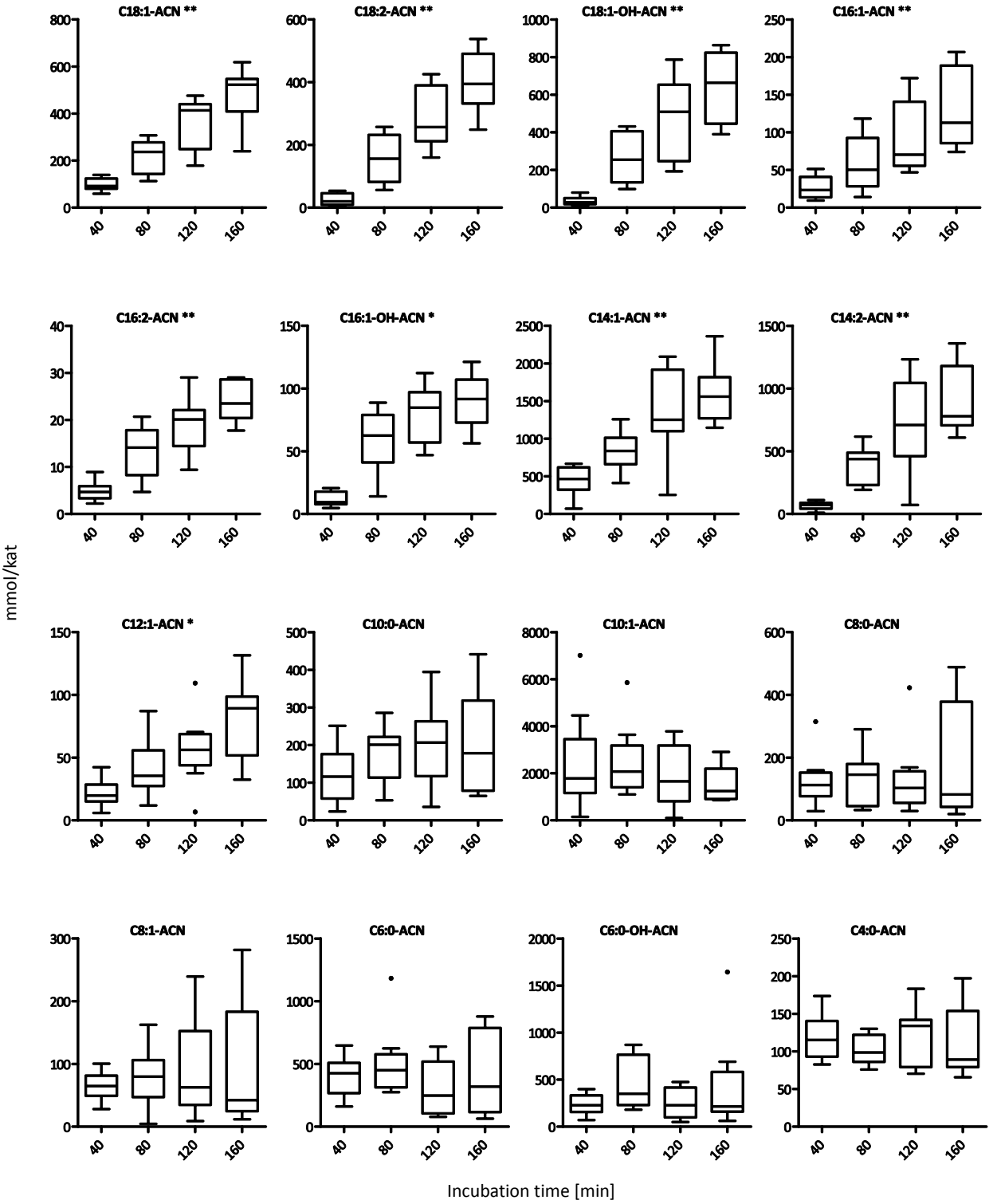

Figure 1.4-3 Determination of optimal incubation time

Depicted are levels of 16 acylcarnitines with various chain lengths extracted from EBV-LCL cells and supernatants after 40, 80, 120, 160 min incubation with 100 µM oleic acid. Acylcarnitine levels were normalized to the CS activity. The results of three independent experiments in triplicates each are shown as box plots. Boxes extend from 1st quartile to 3rd quartile, median is indicated as a horizontal line, whiskers are drawn equal to 1.5 times the interquartile distance. * = $p < 0.001$, **= $p < 2.20 \times 10^{-4}$ (Bonferroni corrected significance levels) by Kruskal-Wallis one-way ANOVA. ACN = acylcarnitine.

1.4.2 Genotype effect on mitochondrial acylcarnitine flux

To compare genotype effects on FAO the mitochondrial metabolite flux assay was applied to EBV-LCLs homozygous for the major T allele, the minor C allele or heterozygous for the variant rs2014355. Therefore, three EBV-LCLs homozygous for the major T allele, five EBV-LCLs homozygous for the minor C allele and two heterozygous EBV-LCLs (Table 1.2-1) were incubated with 100 µM oleic acid for 160 min.

1.4.2.1 CS activity of EBV-LCLs

The measured acylcarnitine levels were normalized to the CS activity to adjust for differences in number and activity of mitochondria in the various EBV-LCLs. This procedure is supported by the observation that CS activity shows a high variability in the different EBV-LCLs (Figure 1.4-4). Of note there was a significant difference in CS activity in heterozygous EBV-LCLs compared to EBV-LCLs homozygous for the minor C allele (Figure 1.4-4). However, a genotype effect is rather unlikely, as no significant difference was found in CS activity of EBV-LCLs homozygous for the major T allele and the minor C allele (Figure 1.4-4). Since number and activity of mitochondria might lead to differences in FAO, comparison of FAO flux in EBV-LCLs with varying genotype requires normalization to the activity levels of CS.

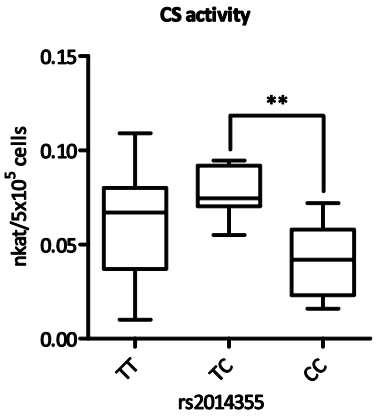

Figure 1.4-4: CS activity of EBV-LCLs depicted by genotype
CS activity in cell lysates of major T allele carriers (n = 3), heterozygous allele carriers (n = 2) and homozygous C allele carriers (n = 5) was measured spectrophotometrically. Boxes extend from 1st quartile to 3rd quartile, median is indicated as a horizontal line, whiskers are drawn equal to 1.5 times the interquartile distance. ** = $p < 0.01$, Kruskal-Wallis one-way ANOVA with Dunn's post hoc test.

1.4.2.2 Increased acylcarnitine levels after substrate loading with oleic acid

Overall, independent of the genotype most acylcarnitines levels derived from oleic acid breakdown were higher if the EBV-LCLs were incubated with oleic acid (Table 1.4-1) compared to cells that were incubated without oleic acid (Table 1.4-2), suggesting that in the case of loading with oleic acid the measured acylcarnitines were derived from oleic acid breakdown.

Table 1.4-1: Genotype effect on acylcarnitine levels after incubation with oleic acid
Depicted are the levels of 16 acylcarnitines after 160 min incubation with 100 µM oleic acid. Acylcarnitine levels were normalized to the CS activity. Values of 3-6 independent experiments per EBV-LCL in triplicates each are expressed as mean ± SD. Adjusted p-value < 0.00113 (Bonferroni corrected significance levels), Kruskal-Wallis one-way ANOVA.

	EBV-LCLs rs2014355 TT		EBV-LCLs rs2014355 TC		EBV-LCLs rs2014355 CC		
	Mean ± SD (mmol/kat)	n	Mean ± SD (mmol/kat)	n	Mean ± SD (mmol/kat)	n	p value *
C18.1	413.20 ± 394.44	38	873.89 ± 762.92	30	566.09 ± 341.03	45	0.0105
C18:2	269.03 ± 268.68	36	507.86 ± 429.70	30	216.85 ± 250.41	40	0.0164
C18:1-OH	384.04 ± 366.63	36	739.71 ± 654.02	30	268.33 ± 352.54	45	0.0034
C16:1	87.85 ± 87.61	36	142.29 ± 132.88	30	88.24 ± 62.53	44	0.0916
C16:2	21.77 ± 16.51	36	32.30 ± 22.14	29	27.21 ± 21.03	37	0.1610
C16:1-OH	93.33 ± 78.22	37	153.90 ± 116.11	30	109.15 ± 112.53	42	0.1418
C14:1	1608.66 ± 1115.73	38	2884.63 ± 4037.22	30	1965.42 ± 1788.94	45	0.9444
C14:2	599.49 ± 459.75	38	1050.36 ± 1381.19	30	485.50 ± 662.64	45	0.0694
C12:1	54.26 ± 43.21	37	53.40 ± 56.14	30	49.92 ± 52.80	39	0.7203
C10:0	244.01 ± 215.38	34	312.24 ± 241.94	30	477.87 ± 450.94	42	0.0275
C8:0	184.28 ± 136.45	38	211.84 ± 174.54	27	326.58 ± 230.07	39	0.0157
C8:1	103.58 ± 77.42	37	101.39 ± 85.68	30	182.28 ± 167.44	42	0.0169
C6:0	488.57 ± 349.31	38	701.04 ± 704.65	29	726.92 ± 469.13	44	0.0479
C4:0	**130.37 ± 65.47**	**38**	**248.14 ± 194.83**	**30**	**268.12 ± 145.00**	**44**	**< 0.0001**
C4:0-OH	141.95 ± 124.17	38	110.12 ± 100.04	30	177.35 ± 100.52	41	0.0041
C2:0	7103.22 ± 4589.46	38	12265.24 ± 8046.96	30	10766.54 ± 10233.22	45	0.0317

EBV-LCL = Epstein-Barr virus transformed lymphoblastoid cell line, SD = Standard deviation, * Kruskal-Wallis one-way ANOVA

In the EBV-LCLs carrying the TT and TC genotype the long-chain acylcarnitine levels were 2 fold to 44 fold higher, whereas middle- and short-chain acylcarnitines were up to 2 fold higher upon incubation with oleic acid compared to incubation without oleic acid. Concerning the EBV-LCLs homozygous for the minor C allele, the difference in long-chain acylcarnitine levels between incubation with oleic acid and without oleic acid was lower (1.2 fold to 13 fold) compared to the other genotypes. However, the higher levels of medium- and short-chain acylcarnitines after incubation with oleic acid compared to incubation without oleic acid were in a similar dimension as in the other genotypes. Of note, the C6:0- and C4:0-OH-acylcarnitine levels were decreased after incubation with oleic acid compared to incubation without oleic acid in the EBV-LCLs homozygous for the minor C allele. To sum up, the incubation with oleic acid for 160 min revealed higher acylcarnitine levels for most of the analysed metabolites (e.g. C16:1-acylcarnitine in rs2014355 TT: 87.85 ± 87.61) compared to incubation without oleic acid (e.g. C16:1-acylcarnitine in rs2014355 TT: 41.93 ± 44.23). Nevertheless, the fact that acylcarnitine levels were also detectable after incubation without oleic acid infers that EBV-LCLs use endogenous fatty acids as fuel in the absence of other energy substrates. Incubation with oleic acid enhances FAO and thereby increases oleic acid break down intermediates.

Table 1.4-2: Genotype effect on acylcarnitine levels after incubation without oleic acid
Depicted are the levels of 16 acylcarnitines after 160 min incubation without oleic acid. Acylcarnitine levels were normalized to the CS activity. Values of 3-6 independent experiments per cell line in triplicates each are expressed as mean ± SD. Adjusted p-value < 0.00113 (Bonferroni corrected significance levels), Kruskal-Wallis test one-way ANOVA.

	EBV-LCLs rs2014355 TT		**EBV-LCLs rs2014355 TC**		**EBV-LCLs rs2014355 CC**		
	Mean ± SD (mmol/kat)	n	Mean ± SD (mmol/kat)	n	Mean ± SD (mmol/kat)	n	p value *
C18.1	29.88 ± 49.54	35	35.53 ± 26.59	29	42.27 ± 53.97	46	0.1402
C18:2	**11.75 ± 15.37**	**31**	**24.44 ± 16.85**	**25**	**29.92 ± 40.20**	**37**	**0.0004**
C18:1-OH	11.67 ± 17.46	35	16.53 ± 12.51	26	20.73 ± 28.72	40	0.0501
C16:1	41.93 ± 44.23	34	58.82 ± 52.21	28	72.10 ± 92.80	38	0.0714
C16:2	5.86 ± 4.16	30	5.33 ± 2.79	26	8.42 ± 9.96	35	0.9883
C16:1-OH	13.89 ± 13.60	32	18.70 ± 12.64	25	32.84 ± 48.24	43	0.0703
C14:1	83.46 ± 107.44	35	101.03 ± 98.87	29	117.42 ± 144.97	46	0.6553
C14:2	25.77 ± 19.60	33	57.78 ± 57.29	23	52.39 ± 67.01	41	0.1272
C12:1	29.86 ± 43.16	32	20.64 ± 16.59	29	27.15 ± 27.27	43	0.9241
C10:0	153.07 ± 99.78	33	269.67 ± 203.80	27	336.41 ± 342.99	40	0.0440
C8:0	131.97 ± 103.91	34	139.93 ± 74.38	27	284.27 ± 296.70	43	0.0194
C8:1	75.23 ± 54.90	35	50.58 ± 31.52	27	102.96 ± 95.16	43	0.0859
C6:0	419.96 ± 277.14	35	554.00 ± 496.62	29	776.71 ± 665.88	47	0.1580
C4:0	110.50 ± 48.23	35	185.49 ± 150.78	27	230.69 ± 230.45	48	0.2130
C4:0-OH	124.86 ± 91.79	33	95.12 ± 56.43	27	215.86 ± 256.59	42	0.0306
C2:0	5282.75 ± 4156.94	35	8110.28 ± 3388.97	29	9002.69 ± 8926.42	48	0.0229

EBV-LCL = Epstein-Barr virus transformed lymphoblastoid cell line, SD = Standard deviation, * Kruskal-Wallis one-way ANOVA

1.4.2.3 Genotype-dependent alteration of acylcarnitine levels

The incubation without oleic acid revealed significant genotype-dependent differences in C18:2-, C18:0-, C16:0-, C6-DC- and C3:0-acylcarnitine levels (Figure 1.4-5a-e). Except for C3:0-acylcarnitine (which lost significance after correction for multiple testing) (Figure 1.4-5e) and C6:0-DC-acylcarnitine (Figure 1.4-5d) the mean acylcarnitine levels were significantly higher in the EBV-LCLs homozygous for the minor C allele compared to the EBV-LCLs homozygous for the major T allele (Figure 1.4-5a, b, c). The heterozygous EBV-LCLs revealed intermediate acylcarnitine levels except for C6:0-DC-acylcarnitine (Figure 1.4-5d). The C18:2-acylcarnitine level was significantly higher in heterozygous EBV-LCLs than in EBV-LCLs homozygous for the major T allele.

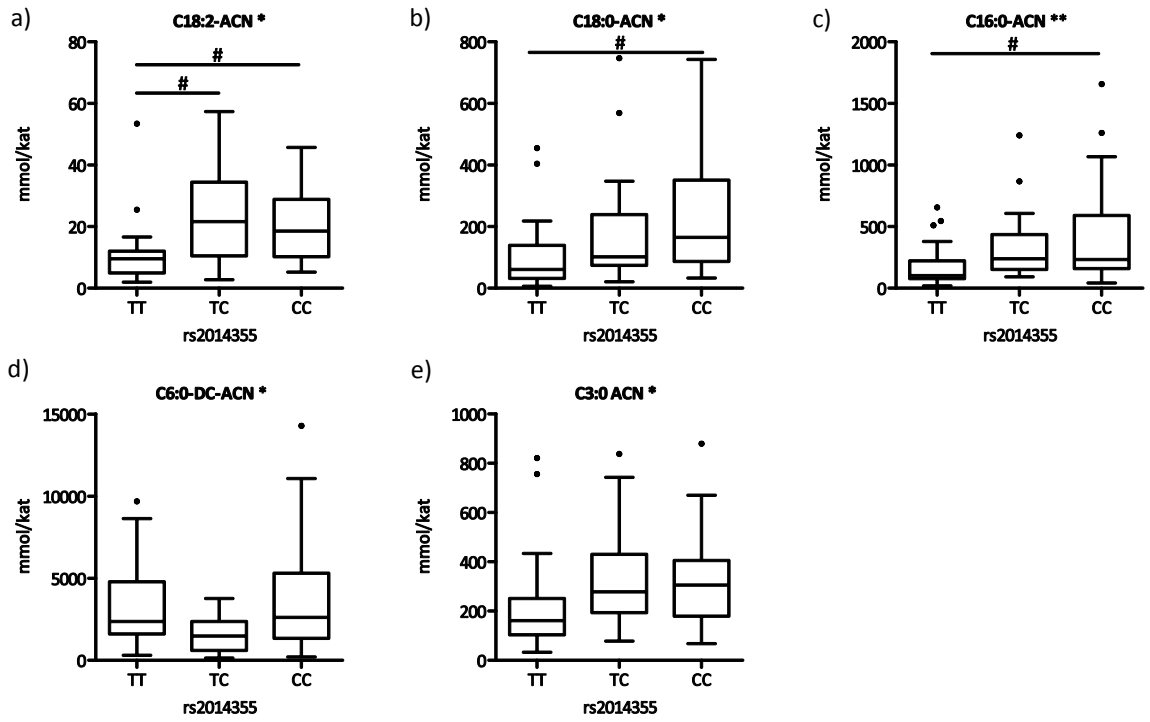

Figure 1.4-5: Acylcarnitines affected by genotype after incubation without oleic acid
Depicted are the levels of five acylcarnitines a) - e) that differed significantly between genotypes after 160 min incubation without oleic acid. Acylcarnitine levels were normalized to the CS activity. Values of 3-6 independent experiments per EBV-LCL in triplicates are shown as box plots (Boxes extend from 1st quartile to 3rd quartile, median is indicated as a horizontal line, whiskers are drawn equal to 1.5 times the interquartile distance. * = $p < 1.13 \times 10^{-3}$, ** = $p < 2.20 \times 10^{-4}$ (Bonferroni corrected significance levels), Kruskal-Wallis one-way ANOVA. # = $p < 1.13 \times 10^{-3}$ (Dunn's post hoc test), ACN = acylcarnitine.

The incubation with oleic acid resulted in significant genotype-dependent differences in C4:0- and C6:0-DC-acylcarnitine levels (Figure 1.4-6a and b). The mean C4:0-acylcarnitine level was significantly higher in the EBV-LCLs homozygous for the minor C allele compared to EBV-LCLs homozygous for the major T allele supporting a genotype-dependent effect (Figure 1.4-6a). Nevertheless, the C6:0-DC-acylcarnitine level was not significantly different between the homozygous genotypes. However, the C6:0-DC-acylcarnitine level in the heterozygous EBV-LCLs were significantly lower than in the EBV-LCLs homozygous for the major T and the minor C allele (Figure 1.4-6b) similar to the results obtained if incubated without oleic acid (Figure 1.4-5d).

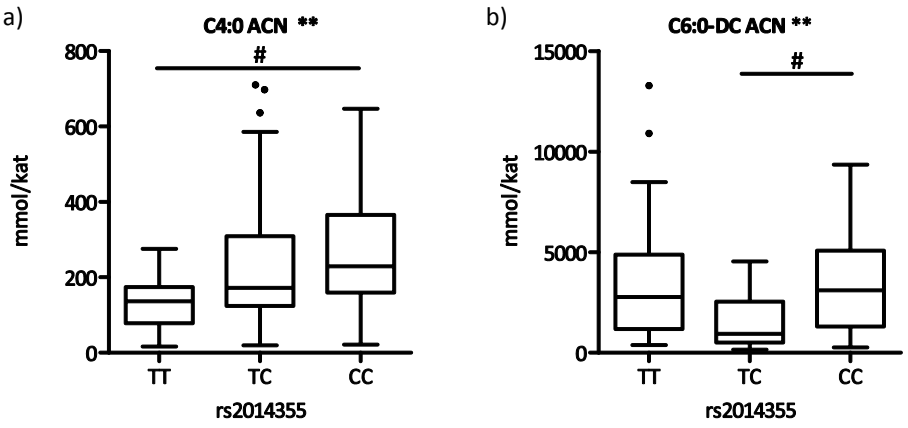

Figure 1.4-6: Metabolites affected by genotype after incubation with oleic acid
Depicted are a) C4:0-acylcarnitine levels and b) C6:0-DC-acylcarnitine levels which differed significantly between genotypes after 160 min incubation with 100 µM oleic acid. Acylcarnitine levels were normalized to the CS activity. Values of 3-6 independent experiments per EBV-LCL in triplicates are shown as box plots (Boxes extend from 1st quartile to 3rd quartile, median is indicated as a horizontal line, whiskers are drawn equal to 1.5 times the interquartile distance. * = $p < 1.13 \times 10^{-3}$, ** = $p < 2.20 \times 10^{-4}$ (Bonferroni corrected significance levels), Kruskal-Wallis one-way ANOVA. # = $p < 1.13 \times 10^{-3}$ (Dunn's post hoc test), ACN = acylcarnitine.

To evaluate if the difference in acylcarnitine levels attributes to each copy of allele, a linear regression was calculated under assumption of the additive genetic model (Lewis 2002). Calculations of linear regressions dependent on rs2014355 genotype for acylcarnitine levels measured after incubation without oleic acid revealed significant higher C16:0- and C18:0-acylcarnitine levels ($p = 1.55 \times 10^{-4}$ and $p = 5.34 \times 10^{-3}$, respectively) in carriers of the minor C allele. This indicates both, that fatty acids are metabolized by FAO in EBV-LCLs and furthermore that in EBV-LCLs the rs2014355 minor C allele associates with reduced oxidation of endogenous long-chain fatty acids.

Significant allele-dependent difference of C4:0-acylcarnitine levels were found after incubation with ($p = 3.50 \times 10^{-6}$) and without ($p = 0.03$) oleic acid, respectively. However, the genotype effect was more pronounced after incubation with oleic acid (Table 1.4-1) than without oleic acid (Table 1.4-2) and leads to a lower p-value, which substantiates the assay as useful to trigger minor genotype effects.

1.4.3 Genotype effect on ACADS gene expression

It was shown that trait-associated loci in non-coding regions are highly enriched for eQTLs (Nicolae et al. 2010; Nica et al. 2011) (Claussnitzer M, personal communication), suggesting c*is*-regulatory potential for many intronic or intergenic SNPs that affects gene expression.

Thus, gene expression of *ACADS* was measured in EBV-LCLs and primary human preadipocytes with different genotypes under normal growth conditions. ACADS mRNA expression was significantly lower in EBV-LCLs homozygous for the minor C allele (Figure 1.4-7a) but not in homozygous (CC) primary human preadipocytes compared to homozygous carriers of the major T allele (Figure 1.4-7b). Complementary, ACADS protein levels were significantly lower in EBV-LCLs homozygous for the minor C allele if compared to EBV-LCLs homozygous for the major T allele (Figure 1.4-7c). On the contrary, ACADS protein levels were significantly higher in preadipocytes homozygous for the minor C allele compared to preadipocytes homozygous for the major T allele (Figure 1.4-7d). Also in primary adipocytes differentiated until day 18, there was a tendency towards higher ACADS protein levels in adipocytes homozygous for the minor C allele compared to adipocytes homozygous for the major T allele (Figure 1.4-7e). These results indicate a genotype-triggered down-regulation of the ACADS mRNA expression in EBV-LCLs by the minor C allele which is reflected in lower protein levels. The opposite was observed in primary human preadipocytes and adipocytes, where the minor C allele triggered increased ACADS protein levels.

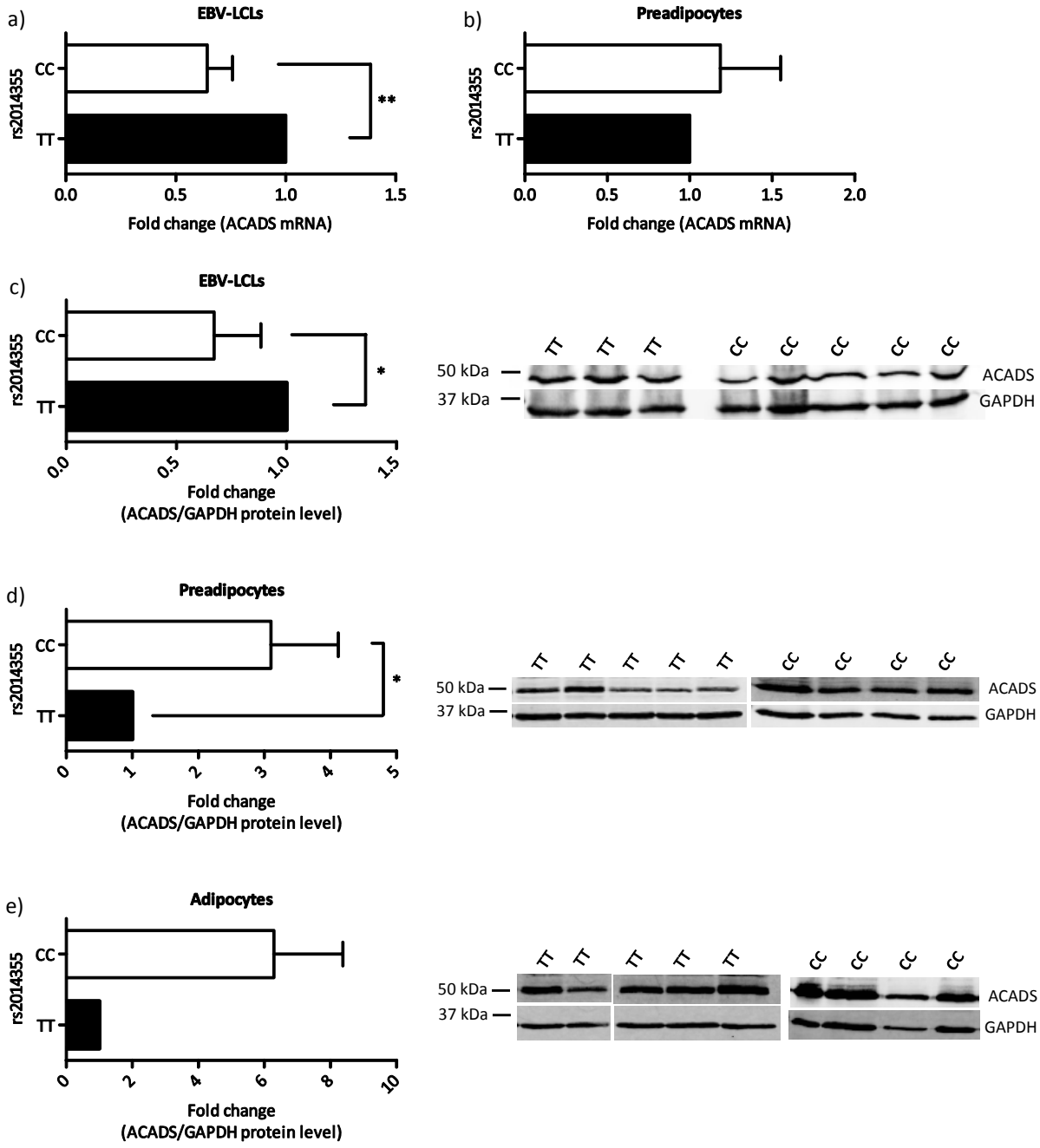

Figure 1.4-7: Expression of ACADS mRNA and protein levels in EBV-LCLs, human primary preadipocytes and adipocytes

a) EBV-LCL mRNA of three homozygous major allele carriers (rs2014355 TT) and five homozygous minor allele (rs2014355 CC) carriers was analysed by RT-qPCR. b) Preadipocyte mRNA of six homozygous major allele carriers (rs2014355 TT) and four homozygous minor allele (rs2014355 CC) carriers were analysed by RT-qPCR. c) Western blot analysis of ACADS protein levels was carried out in 10 µg protein lysates of EBV-LCLs homozygous for the major T allele (n = 3) and homozygous for the minor C allele (n = 5); in 20 µg protein lysates of d) primary human preadipocytes and e) human primary adipocytes (day 18) homozygous for major T allele (n = 5) and homozygous for the minor C allele (n = 4). Band intensities were analysed and quantified using the Odyssey IR Imaging System (LI-COR, Bioscience) and ACADS was normalized to GAPDH. The RGI was calculated as arithmetic mean of GAPDH and YWHAZ in each EBV-LCL and preadipocyte sample. Fold changes were calculated using the ΔΔCt method. Values are mean + SD. * = $p < 0.05$; ** = $p < 0.01$; two-tailed, one sample t-test.

1.4.4 *Cis*-regulatory SNPs in LD with rs2014355

To measure allele-dependent *cis*-regulatory activity of SNPs in LD with rs2014355 predicted by PMCA, reporter assays were used to quantify allele-dependent changes in relative luciferase activity in a liver cell line (Huh7) and an adipocyte cell line (3T3L1). A statistically significant repressing allelic effect was found for the rs10431384 minor G allele (in LD: r^2 = 0.64 with rs2014355, European population, 1,000 Genome Phase 1) in Huh7 cells (Figure 1.4-8a) as well as in 3T3L1 cells compared to the major A allele (Figure 1.4-9a) with a mean of 0.3 fold and 0.4 fold decrease luciferase activity, respectively. Activating allelic effects were found for the rs10431386 minor T allele (in LD: r^2 = 0.65 with rs2014355, European population, 1,000 Genome Phase 1) and the rs35599677 minor A allele (in LD: r^2 = 0.94 with rs2014355, European population, 1,000 Genome Phase 1) in Huh7 cell (Figure 1.4-8b, c), and the rs3999408 minor A allele (in LD: r^2 = 0.93 with rs2014355, European population, 1,000 Genome Phase 1) in 3T3L1 compared to the major C, G and G alleles, respectively (Figure 1.4-9d).

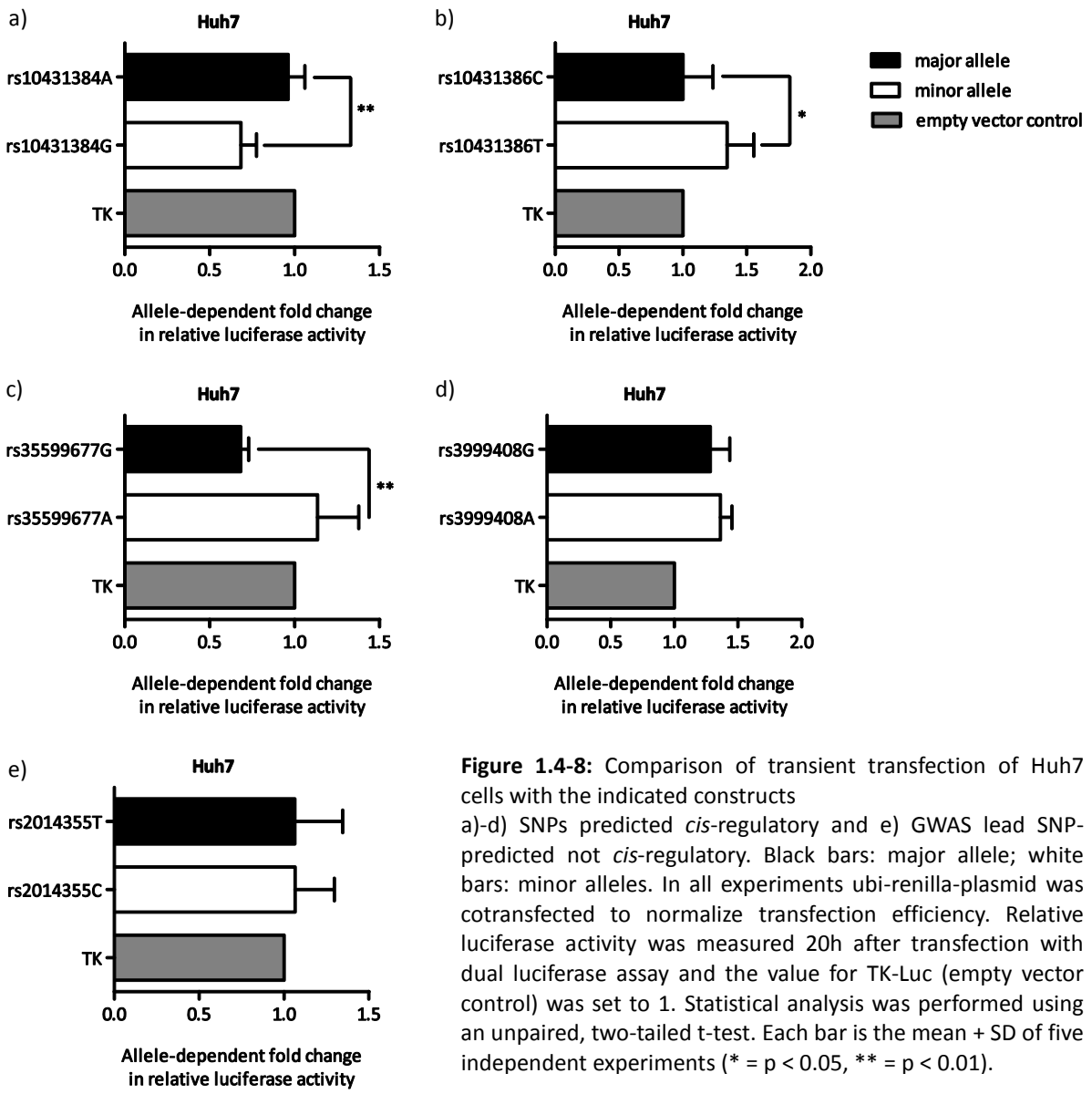

Figure 1.4-8: Comparison of transient transfection of Huh7 cells with the indicated constructs
a)-d) SNPs predicted *cis*-regulatory and e) GWAS lead SNP-predicted not *cis*-regulatory. Black bars: major allele; white bars: minor alleles. In all experiments ubi-renilla-plasmid was cotransfected to normalize transfection efficiency. Relative luciferase activity was measured 20h after transfection with dual luciferase assay and the value for TK-Luc (empty vector control) was set to 1. Statistical analysis was performed using an unpaired, two-tailed t-test. Each bar is the mean + SD of five independent experiments (* = $p < 0.05$, ** = $p < 0.01$).

Allele-specific activating effects of rs10431386 minor T allele and rs35599677 minor A allele showed a mean 1.4 fold to 1.7 fold change in reporter gene activity in Huh7 cells (Figure 1.4-8b, c), and the rs3999408 minor A allele a mean 1.5 fold change in reporter gene activity in 3T3L1 cells (Figure 1.4-9d). Notably, the minor C allele of the tag SNP (rs2014355) used in the GWASs did not exhibit any *cis*-regulatory effects in either Huh7 cells (Figure 1.4-8e) or 3T3L1 cell (Figure 1.4-9e).

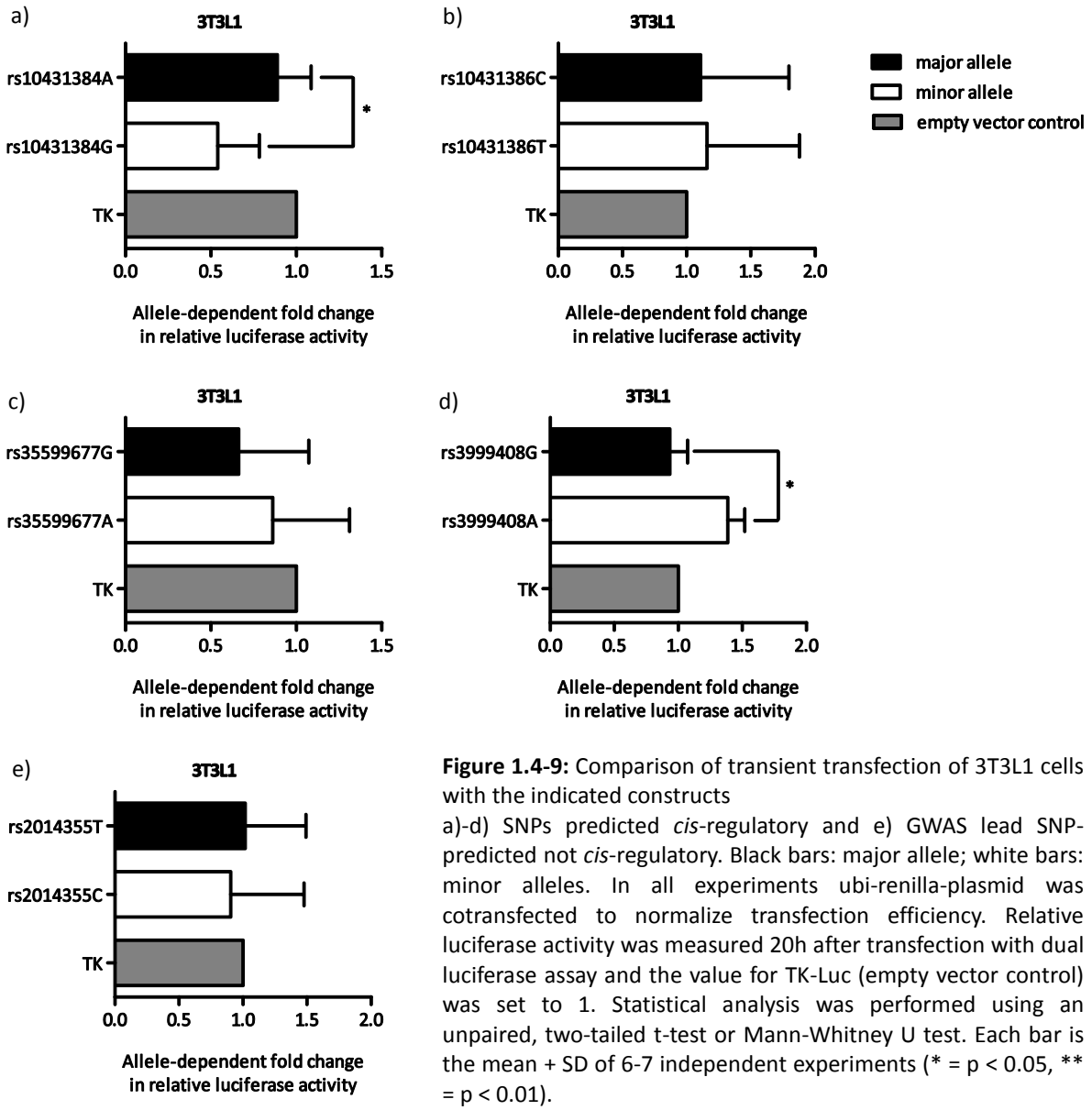

Figure 1.4-9: Comparison of transient transfection of 3T3L1 cells with the indicated constructs
a)-d) SNPs predicted *cis*-regulatory and e) GWAS lead SNP-predicted not *cis*-regulatory. Black bars: major allele; white bars: minor alleles. In all experiments ubi-renilla-plasmid was cotransfected to normalize transfection efficiency. Relative luciferase activity was measured 20h after transfection with dual luciferase assay and the value for TK-Luc (empty vector control) was set to 1. Statistical analysis was performed using an unpaired, two-tailed t-test or Mann-Whitney U test. Each bar is the mean + SD of 6-7 independent experiments (* = $p < 0.05$, ** = $p < 0.01$).

1.4.5 Inducible knock-down of ACADS protein in stable Huh7 cells

1.4.5.1 Knock-down efficiency using different doxycycline concentrations and incubation times

To establish gradual knock-downs, Huh7 cells, transduced with a tet-inducible shRNA for down-regulation of ACADS (shACADS), were incubated with doxycycline concentrations ranging from 0 - 50 ng/ml for 3 or 5 days.

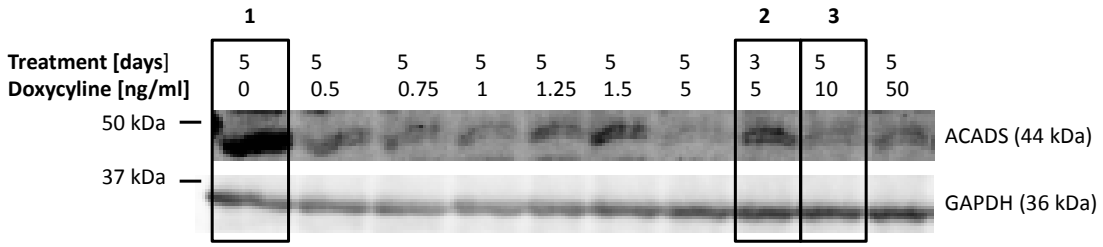

Figure 1.4-10: Western blot analysis of ACADS protein knock-down in stable-transduced shACADS Huh7 cells
Western blotting analysed 10 µg of cell lysate per sample. Protein was harvested after 3 and 5 days of treatment with 0, 0.5, 0.75, 1, 1.25, 1.5, 5, 10 and 50 ng/ml doxycycline. Boxes indicate conditions chosen for further experiments: (1) null knock-down, (2) intermediate knock-down, (3) maximal knock-down.

Western blot analysis revealed successful knock-downs of ACADS protein levels with several concentrations (Figure 1.4-10). For further functional assays in gradual knock-downs the most reproducible (data not shown) incubation time and doxycycline concentration inducing null knock-down (1), intermediate knock-down (2) and maximal knock-down (3) (boxes Figure 1.4-10) were chosen. The intermediate- and maximal knock-down efficiencies were 81% and 95%, respectively, determined by analysis and quantification of band intensities using the Odyssey IR Imaging System (LI-COR, Bioscience). ACADS protein levels were normalized to GAPDH protein levels and normalized ACADS protein levels of the intermediate- and maximal knock-down were compared to the null knock-down.

1.4.5.2 ACADS knock-down leads to decelerated FAO and decreases mitochondrial OCR

In order to examine FAO flux (acylcarnitine-measurement) and mitochondrial respiration (O_2-consumption measurement) four independent experiments were conducted as described in Figure 1.3-3.

Comparison of knock-down efficiency of four independent experiments

RT-qPCR and western blot analyses were performed to assess knock-down efficiencies in the four independent experiments. Considering, the three selected conditions (null-, intermediate-, and maximal knock-down exhibited comparable knock-down efficiencies on protein (Figure 1.4-11) and mRNA level (Figure 1.4-12).

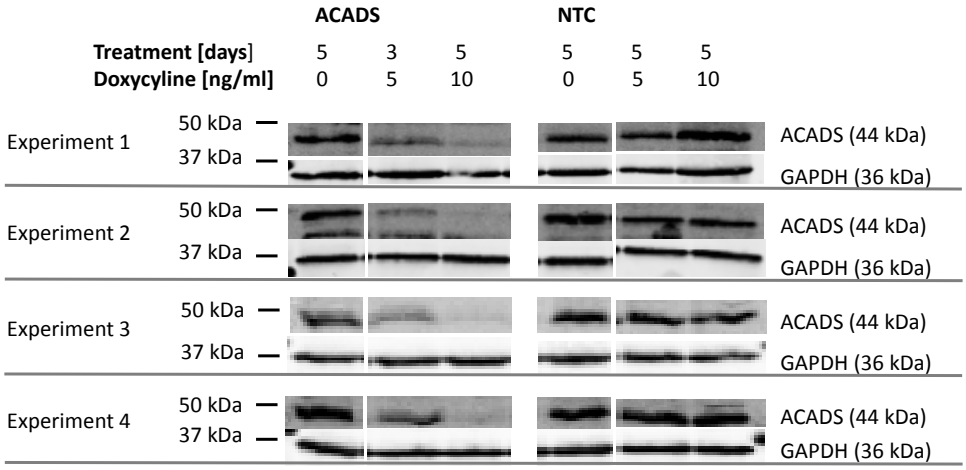

Figure 1.4-11: Western blot analysis of ACADS protein knock-downs in stable-transduced Huh7 cells
Western blotting analysed 10 µg of cell lysate per sample for 4 independent experiments. Protein was harvested after 3 or 5 days of treatment with 0, 5, and 10 ng/ml doxycycline.

The significant down-regulation of ACADS mRNA was similar in the intermediate- (5 ng/ml doxycycline) and maximal (10 ng/ml doxycycline) shACADS knock-down Huh7 cells (82% and 84%, respectively) (Figure 1.4-12) compared to the null (0 ng/ml doxycycline) knock-down shACADS Huh7 cells. However, on protein level the intermediate- and maximal knock-down shACADS Huh7 cells resulted in a clear gradual knock-down on ACADS protein levels, the intermediate- and maximal knock-down shACADS Huh7 cells exhibited knock-down efficiencies of 71.5 ± 8.7% and 92.8 ± 3.8%, respectively (Figure 1.4-11). A similar treatment in Huh7 cells transduced with a tet-inducible non-target shRNA (shNTC) revealed no effect on both, protein (Figure 1.4-11) and mRNA levels (Figure 1.4-12). Comparison of ACADS mRNA expression levels in shACADS and shNTC Huh7 without doxycycline treatment revealed no differences ($p = 0.964$, one sample t-test, $n = 4$), proving that the lentiviral shRNA construct is solely active upon doxycycline treatment without any leakiness.

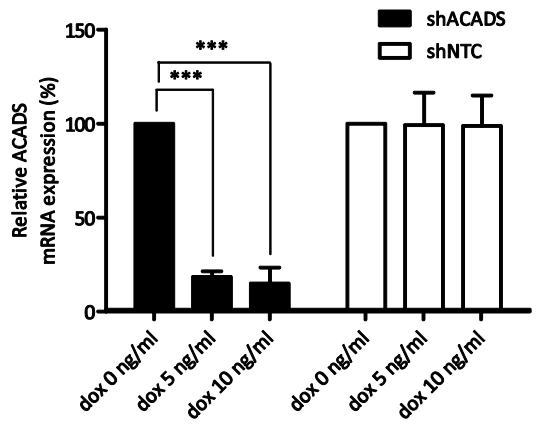

Figure 1.4-12: qPCR analysis of ACADS mRNA knock-down in stable-transduced Huh7 cells
RT-qPCR analysed mRNA of four independent experiments. mRNA was harvested after 3 or 5 days of treatment with 0, 5, and 10 ng/ml doxycycline. The RGI was calculated as arithmetic mean of GAPDH and PPIA in each sample. Fold changes were calculated using the ΔΔCt method. Values are mean + SD. *** = $p < 0.001$, one sample t-test. ACADS = acyl-CoA dehydrogenase short-chain, ACN = acylcarnitine, dox = doxycycline, NTC = non-target control.

Baseline C4:0-acylcarnitine levels of shACADS and shNTC Huh7 cells

Baseline C4:0-acylcarnitine measurement in null-, intermediate- and maximal knock-down shACADS Huh7 cells revealed an accumulation of C4:0-acylcarnitine in the intermediate- and maximal knock-down shACADS Huh7 cells that was significantly higher in the maximal knock-down shACADS Huh7 cells compared to null knock-down shACADS Huh7 cells (Figure 1.4-13). Parallel C4:0-acylcarnitine measurement in shNTC Huh7 cells with a similar treatment did not reveal any significant differences (Figure 1.4-13).

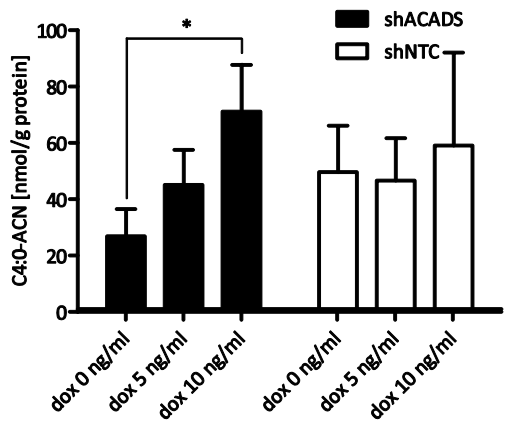

Figure 1.4-13: Intracellular C4:0-acylcarnitine measurement in shACADS and shNTC Huh7 cells
Intracellular C4:0-acylcarnitine measurement in null- (shACADS dox 0 ng/ml), intermediate- (shACADS dox 5 ng/ml) and maximal knock-down (shACADS dox 10 ng/ml) shACADS Huh7 cells after 1h starvation compared to similar treated stable cell lines transduced with control vector with non-target shRNA (shNTC). Values of four independent experiments are expressed as mean + SD. * = $p < 0.05$, Kruskal-Wallis one-way ANOVA with Dunn's post hoc test. ACADS = acyl-CoA dehydrogenase short-chain, ACN = acylcarnitine, dox = doxycycline, NTC = non-target control.

Time course of acylcarnitine flux induced by palmitic acid loading in shACADS- and shNTC Huh7 cells

Short-term time courses of intracellular acylcarnitine flux were measured immediately after palmitic acid loading in null-, intermediate-, and maximal knock-down shACADS- and shNTC Huh7 cells to monitor induced FAO flux. A total of 21 measured acylcarnitines were above the limit of quantification. Twelve of these detectable acylcarnitines were used as proxies for acyl-CoA metabolites of mitochondrial palmitic acid β-oxidation. Therefore, acylcarnitines

(grey-shaded boxes) were assigned as substrate to one of the four FAO enzymatic reactions (Figure 1.4-14). Some substrates of the enoyl-CoA hydratase and the 3-hydroxyacyl-CoA dehydrogenase in the simultaneous measured acylcarnitine panel (Appendix Table A.2) were below the detection limit.

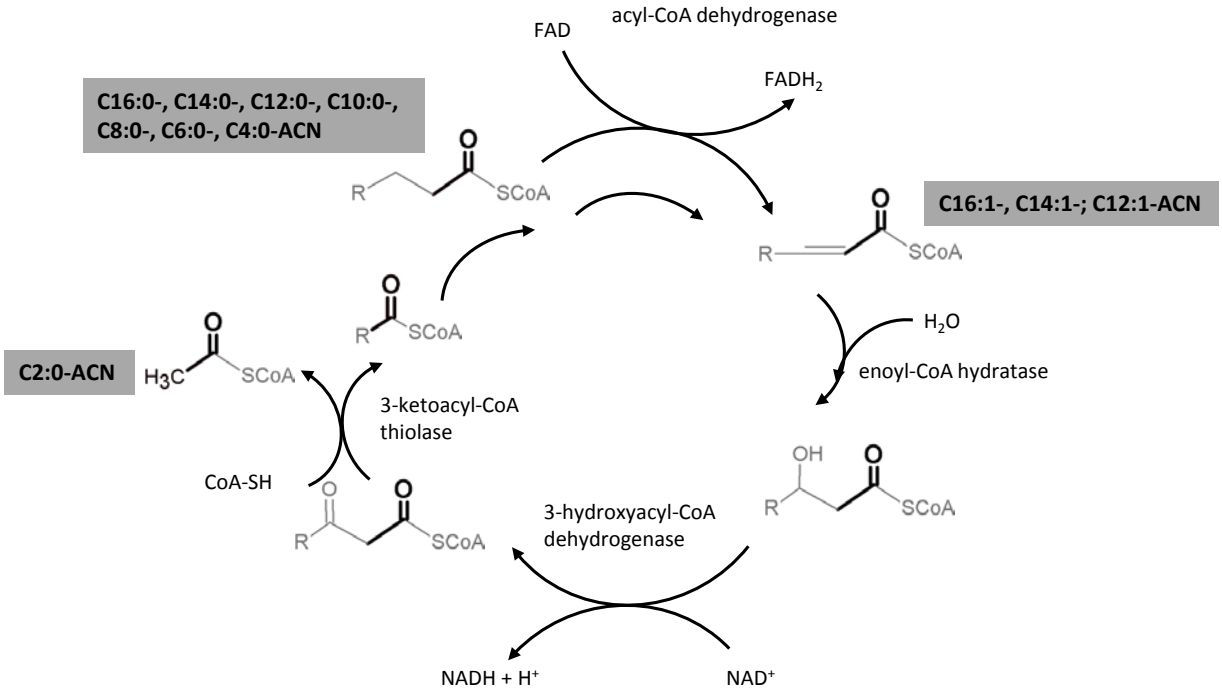

Figure 1.4-14: Assignment of detected acylcarnitines by HPLC-MS/MS to corresponding enzymatic FAO reactions
Twelve intermediate acylcarnitines from cell extracts reflecting the mitochondrial acyl-CoA pool with corresponding chain lengths were measured as breakdown products of palmitic acid (shaded in grey). An extensive description of FAO is given in chapter 1.1.3.

Enzyme-reaction specific patterns were observed in maximal knock-down shACADS Huh7 cells' time course measurements of the assigned acylcarnitine levels after incubation with palmitic acid (Figure 1.4-15). Interestingly, the pattern of the acyl-CoA dehydrogenase substrates was observed in the intermediate knock-down shACADS Huh7 cells only for the medium-chain acylcarnitines (Figure 1.4-15).

In contrast to all other detectable acylcarnitine levels, at baseline (0 min) the C4:0-acylcarnitine levels were gradually increased in intermediate- (45.1 ± 12.41 nmol/g protein) and maximal knock-down (71.16 ± 16.54 nmol/g protein) shACADS Huh7 cells which was significantly higher than in null knock-down shACADS Huh7 cells (26.89 ± 9.65 nmol/g protein) (Figure 1.4-13). After seven minutes of incubation with palmitic acid the increase in

C4:0-acylcarnitine level was significantly higher in the maximal knock-down shACADS Huh7 cells (129.94 ± 20.51 nmol/g protein) compared to the null knock-down shACADS Huh7 cells (60.95 ± 10.97 nom/g protein), whereas the C4:0-acylcarnitine level in intermediate knock-down shACADS Huh7 cells (92.9 ± 14.5 nmol/g protein) was higher compared to null knock-down shACADS Huh7 cells but lower than in the maximal knock-down shACADS Huh7 cells (Figure 1.4-16a). Interestingly, at the same time point (7 min) the main products (C16:1-; C14:1-; C12:1-acylcarnitine) of the very long-chain acyl-CoA dehydrogenase (VLCAD), which are likewise substrates for the long-chain enoyl-CoA hydratase, were also increased in maximal knock-down shACADS Huh7 cells compared to null knock-down shACADS Huh7 cells (Figure 1.4-15). Likewise, an increase of C2:0-acylcarnitine level was observed (Figure 1.4-17a) which represents acetyl-CoA that is cleaved off acyl-CoAs in each cycle of FAO (Figure 1.4-14). At this time point all other acylcarnitines did not differ between the three knock-down conditions (Figure 1.4-15).

Fourteen minutes after addition of palmitic acid the levels of acyl-CoA dehydrogenase substrates were decreased in the maximal knock-down shACADS Huh7 cells compared to the previous measurement (7 min) (Figure 1.4-15). Furthermore, C16:0-, C14:0-, C12:0-, C10:0-, C8:0- and C6:0-acylcarnitine levels were lower in the maximal knock-down shACADS Huh7 cells compared to the null knock-down shACADS Huh7 cells, an effect reaching significance for C10:0-, C8:0-, and C6:0-acylcarnitine levels. The C10:0-, C8:0-and C6:0-acylcarnitine levels in the intermediate knock-down shACADS Huh7 cells were between the levels in null- and maximal shACADS knock-down Huh7 cells (Figure 1.4-15). Palmitic acid is converted into C16:0-acylcarnitine by the CPT I located in the outer mitochondrial membrane. A lower C16:0-acylcarnitine level in the intermediate- and the maximal knock-down shACADS Huh7 cells might indicate an inhibition of CPT I and further the lower C16:0-acylcarnitine supply might accounts for the lower levels of break down product (C14:0-, C12:0-, C10:0-, C8:0- and C6:0-acylcarnitine) of the subsequent FAO cycles. Of note, the intracellular C4:0-acylcarnitine level was decreased in the maximal knock-down shACADS Huh7 cells compared to the previous time point (Figure 1.4-16a), whereas the level increased in the supernatant (Figure 1.4-16b). This observation may reflect an efflux of accumulating C4:0-acylcarnitine from the cell into the supernatant.

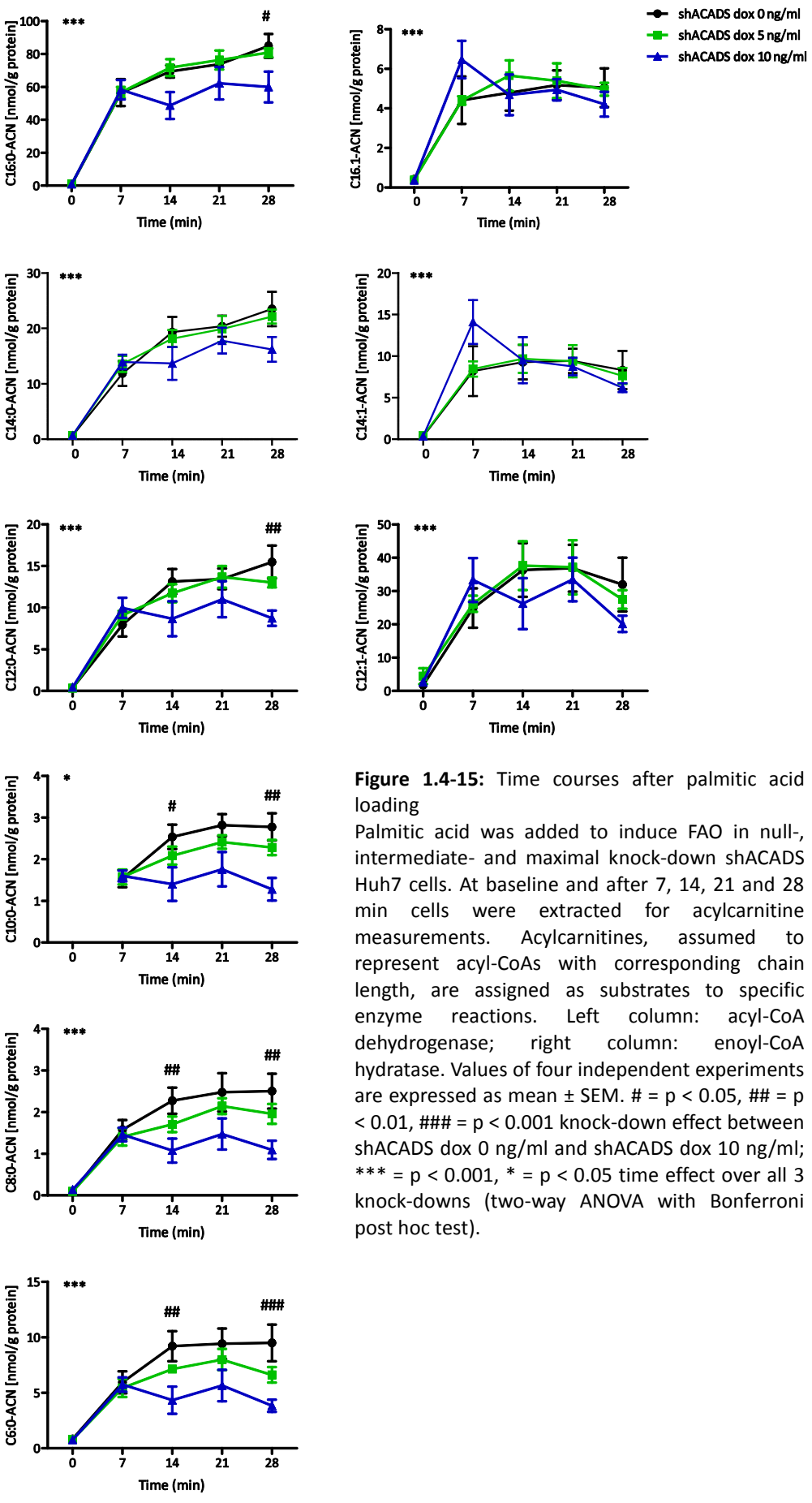

Figure 1.4-15: Time courses after palmitic acid loading

Palmitic acid was added to induce FAO in null-, intermediate- and maximal knock-down shACADS Huh7 cells. At baseline and after 7, 14, 21 and 28 min cells were extracted for acylcarnitine measurements. Acylcarnitines, assumed to represent acyl-CoAs with corresponding chain length, are assigned as substrates to specific enzyme reactions. Left column: acyl-CoA dehydrogenase; right column: enoyl-CoA hydratase. Values of four independent experiments are expressed as mean ± SEM. # = $p < 0.05$, ## = $p < 0.01$, ### = $p < 0.001$ knock-down effect between shACADS dox 0 ng/ml and shACADS dox 10 ng/ml; *** = $p < 0.001$, * = $p < 0.05$ time effect over all 3 knock-downs (two-way ANOVA with Bonferroni post hoc test).

21 min after incubation with palmitic acid there was a trend towards increasing acylcarnitine levels (except for C14:1- and C4:0-acylcarnitine which were similar at 14 min) (Figure 1.4-15 and 1.4-16a) compared to the previous time point. After 28 min, there was a trend towards decreasing acylcarnitine levels in maximal knock-down shACADS Huh7 cells (except for C2:0-acylcarnintine level which increased) (Figure 1.4-17a). Noteworthy, C16:0-, C14:0-, C12:0-, C10:0-, C8:0- and C6:0-acylcarnitine levels of the maximal knock-down shACADS Huh7 cells did not revert to the levels of null knock-down shACADS Huh7 cells and were significantly lower after 28 min (except for C14:0-acylcarnitine levels). These observations indicate maintenance of the enzyme activity rates adjusted in the first 14 min of palmitic acid incubation.

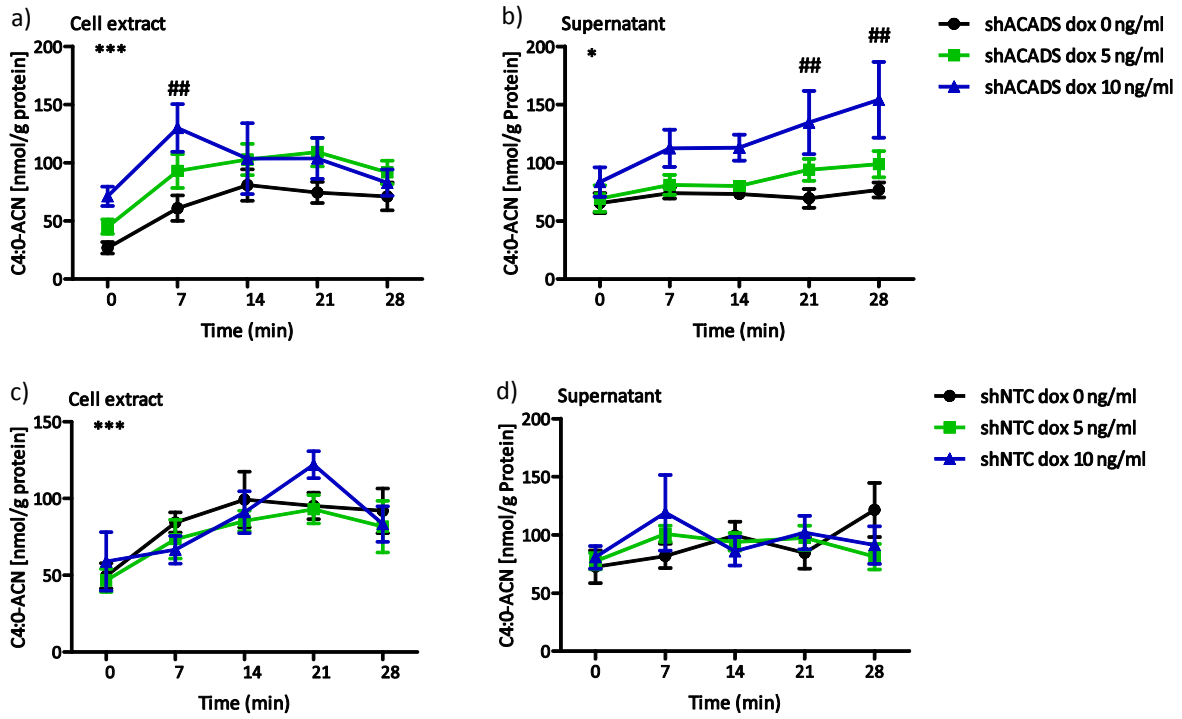

Figure 1.4-16: Time courses of C4:0-acylcarnitine levels after palmitic acid loading in cell extract and supernatant
Palmitic acid was added to induce FAO in a), b) shACADS and c), d) shNTC cells. At baseline and after 7, 14, 21 and 28 min acylcarnitine levels were measured in supernatants and cell extracts. Values of four independent experiments are expressed as mean ± SEM. ## $p < 0.01$ knock-down effect between shACADS dox 0 ng/ml and shACADS dox 10 ng/ml; * $p < 0.05$, *** $p < 0.001$ time effect over all 3 knock-downs (two-way ANOVA with Bonferroni post hoc test).

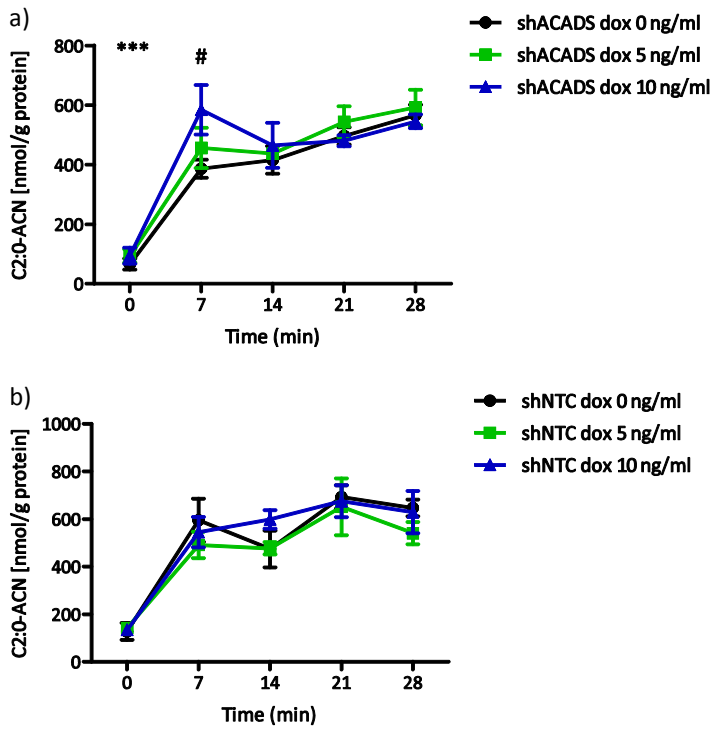

Figure 1.4-17: Time courses of C2:0-acylcarnitine levels after palmitic acid loading
Palmitic acid was added to induce FAO in a) shACADS and b) shNTC Huh7 cells. At baseline and after 7, 14, 21 and 28 min acylcarnitines were measured in cell extracts. Values of four independent experiments are expressed as mean ± SEM. # $p < 0.05$ knock-down effect between shACADS dox 0 ng/ml and shACADS dox 10 ng/ml; *** $p < 0.001$, time effect over all 3 knock-downs (two-way ANOVA with Bonferroni post hoc test).

Vitally, the same experiment was carried out in shNTC Huh7 cells with exactly the same treatment. Notably, none of the above described observations were found in the control cells (Figure 1.4-16c and d, Figure 1.4-17b, Figure 1.4-18) showing the specificity of the ACADS knock-down and excluding side effects of doxycycline and the vector construct.

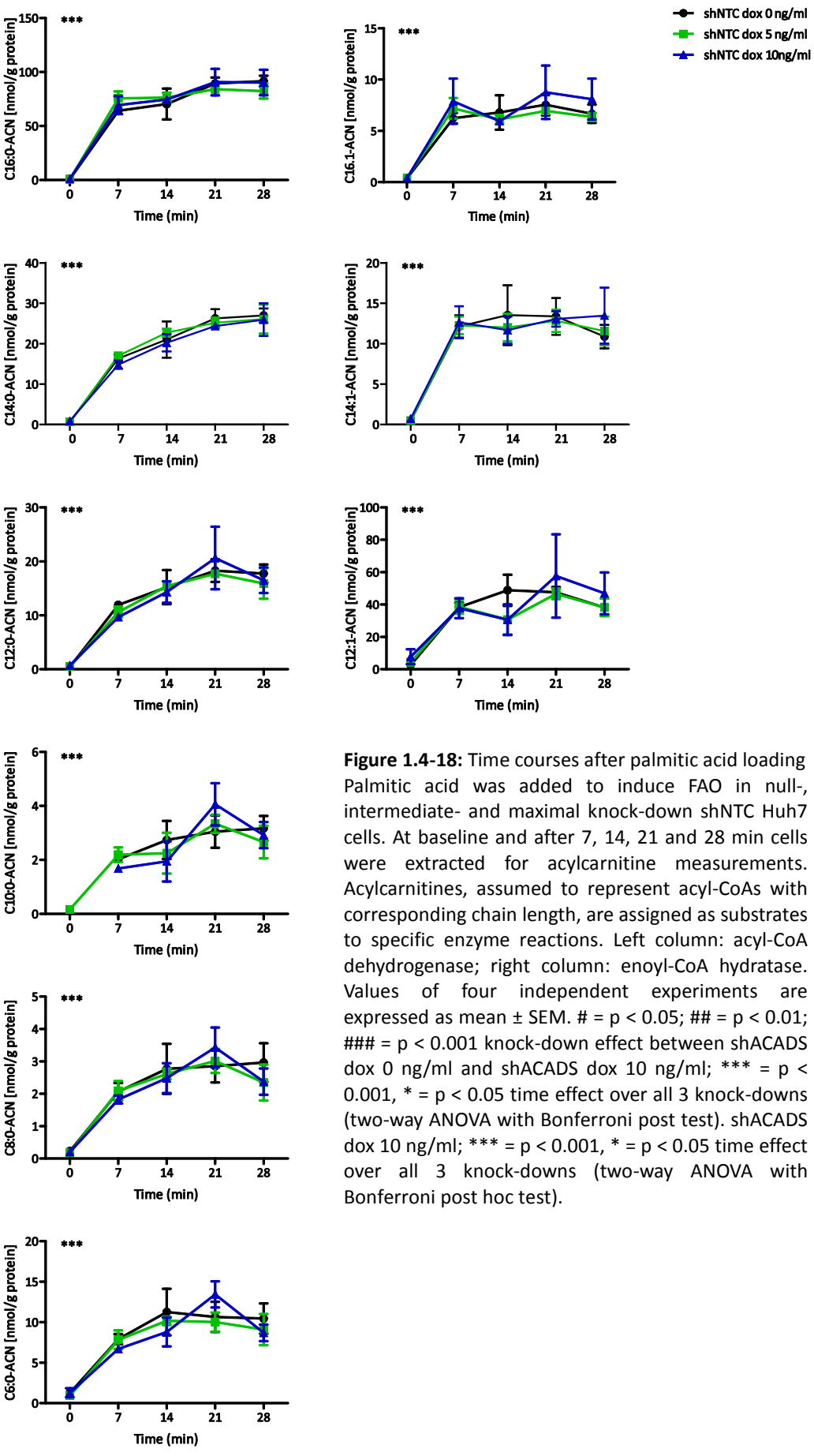

Figure 1.4-18: Time courses after palmitic acid loading Palmitic acid was added to induce FAO in null-, intermediate- and maximal knock-down shNTC Huh7 cells. At baseline and after 7, 14, 21 and 28 min cells were extracted for acylcarnitine measurements. Acylcarnitines, assumed to represent acyl-CoAs with corresponding chain length, are assigned as substrates to specific enzyme reactions. Left column: acyl-CoA dehydrogenase; right column: enoyl-CoA hydratase. Values of four independent experiments are expressed as mean ± SEM. # = $p < 0.05$; ## = $p < 0.01$; ### = $p < 0.001$ knock-down effect between shACADS dox 0 ng/ml and shACADS dox 10 ng/ml; *** = $p < 0.001$, * = $p < 0.05$ time effect over all 3 knock-downs (two-way ANOVA with Bonferroni post test). shACADS dox 10 ng/ml; *** = $p < 0.001$, * = $p < 0.05$ time effect over all 3 knock-downs (two-way ANOVA with Bonferroni post hoc test).

Monitoring of branched-chain amino acid intermediates revealed that C5:0-acylcarnitine (Figure 1.4-19a, b) but not C3:0-acycarnitine (Figure 1.4-19c, d) was significantly decreased during the time course in both shACADS and shNTC Huh7 cells. There was no significant difference between null-, intermediate- and maximal knock-down shACADS Huh7 cells.

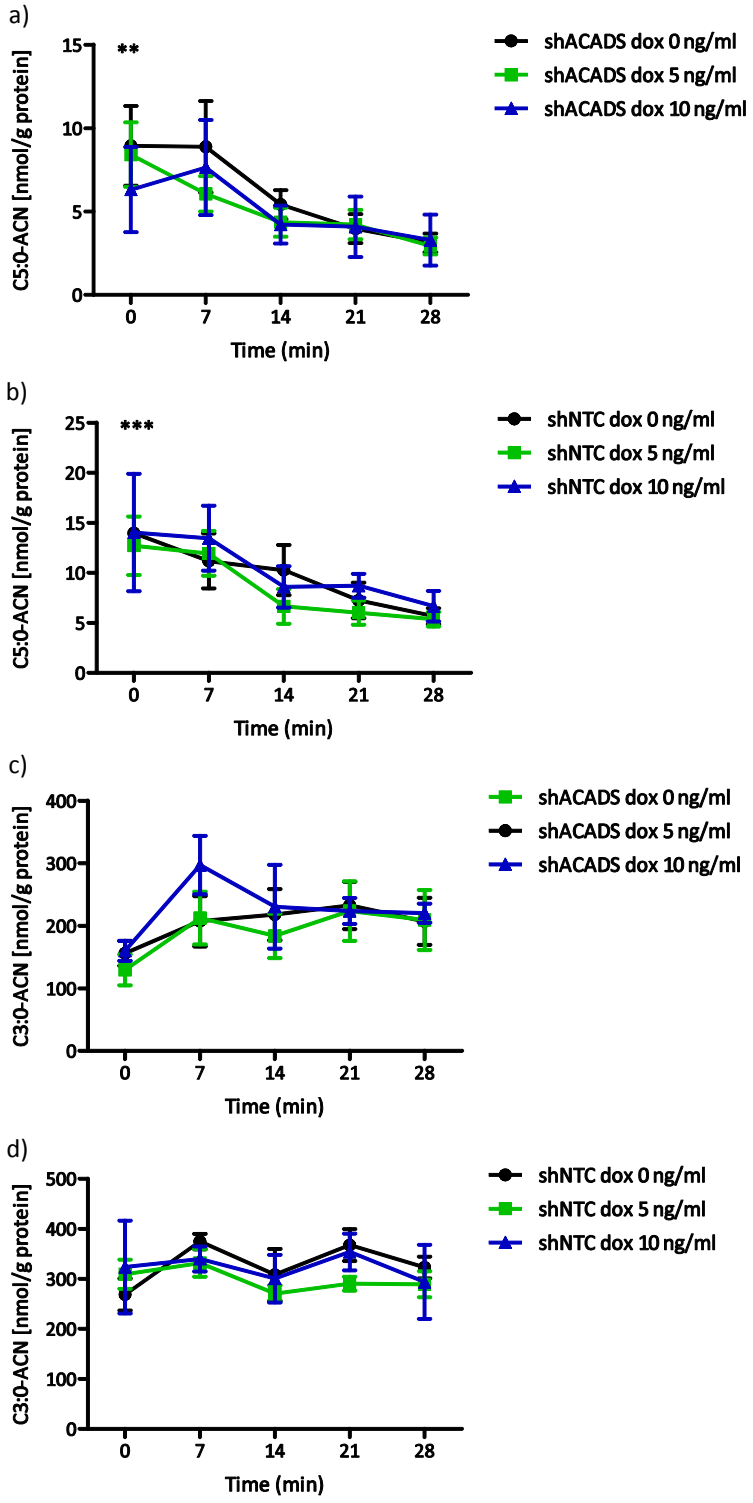

Figure 1.4-19: Time course of C5:0- and C3:0-acylcarnitine levels after incubation with palmitic acid Time course of a), b) C5:0-acylcarnitine levels and c), d) C3:0-acylcarnitine levels after incubation with palmitic acid of a), c) shACADS and b), d) shNTC Huh7 cells. At baseline and after 7, 14, 21 and 28 min acylcarnitines were measured in cell extracts. Values of four independent experiments are expressed as mean ± SEM. ** = $p < 0.05$, *** = $p < 0.001$ time effect over all 3 knock-downs (two-way ANOVA with Bonferroni post hoc test).

OCR in gradual knock-down cell lines

To evaluate the overall metabolic activity of shACADS and shNTC Huh7 cells, continuous measurements of OCR were collected over time after stimulation of FAO by palmitic acid, mitochondrial uncoupling by FCCP and inhibition by etomoxir using Seahorse XF Flux Analyzer.

To avoid an influence of variable cell number on the experimental outcome, the total protein per well for each of the shNTC and shACADS Huh7 cells was measured, as it was demonstrated that the protein amount correlates with the cell number (Zhou et al. 2012).

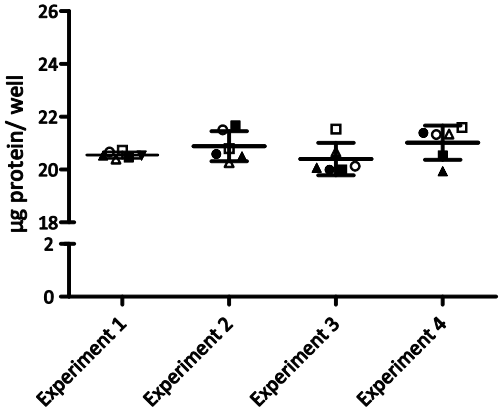

Figure 1.4-20: Protein amount per well of the 96 well plate used for Seahorse measurement
shACADS and shNTC Huh7 cells were lysed in 0.2 M NaOH and the protein amount was determined by the RCDC assay (Bio-Rad, München, Germany). Closed circles: shACADS 0 ng/ ml doxycycline, closed square: shACADS 5 ng/ml doxcycyline, closed triangle: 10 ng/ml doxcycyline, open circles: shNTC 0 ng/ ml doxycycline, open squares: shNTC 5 ng/ml doxycycline, open triangles: shNTC 10 ng/ml doxycycline. Depicted are single values and mean ± SD; one-way ANOVAs comparing protein amounts of shACADS and shNTC Huh7 cells, experiments did not reveal statistical significances.

There were no significant differences in protein amount/well between any of the shACADS and shNTC cell lines (Figure 1.4-20) assuming similar cell numbers/well. Therefore, the OCR values were not normalized.

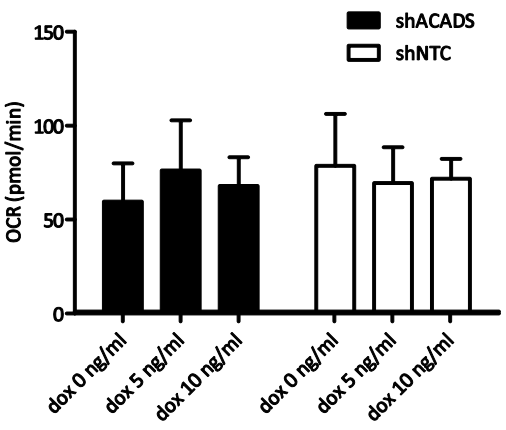

Figure 1.4-21: Basal OCR after 1h starvation of all shACADS and shNTC Huh7 cells
Absolute extracellular O_2 measurement in null- (shACADS dox 0 ng/ml), intermediate- (shACADS dox 5 ng/ml) and maximal (shACADS dox 10 ng/ml) knock-down shACADS Huh7 cells after 1h starvation compared to similar treated shNTC Huh7 cells. Values of four independent experiments are expressed as mean + SD. One-way ANOVA with Dunnett's post hoc test did not reveal any significant differences between null-, intermediate- and maximal knock-downs shACADS and shNTC Huh7 cells. ACADS = acyl-CoA dehydrogenase short-chain, dox = doxycycline, NTC = non-target control, OCR = oxidative consumption rate.

Cells were starved for 1h before OCR measurements were started. During starvation the cells had no access to any energy substrates, like carbohydrates, fatty acid and protein, in the

assay buffer. The baseline OCR (pmol/min) (Figure 1.4-21) did not reveal significant differences between any of the shACADS and shNTC Huh7 cells.

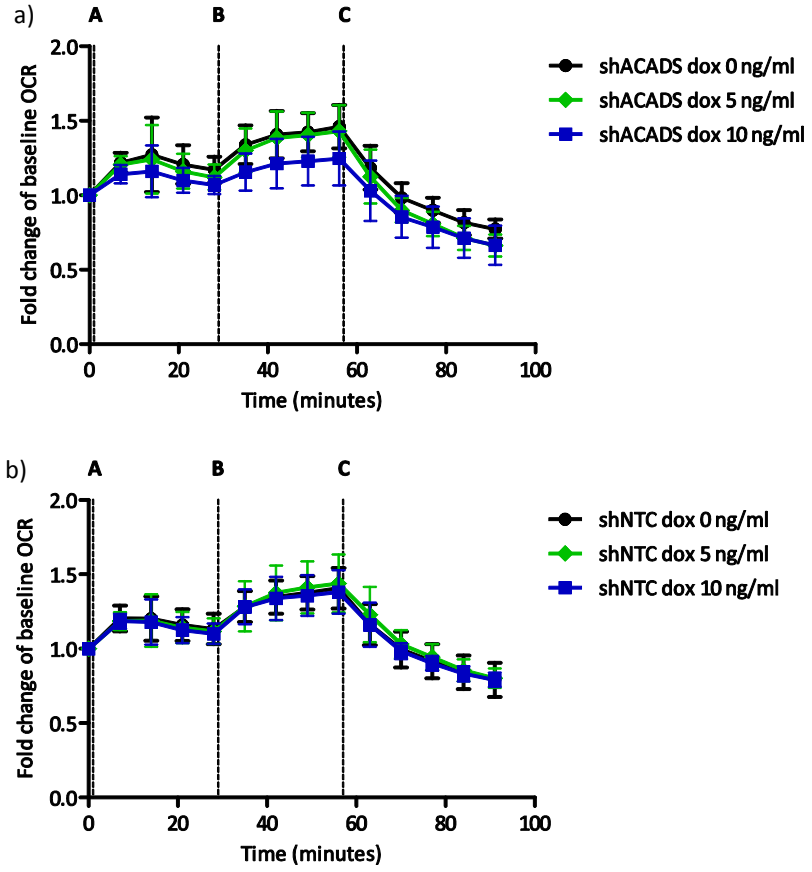

Figure 1.4-22: Fold change of baseline OCR after stimulation of FAO, mitochondrial uncoupling and inhibition of FAO
a) Relative extracellular O_2 measurement in control shNTC Huh7 cells and b) null- (shACADS dox 0 ng/ml), intermediate- (shACADS dox 5 ng/ml) and maximal knock-down (shACADS dox 10 ng/ml) shACADS Huh7 cells after 1h starvation. A = injection of palmitic acid (200 µM), B = injection of FCCP (100 µM), C = injection of etomoxir (100 µM). OCR baseline measurements were normalized to one and the following values are expressed as fold change of basal level. Values of four independent experiments are expressed as mean ± SD. ACADS = acyl-CoA dehydrogenase short-chain, dox = doxycycline, NTC = non-target control, OCR = oxidative consumption rate.

OCR baseline measurements were normalized to one and the following values are expressed as fold change of basal level. Palmitic acid was injected to stimulate FAO by being the only offered substrate (Figure 1.4-22a A, b A). The addition of palmitic acid led to an increase in OCR in all shACADS and shNTC Huh7 cells (1.4-22a, b). The maximum peak of fold change of baseline OCR after palmitic acid injection was significantly higher compared to baseline in the shNTC dox 0 ng/ml and the shNTC dox 10 ng/ml Huh7 cells but not in the shACADS Huh7 cells (1.4-23a). The addition of the uncoupler FCCP (Figure 1.4-22a B, b B) (to trigger maximal

oxygen consumption) induced an increase of OCR in all shACADS and shNTC Huh7 cells. The maximum peak of fold change of baseline OCR after FCCP injection was significantly higher compared to baseline in all shACADS and shNTC Huh7 cells except in the maximal knock-down shACADS (10 ng/ml) Huh7 cells (Figure 1.4-23b). Next, the CPT I inhibitor etomoxir was added to block FAO (Figure 1.4-22a C, b C). The addition of etomoxir inhibited the OCR significantly in all shACADS and shNTC Huh7 cells (Figure 1.4-23c). In the maximal knock-down shACADS Huh7 cells the fold changes of baseline OCR were lower at each time point compared to the null knock-down shACADS Huh7 cells (Figure 1.4-22a) which was statistically significant for the maximal fold change after palmitic acid and FCCP injection (Figure 1.4-23a, b). Further, intermediate shACADS knock-down Huh7 cells exhibited fold changes of baseline OCR that were lower than in null knock-down shACADS Huh7 cells, but higher than in maximal knock-down shACADS Huh7 cells at almost all time points (Figure 1.4-22a).

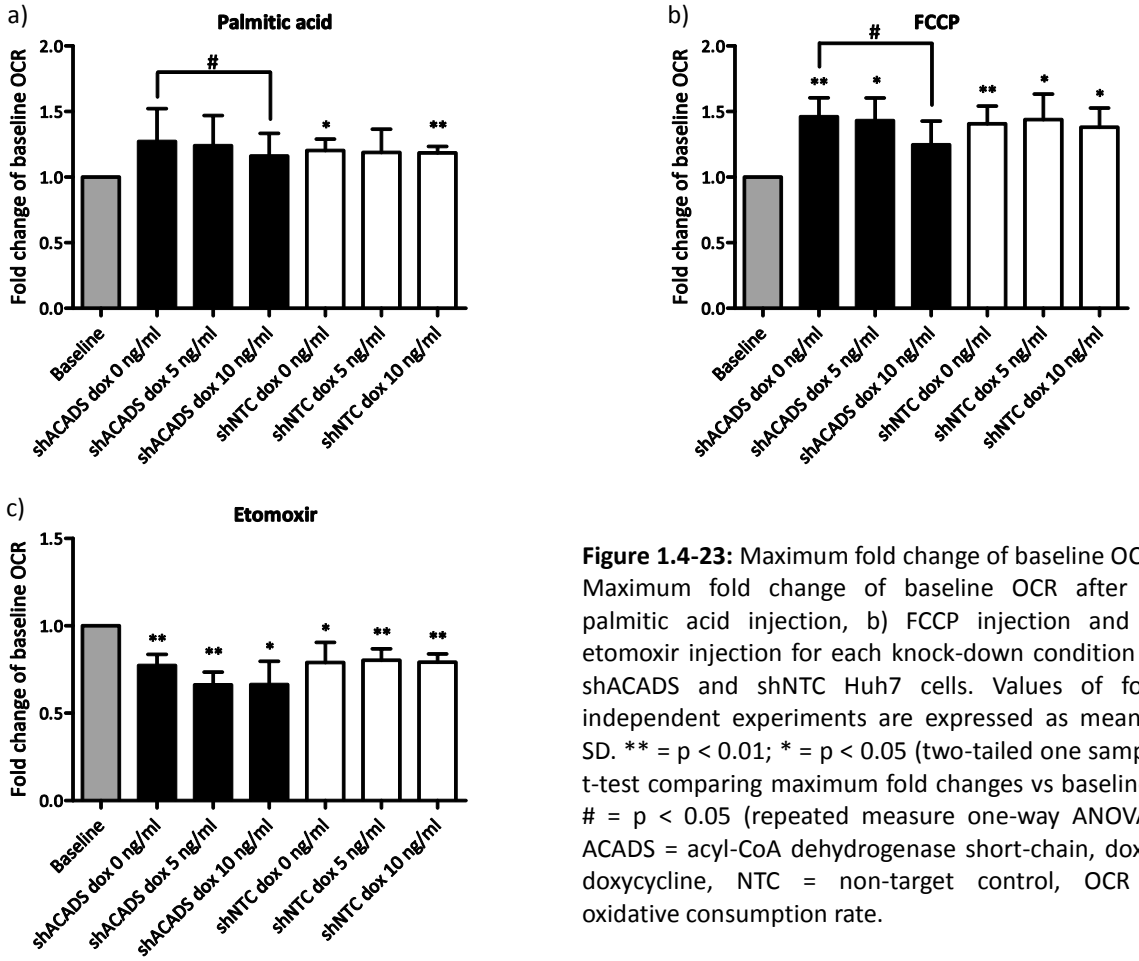

Figure 1.4-23: Maximum fold change of baseline OCR Maximum fold change of baseline OCR after a) palmitic acid injection, b) FCCP injection and c) etomoxir injection for each knock-down condition of shACADS and shNTC Huh7 cells. Values of four independent experiments are expressed as mean + SD. ** = $p < 0.01$; * = $p < 0.05$ (two-tailed one sample t-test comparing maximum fold changes vs baseline). # = $p < 0.05$ (repeated measure one-way ANOVA). ACADS = acyl-CoA dehydrogenase short-chain, dox = doxycycline, NTC = non-target control, OCR = oxidative consumption rate.

Summing up, in contrast to the baseline values a time course, monitoring the stimulation and inhibition of mitochondrial respiration, revealed differences between null-, intermediate- and maximal shACADS knock-down Huh7 cells. The increase in fold change of baseline OCR after palmitic acid injection indicates a stimulation of FAO. The fact that the fold change of baseline OCR in maximal knock-down shACADS Huh7 cells was lower than in the other shACADS Huh7 cells and did not increase significantly after FCCP injection, suggests a decreased mitochondrial respiration probably induced by impaired interaction of FAO and electron transport chain and reduced availability of reducing equivalents.

Efflux of acylcarnitines

Additional to the cell extract the acylcarnitine levels were measured in cell supernatants. A total of 7 measured acylcarnitines were above the limit of quantification. To investigate if the extracellular acylcarnitine levels are related to the intracellular levels, correlations were calculated. Overall, the correlation analysis revealed significant correlations of intra- and extracellular acylcarnitines (Figure 1.4-24), indicating that the measured acylcarnitine levels in the supernatant represent the intracellular acylcarnitine pool.

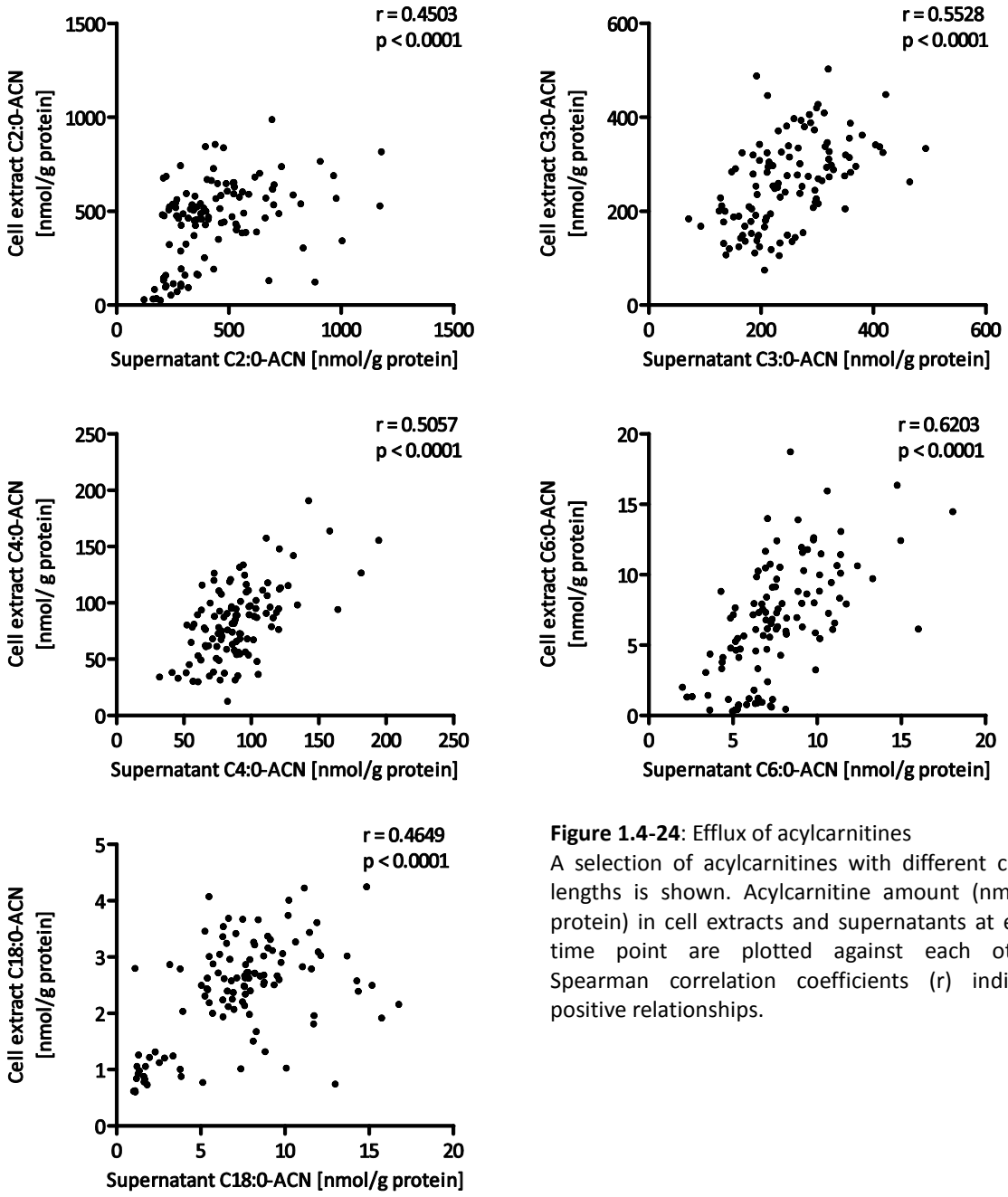

Figure 1.4-24: Efflux of acylcarnitines
A selection of acylcarnitines with different chain lengths is shown. Acylcarnitine amount (nmol/g protein) in cell extracts and supernatants at each time point are plotted against each other. Spearman correlation coefficients (r) indicate positive relationships.

1.5 Discussion

1.5.1 Measurement of FAO flux in genotyped EBV-LCLs confirms association of rs2014355 with biochemical phenotype

GWASs revealed that subjects carrying the rs2014355 C allele are characterized by a decreased plasma C3/C4-acylcarnitine ratio compared to the average population (Gieger et al. 2008; Illig et al. 2010). It was hypothesized that this implies a reduced activity of the enzyme ACADS. To confirm this hypothesis based on fasted plasma measurements, an *in vitro* assay to quantify FAO flux was adapted for the use in genotyped EBV-LCLs, generated from a subpopulation of the KORA-Cohort (http://www.helmholtz-muenchen.de/kora). EBV-LCLs reflect a wide range of metabolic pathways that are specific to the donors, and therefore provide a valuable tool for molecular and functional studies (Amoli et al. 2008; Caron et al. 2002).

A variety of methodologies including *in vitro* functional studies like FAO rate, acylcarnitine profiling subsequent to fatty acid loading, and enzyme studies were used to investigate mitochondrial FAO disorders (Sim et al. 2002). Ensenauer et al. established an assay to quantify FAO function in intact mitochondria. This approach was developed to facilitate highly sensitive, simple, and fast monitoring of lipid-induced metabolic dysfunction and pharmacological effects on FAO (Ensenauer et al. 2012). The assay, formerly used in fibroblasts, primary adipocytes, and adipocyte cell lines was successfully adapted for EBV-LCLs in this thesis.

EBV-LCLs may have pronounced batch effects related to preparation and/or growth rates (Caliskan et al. 2011). Indeed, CS activity in the heterozygous EBV-LCLs was significantly higher compared to the EBV-LCLs homozygous for the minor C allele, which is however unlikely to be a genotype effect. Therefore, the CS activity as a stable marker of mitochondrial mass (Patti and Corvera 2010) and routinely used in the *in situ* metabolite flux assay (Ensenauer et al. 2012), is a valuable factor for normalization of the mitochondrial metabolite flux.

The primary focus of this assay was the result of the C4:0-acylcarnitine measurement since butyryl (C4:0)-CoA is the primary substrate for ACADS (Ghisla and Thorpe 2004; Modre-

Osprian et al. 2009) and enzyme deficiency leads to accumulation of C4:0-CoA by-products including C4:0-acylcarnitine (Corydon et al. 1996). Indeed, C4:0-acylcarnitine accumulated in the EBV-LCLs heterozygous and homozygous for the minor C allele compared to the EBV-LCLs homozygous for the major T allele under both conditions, incubation with and without oleic acid. Interestingly, the use of an additive genetic model assuming a trend per copy of the minor C allele revealed the lowest p-value for C4:0-acylcarnitine after incubation with oleic acid. This is in line with the findings of a study that compared different *in vitro* profiling methods to distinguish the reduced ACADS activity associated with homozygosity of the ACADS variant rs1799958 (AA) or heterozygosity (G/T) compared to wild type (TT) in sequenced fibroblasts. In this study a moderately reduced ACADS enzyme activity for homozygotes compared to the wild type and an intermediate effect for the heterozygotes was reported (Young et al. 2003). To sum up, the accumulation of C4:0-acylcarnitine, after induction of FAO in EBV-LCLs carrying the minor C allele, confirms the hypothesis that the reported association of rs2014355 with the plasma C3/C4-ratio is caused by an impaired ACADS function.

The mitochondrial metabolite flux assay used in this thesis measures ACADS activity indirectly. The direct measurement of the ACADS enzyme activity by using the electron transfer flavoprotein (ETF)-based assay developed by Frerman and Goodman (Frerman and Goodman 1985) was reported to be notoriously difficult (Wanders et al. 1999). Besides, while this approach is reliable for detecting a severe ACADS deficiency, variable results have been reported when fibroblasts were used carrying the ACADS variants (rs1799958 and rs1800556), due to the low ACADS activity in this cell type (Young et al. 2003). The ACADS activity in EBV-LCLs is similar or even lower than in the fibroblasts and therefore the alternative technique of *in vitro* acylcarnitine profiling in which EBV-LCLs are incubated with fatty acids in the presence of excess L-carnitine was the method of choice to indirectly measure ACADS activity in this thesis.

Hornbak et al. proposed that reduced FAO associated with rs2014355 CC could predispose some individuals to type 2 diabetes mellitus (Hornbak et al. 2011). A study comparing the protein expression of the liver, heart, and skeletal muscle of diabetes-prone rats and matched control rats revealed that the FAO pathway was up-regulated except for ACADS. This could potentially cause the buildup of short-chain fatty acyl-CoA, which was in

conjunction with an increase of carnitine acyltranslocase suggesting that short-chain acylcarnitines may be released from the diabetic liver, allowing the recycling of CoA in the presence of decreased flux through ACADS (Johnson et al. 2009). This hypothesis is reflected by the finding that short-chain acylcarnitines are increased in the plasma of diabetic patients (Bene et al. 2013; Mihalik et al. 2010). The biochemical phenotype associated with rs2014355 CC resembles one of the clinical features observed in type 2 diabetes which allows the assumption that variants inducing ACADS activity decrease might predispose for the development of type 2 diabetes. However, the study of Hornbak et al., as well as a previously published meta-analysis (Zeggini et al. 2008; Morris et al. 2012) showed that the analysed ACADS variant (rs2014355 CC) did not associate directly with an increased risk to develop type 2 diabetes in humans. Therefore, the association of rs2014355 with insulin resistance and type 2 diabetes remains controversial and needs further investigation.

Complementary, additional acylcarnitines, especially long-chain acylcarnitines, were significantly different between the genotypes. However, only C16:0- and C18:0-acylcarnitine revealed a significant effect per allele copy. Alterations of long-chain acylcarnitines have not been published in the context of ACADS deficiency. Nevertheless, to take up the issue of the previous paragraph, a human study showed that fasting plasma acylcarnitine levels during euglycemic clamp in type 2 diabetic patients revealed an increase of long-chain acylcarnitine species including C16:0- and C18:0-acylcarnitine (Morris et al. 2012). In contrast Adams et al. did not find increased C16:0- and C18:0-acylcarnitine levels in plasma samples of type 2 diabetic African-American women (Adams et al. 2009) and Bene et al. even reported a decrease of C16:0-acylcarntines in sera from a mixed (males and females) type 2 diabetes population (Bene et al. 2013). Concluding, the current literature is controversial concerning the association of plasma acylcarnitines and type 2 diabetes and additional investigation is needed especially in view of the source, destination and function of plasma acylcarnitines.

Further, the interpretation of altered acylcarnitine species has to be taken with care if they are not significant in the additive genetic model. For example, C6:0-DC-acylcarnitine was highly significantly different between the groups after both incubation with and without oleic acid. However, the C6:0-DC-acylcarnitine level was lower in the heterozygous EBV-LCLs compared to the two homozygous groups, indicating the possibility for genetic variation in genes coding for proteins of the leucine catabolism and/or ketone body formation (Roe et al.

1986). It has to be kept in mind that the complete genetic background of the used EBV-LCLs is unknown and possible gene variations in other loci could be responsible for biochemical alterations rather than attributing all effects to the variation in the ACADS locus.

As mentioned above EBV-LCLs are the preferred choice of storage for patients' genetic material (Amoli et al. 2008) and numerous genetic studies including several GWASs have EBV-LCLs stored in biobanks (Wichmann et al. 2005, Craddock et al. 2010; McCarroll et al. 2008; Simon-Sanchez et al. 2007). Therefore, the here presented assay provides a tool to investigate further gene variants associated with FAO disorders in ready to use biobank material. However, it has to be taken into consideration that genetic instability of EBV-LCLs might cause the accumulation of genetic modifications following their long-term subculture (Oh et al. 2013). The passage number of the EBV-LCLs obtained from the Helmholtz Zentrum München used in the present thesis is unknown; therefore the SNPs of interest were re-sequenced at the Helmholtz Zentrum München which should be a routine procedure before conducting any experiments.

1.5.2 Allele-specific gene and protein expression in cellular models

Understanding the biological pathways and mechanisms mediating the genotype-phenotype correlation identified by GWASs remains a major challenge (Mirkov et al. 2012). Here the elucidation of the biologic mechanism that causes the reduced C3/C4-acylcarnitine ratio associated with rs2014355 was successfully approached by the application of the *in situ* mitochondrial metabolite flux assay. The results indicate that an accumulation of C4:0-acylcarnitine is induced by a decreased ACADS activity. Considerably, the SNP rs1799958 appeared in LD (r^2 = 1.0, European population, 1,000 Genome Phase 1) with rs2014355 in all EBV-LCLs used in this thesis. There is a substantial body of literature stating that rs1799958 encodes proteins with reduced catalytic activity and/or thermostability (Corydon et al. 2001; Gregersen et al. 1998; Corydon et al. 1996). Pedersen et al. proposed that rs1799958 exhibited a temperature-sensitive misfolding and aggregation tendency due to the Gly209Ser exchange in comparison to the wild type, which suggests that the ACADS protein is less efficient in C4:0 acetyl-CoA conversion in carriers of the minor A allele (Pedersen et al. 2003; Pedersen et al. 2008).

In addition to effects on enzyme activity, one might assume that associated SNPs in nontranscribed genomic regions have regulatory effects on the transcriptional level, thereby affecting ACADS mRNA expression. Therefore, rs2014355-dependent expression level of ACADS mRNA and protein was examined. Genotype-dependent decreases in ACADS mRNA and protein levels of EBV-LCLs homozygous for the minor C allele were found. There are concerns that EBV transformation itself, as well as non-genetic factors like amount of and individual response to the EBV virus, the history and passage in cell culture, and culture condition can alter the expression levels of a subset of genes (Carter et al. 2002). Nevertheless, studies evaluating gene expression profiles of EBV-LCLs compared to primary B cells showed that differences in gene expression levels are of small magnitude (Caliskan et al. 2011). Still, ACADS gene expression was also analysed in primary human preadipocytes and did not reveal any genotype-dependent differences. However, the protein levels in primary human preadipocytes were higher in preadipocytes homozygous for the minor C allele compared to the major T allele, which was also shown in mature adipocytes. To cap it all, Mirkov et al reported an association of the rs2014355 C-allele with increased ACADS mRNA levels in human liver tissue samples (Mirkov et al. 2012). One explanation for these inconsistent data is offered by recent findings demonstrating that common variants affecting gene regulation act predominantly in a cell type-specific manner (Dimas et al. 2009; Neph et al. 2012; Maurano et al. 2012). Another explanation might be based on activating and repressing *cis*-regulatory SNPs in LD with rs2014355. Indeed, based on PMCA, an analysis to define regions with *cis*-regulatory potential surrounding a set of linkage SNPs (Claussnitzer M, personal communication), repressing as well as activating allelic effects were found for four SNPs in strong LD with rs2014355. Interestingly, the *cis*-regulatory potential varied between the used liver- and adipocyte cell line which is in line with the above stated tissue specificity of gene regulation. Of note, rs2014355 (also analysed in the reporter gene assay although not predicted *cis*-regulatory) did not exhibit any regulatory effects although it is assigned as GWAS lead SNP. To sum up, each single variant showing activating or repressing *cis*-regulatory activity – or a combined effect of several variants – could contribute to a tissue dependent alteration in ACADS mRNA and protein expression. In view of the persuasive evidence that the rs1799958 minor A allele associates with less efficient ACADS the here reported activating *cis*-regulatory variants might as well act compensatory by increasing gene expression.

However, to make sure if a transcription factor binds to the region comprising the *cis*-regulatory SNPs, further *ex vivo* studies such as electrophoretic mobility shift assays have to be carried out. This could reveal differential binding of proteins depending on the SNP alleles, and affinity chromatography combined with LC-MS/MS could be used to identify such binding factors. Besides, *in vivo* verification of protein-DNA interaction at a specific genomic locus of interest could be performed using chromatin immunoprecipitation.

1.5.3 Gradual ACADS knock-down revealed specific alterations in acylcarnitine flux and changes in mitochondrial respiration

Functional studies of SNPs are often limited by the availability of relevant cell models (Paul et al. 2011) carrying the corresponding genotype. In this thesis, EBV-LCLs with the genotype of interest were used to study FAO. However, EBV-LCLs are derived from lymphocytes and although they are known to oxidise fatty acids their main energy substrates are glucose and glutamine (Yaqoob et al. 1994). Therefore, a cell culture model was generated from a hepatoma cell line that allowed a partial down-regulation of the ACADS protein level and thereby represents an *in vitro* genotype-phenotype model to study moderate genetic effects from common variants. Here, the ACADS knock-down cell model was used to analyse the effect of ACADS protein levels on intracellular acylcarnitine flux in Huh7 cell extracts, on acylcarnitine levels in Huh7 cell supernatants, as well as mitochondrial respiration in response to induction of FAO. The efficiency of enzyme knock-down was confirmed by both western blot and phenotype analysis (C4:0-acylcarnitine accumulation).

Feedback-control of FAO

The induction of FAO, by offering palmitic acid as solely available energy substrate, revealed an altered acylcarnitine pattern during the time course comparing the intermediate- and maximal knock-down shACADS Huh7 cells to null knock-down shACADS Huh7 cells. Both the intermediate- and maximal knock-down shACADS Huh7 cells led to an initial C4:0-acylcarnitine accumulation at baseline, induced by the reduced or almost complete absence of ACADS protein, respectively. Seven minutes after incubation with palmitic acid both the C4:0-acylcarnitine level and the C16:1-, C14:1-, C12:1-acylcarnitine levels were higher in the maximal knock-down shACADS Huh7 cells compared to the null knock-down shACADS Huh7 cells. C16:1-, C14:1-, C12:1-acylcarnitine are the main products of the VLCAD (Ghisla and

Thorpe 2004), which are likewise substrates for the long-chain enoyl-CoA hydratase (Ishikawa et al. 2004). These results indicate a positive feedback on the VLCAD or a negative feedback on the long-chain enoyl-CoA hydratase. In fact both either an increased VLCAD activity or a decreased long-chain enoyl-CoA hydratase activity would result in a subsequent transient intracellular increase of long-chain enoyl-carnitines, respectively (Ghisla and Thorpe 2004; Ishikawa et al. 2004). The following time courses in the intermediate and maximal knock-down shACADS Huh7 cells compared to the null knock-down shACADS Huh7 cells are distinct by a continuous lower concentration of saturated acylcarnitine levels of all chain lengths. Such reduced levels of acylcarnitines of different chain length may be explained by an inhibitory effect on the CPT I resulting in a reduced formation of C16:0-acylcarnitine from palmitic acid in the maximal knock-down shACADS Huh7 cells. Thereby, less palmitic acid would enter mitochondria and would be oxidised as indicated by the continuously lower concentration of long-, medium-, and short-chain acylcarnitine intermediates resulting from C16:0-acylcarnitine break down (Figure 1.5-1). To confirm this hypothesis CPT-1 enzyme activity needs to be measured during the time course of palmitic acid loading.

So far there have not been intensive investigations on the influence of ACADS deficiency on the control of FAO flux. Although it was demonstrated that ACADS deficiency decreased the oxidation rate of butyrate (Ribes et al. 1998) whereas myristic acid (Tein et al. 1999) oxidation rates were normal. Palmitic acid oxidation rates were shown to be normal by Wanders et al. (Wanders et al. 1999), whereas Ventura et al. found that acylcarnitine production from palmitic acid was decreased (Ventura et al. 1999). However, details on regulatory effects of ACADS deficiency have not been published so far.

Numerous reports suggest that all steps of FAO may be strongly inhibited by their reaction products. The acyl-CoA dehydrogenases are inhibited by their trans-2 enoyl-CoA products (Powell et al. 1987) and the enoyl-CoA hydratases by their 3-hydoxyacyl-CoA products (He et al. 1989). The 3-hydroxyacyl-CoA dehydrogenases can be inhibited by their 3-ketoacyl-CoA products (He et al. 1989) as can the 3-ketoacyl-CoA thiolases by acetyl-CoA (Olowe and Schulz 1980; Yao and Schulz 1996). Therefore, FAO might be regulated by product accumulation at multiple sites (Powell et al. 1987), including the short-, medium-, and long-chain acyl-CoA dehydrogenases. In addition, 3-ketoacyl-CoA compounds can inhibit acyl-CoA dehydrogenases (Davidson and Schulz 1982) and enoyl-CoA hydratases (Waterson and Hill

1972). Further, it was hypothesized that full activity of 2-enoyl-CoA hydratase and L-3-hydroxyacyl-CoA dehydrogenase, of the trifunctional protein, require the downstream enzyme L-3-hydroxyacyl-CoA dehydrogenase 3-ketoacyl-Co thiolase, respectively. It was proposed that both enzymes are subject to a negative feedback by their respective reaction product (Fould et al. 2010). Moreover, high concentrations of acyl-CoAs can alter reaction kinetics of general acyl-CoA dehydrogenase by the butyryl-CoA/crotonyl-CoA couple (Schopfer et al. 1988) indicating that substrates or substrate/product couples can regulate enzyme kinetics. Overall, despite numerous reports indicating a feedback control in FAO at diverse levels of the FAO enzyme cascade, it remains difficult to explain the here observed metabolite patterns resulting from an ACADS knock-down.

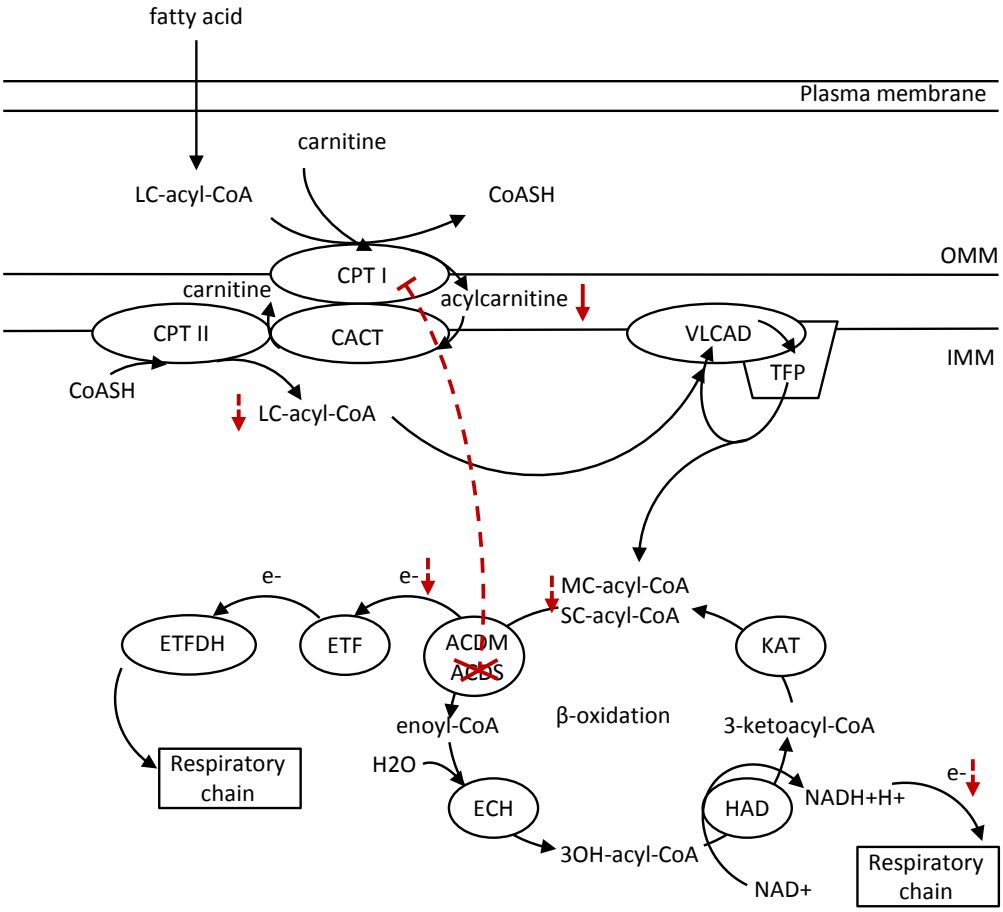

Figure 1.5-1: Schematic illustration of proposed regulatory mechanism in maximal knock-down shACADS Huh7 cells after loading with palmitic acid
ACDM = acyl-CoA dehydrogenase medium-chain, ACDS = acyl-CoA dehydrogenase short-chain, CACT = carnitine acylcarnitine translocase, CPT I = carnitine palmitoyltransferase I, CPT II = carnitine palmitoyltransferase II, ECH = enoyl-CoA hydratase, ETF = electron transfer flavoprotein, ETFDH = electron transfer flavoprotein dehydrogenase, HAD = hydroxyacyl-CoA dehydrogenase, IMM = inner mitochondrial membrane, KAT = ketoacyl-CoA thiolase, LC = long-chain, MC = medium-chain, OMM = outer mitochondrial membrane, SC = short-chain, TFP = trifunctional protein, VLCAD = very long-chain acyl-CoA dehydrogenase.

Noteworthy, Wang et al. provided compelling evidence for the existence of a FAO complex that associates with electron transport chain supercomplexes in mitochondria. The FAO complex was proposed to be dynamic, because CPT-2, VLCAD and trifunctional protein are membrane-bound proteins, whereas ACADM, LCAD and ACADS are all considered "soluble" matrix proteins. The membrane-associated FAO enzyme might form the core of the FAO complex while the other enzymes interact more loosely with this core (Wang et al. 2010). The absence or reduced levels of ACADS might impair the association of the FAO complex proteins and thereby account for a dysfunctional substrate channelling of VLCAD/ enoyl-CoA hydratase.

Overall, the here presented data and numerous literature reports indicate that mitochondrial FAO is a dynamic process that is regulated at multiple sites. Alterations of any component of this complex system could lead to disturbance of the usual FAO flux (Wang et al. 2010).

Neither the feedback mechanism on VLCAD or long-chain enoyl-CoA hydratase nor the inhibition of CPT I, both induced by the ACADS knock-down, are known from studies in human ACADS deficiency. Moreover, it was shown that none of the C2- to C16-acylcarnitines inhibits CPT I in mitochondria isolated from rat liver (Baillet et al. 2000), supposing a Huh7 hepatoma cell line specific effect. Although cancer cells adapt their metabolism to produce all molecules and energy required to promote tumour growth (Solaini et al. 2011), it was demonstrated that Huh7 cells exhibit hepatic markers including expression of albumin and an array of hepatic nuclear receptors. Further, Huh7 cells have the capacity for CYP3A4 induction by phenobarbital treatment, a response that is maintained only in highly differentiated hepatocytes (Zamule et al. 2008). Therefore, Huh7 cells are a useful cell culture model for the liver which is a substantive site of FAO to provide ketone bodies to the peripheral circulation (Eaton et al. 1996). This is an advantage over the usual studies to biochemically confirm ACADS deficiency which are performed in patients' fibroblasts or PBMC by *in vitro* loading with fatty acids. Low activities of ACADS were shown in fibroblasts (Young et al. 2003) requiring long incubation times for *in vitro* loading with fatty acids.

These incubation times last for at least 2h (Ensenauer et al. 2012) up to 120h (Schulze-Bergkamen et al. 2005; Young et al. 2003). Up to now, there are no published studies investigating short-term effects of induced FAO in ACADS deficient cell lines. This suggests

the alternative possibility that the monitored short-term effects are counter- regulated over a longer period of time. Therefore, future investigations should include measurements of prolonged time courses to see when a steady state is reached and if there are more regulatory events preferably in primary human hepatocytes. Additionally, test series with fatty acids of different chain length (e.g. myristic acid) would be of interest to investigate if there are similar results. Also short-term experiments in genotype specific cell lines like fibroblasts could elucidate the findings of this thesis. Furthermore, short- and long-term time course measurements of FAO should be measured in skeletal muscle. A comparison of potential regulatory events in skeletal muscle and liver are of interest because FAO serves a different role in both tissues. FAO provides a major source of ATP for skeletal muscle, whereas hepatic FAO provides ketone bodies to extra-hepatic organs (Eaton 2002).

Noteworthy, acylcarnitines were used as surrogate measures for acyl-CoAs and as proxies for FAO intermediates (Krug et al. 2012; Modre-Osprian et al. 2009). It is usually considered that the observed acylcarnitine profiles reflect the intramitochondrially accumulating acyl-CoAs which are exported out of the mitochondria as their corresponding carnitine esters (Noland et al. 2009; Sim et al. 2002; Ventura et al. 1999; ter Veld et al. 2009). Yet, Violante et al. demonstrated that the profile of acylcarnitines observed in plasma may not fully reflect the profile of acyl-CoA species accumulating within the mitochondrial matrix (Violante et al. 2013). Whether the intracellular measured acylcarnitines represent the acyl-CoA intermediates of FAO or not remains elusive. Future studies should apply direct measurements of acyl-CoAs based on fluorescent derivatives of mass-spectrometry (Eaton 2002) that comprise substrate and products of the 3-hydroxyacyl-CoA dehydrogenase and the 3-ketoacyl-CoA thiolase.

Efflux of accumulating C4:0-acylcarnitine

Plasma C4:0-acylcarnitine accumulation is used as readout for ACADS deficiency. In functional cell culture assays C4:0-acylcarnitine accumulation is mostly measured in supernatants of cells incubated with fatty acids (Violante et al. 2013; Schulze-Bergkamen et al. 2005; Okun et al. 2002; Law et al. 2007; Young et al. 2003) or in pooled cell extract and supernatant (Ensenauer et al. 2012; Ventura et al. 1999). Here, C4:0-acylcarnitine levels were measured separately in cell extracts and supernatants. It was demonstrated, that early accumulating C4:0-acylcarnitine levels in cell extracts from maximal knock-down shACADS

Huh7 cells decreased during the time course after incubation with palmitic acid in the cell extracts while C4:0-acylcarnitine levels in the supernatant accumulated, indicating an efflux of intracellular C4:0-acylcarnitine to the medium. If acyl-CoAs accumulate in the mitochondrial matrix, they deplete free coenzyme A but can also disturb multiple metabolic pathways by inhibition of enzymes especially long-chain acyl-CoAs and long-chain acylcarnitines (Ventura et al. 2007; Bell 1980). The accumulating intermediates can be eliminated from the mitochondrial matrix and extra-mitochondrial compartments as acylglycines, acylcarnitines, or free acids and thereby replenish the free CoA pool (Violante et al. 2013). C4:0-acyl-CoA is converted via alternative pathways into different metabolites: C4:0-carnitine, butyric acid, butyrylglycine and EMA. All of these metabolites may have toxic effects, which could result in the development of clinical symptoms. Indeed, this has been suggested for EMA and butyrate (Leipnitz et al. 2003; Birkebaek et al. 2002). The observed efflux of intracellular accumulating C4:0-acylcarnitine reflects a potential protective mechanism that guards the cell from possible toxic effect of intracellular accumulating C4:0-acylcarnitine and the depletion of free CoA.

C2:0-acylcarnitine levels were not decreased in shACADS knock-downs

Ventura et al. argued that incubation of ACADS-deficient fibroblasts with palmitic acid for 96h resulted in a 66% lower C2:0-acylcarnitine level compared to control cells (Ventura et al. 1999). Similar results were demonstrated by Okun et al. (Okun et al. 2002). Surprisingly, C2:0-acylcarnitine levels were not decreased in the intermediate- and maximal knock-down shACADS Huh7 cells. On top of that, the C2:0-acylcarnitine amount in maximal knock-down shACADS Huh7 cells was transiently higher than in the shACADS control Huh7 cells. Based on the fact that the reaction catalysed by ACADS results in the production of two acetyl-CoAs (Nelson et al. 2008) and the maximal knock-down shACADS Huh7 cells have less FAO substrate available by the proposed inhibition of CPT I, the C2:0-acylcarnitines levels in the intermediate- and maximal knock-down shACADS Huh7 cells are unlikely to originate solely from FAO. Acetyl-CoA is also formed in glucose and amino acid metabolism. Pyruvate which is the output of glycolysis or stems from metabolism of glucogenic amino acids can be converted to acetyl-CoA and ketogenic amino acids can be directly degraded to acetyl-CoA (Nelson et al. 2008). However, studies performed in isolated hepatocytes from starved rats revealed an inhibitory effect of palmitic acid oxidation on hepatic glycolysis and glucose

utilization (Hue et al. 1988; Siess and Wieland 1976), an observation which would exclude glycolysis as acetyl-CoA source. Further considerations have to be taken into account: Firstly, if levels of circulating fatty acids are high, the production of acetyl-CoA from fatty acid breakdown exceeds the cellular energy requirements. To make use of the energy available from the excess acetyl-CoA, ketone bodies are produced (Nelson et al. 2008). Studies in Fao rat hepatoma cells revealed a lack of HMG-CoA synthase and thereby disable Fao cells to perform ketogenesis. This metabolic characteristic could be a common feature in hepatoma cell lines (Prip-Buus et al. 1992). Secondly, hepatoma cells have a truncated TCA exporting citrate into cytosol with consequently decreased concentrations of mitochondrial oxidisable citrate (Deberardinis et al. 2008). An explanation of the finding concerning C2:0-acylcarnitine would go beyond the scope of the current experimental set up. A first step to gain further insights could be investigations of cell metabolism in Huh7 cell lines to elucidate if it reflects the metabolic alteration of hepatoma cells.

Time course measurements during incubation with palmitic acid revealed decreasing C5:0-acylcarnitine levels

C5:0-acylcarnitine was the only measured acylcarnitine that decreased during the time course after incubation with palmitic acid. C5:0-acylcarnitines are comprised of intermediates in mitochondrial isoleucine and leucine catabolism (Newgard 2012). The regulatory effects of fatty acids on the oxidative decarboxylation of leucine and 4-methyl-2-oxopentanoate were investigated in the isolated rat heart. Infusion of the long-chain fatty acid palmitic acid resulted in both an inactivation of the branched-chain 2-oxo acid dehydrogenase and an inhibition of the measured metabolic flux through this enzyme complex (Buxton et al. 1984). Therefore, the decrease of C5:0-acylcarnitine might be explained by the inhibition of palmitic acid on leucine catabolism. This is in line with the observation from the Human Metabolome Study which revealed that C5:0-acylcarnitine was not affected in times of elevated FAO, e.g. during fasting or exercise (Krug et al. 2012). Surprisingly, the C3:0-acylcarnitine amount which is by-product of both isoleucine and valine catabolism (Newgard 2012) remained unchanged throughout the time course, although the same enzyme complexes catalyse the catabolism of isoleucine, leucine and valine.

Influence of shACADS knock-downs on mitochondrial respiration

Optimal assay conditions for FAO measurement in Huh7 cells, using Seahorse technology, were determined based on the Seahorse user protocols (Seahorse Bioscience Inc) for Huh7 cells (Portius 2012). It was demonstrated, that the induction of OCR in the maximal knock-down shACADS Huh7 cells was reduced compared to the intermediate knock-down and the null knock-down shACADS Huh7 cells by stimulation with palmitic acid and FCCP, while baseline OCR was similar in all shACADS and shNTC Huh7 cells. The rate of respiration in mitochondria is tightly regulated by cellular energy demands; it is generally limited by the availability of adenosine diphosphate (ADP) as a substrate for phosphorylation. Intracellular concentration of ADP is only one measure of the energy status of cells. Another related measure is the [ATP]/([ADP][P_i]) ratio which is normally very high, so the ATP-ADP system is almost fully phosphorylated. Only if ADP is available for oxidative phosphorylation, the rate of respiration increases to generate ATP (Nelson et al. 2008). A mechanism to control FAO flux is particularly important in tissues for which the primary function of FAO is provision of ATP for contraction, such as skeletal and cardiac muscle (Eaton 2002). However, control mechanisms of FAO flux were also shown in the liver (Latipää et al. 1986; Bremer and Wojtczak 1972). FAO provides ATP via acetyl-CoA production and additionally by direct generation of reducing equivalents (Fould et al. 2010). FAO is linked to the respiratory chain at two stages, that of the 3-hydroxyacyl-CoA dehydrogenase at complex I via NAD+/NADH, and the acyl-CoA dehydrogenases to ubiquinone via ETF and its oxidoreductase. Inhibition of either of these stages leads to inhibition of FAO in rat liver mitochondria (Latipää et al. 1986; Bremer and Wojtczak 1972). To sum up, ATP and ADP concentrations set the rate of FAO via the ETF- or NADH linked step. However, the results of this thesis indicate that under this specific experimental set up the maximal ACADS knock-down seems to decelerate mitochondrial respiration. Thus, a reduction in the amount of reducing equivalents and acetyl-CoA induced by the ACADS knock-down, as well as by the hypothesized inhibitory effect on the CPT I resulting in a reduced substrate supply could be one reason. Therefore, further experiments should include measurements of NAD+/NADH, FAD/$FADH_2$ and acetyl-CoA as well as the above mentioned CPT I activity.

Amaral et al. presented data which indicate that EMA, a metabolite of butyryl-CoA, disturbs mitochondrial homeostasis by reducing succinate- and malate-supported oxygen

consumption through a competitive inhibition of the mitochondrial dicarboxylate carrier in rat brain mitochondria (Amaral et al. 2012). Beyond, Wang et al. provided evidence for the existence of a FAO complex that is physically associated with electron transport chain supercomplexes in mitochondria (Wang et al. 2010). Therefore, the lack of ACADS might diminish FAO complex formation and interaction with the electron transport chain, and thereby affects the electron transfer from FAO to the electron transport chain and leads to a reduced OCR. To confirm this hypothesis the interaction of FAO and electron transport chain should be measured by applying a "bridging assay" which reflects the interaction of FAO and electron transport chain as measured by reduction of cytochrome *c* in response to the oxidation of an acyl-CoA substrate (Wang et al. 2010). Further enlightenment of the observations could be obtained by measurements of ATP/ADP concentrations and the mitochondrial membrane potential, as well as the formation of EMA as potential inhibitor of mitochondrial respiration.

There is evidence that the FAO pathway plays a role in reactive oxygen species (ROS) generation. It was anticipated that relative amounts of ETF and various partner dehydrogenases are a potential regulatory mechanisms in ROS generation (Rodrigues and Gomes 2012). Indeed, it was proposed that ACADS deficiency is associated with increased oxidative stress that likely contributes to the pathophysiology of ACADS deficiency (Schmidt et al. 2010; Zolkipli et al. 2011; Gregersen et al. 2012). To substantiate the hypothesis of increased ROS generation in this specific cell culture model, a vital additional experiment would be the measurement of intracellular ROS production in combination with the induction of FAO.

Beyond, one more connection between ACADS knock-down and mitochondrial energy metabolism is the interplay between FAO and the TCA. The entrance of acetyl-CoA into the TCA might be diminished because of lacking oxaloacetate synthesized in an anaplerotic reaction from pyruvate (endproduct of glycolysis) due to glucose depletion by starvation of the cells (Nelson et al. 2008). This would also lead to a decrease in reducing equivalents for electron transfer in the respiratory chain. Further, acyl-CoAs showed an inhibitory impact on the pyruvate dehydrogenase complex and alpha-ketoglutarate dehydrogenase complex activity. Both are the rate limiting enzymes of the TCA cycle, whereas the corresponding acylcarnitines did not affect pyruvate dehydrogenase complex activity, but had a small

inhibitory impact on alpha-ketoglutarate dehydrogenase complex activity (Sauer et al. 2008). This provides a further potential explanation for the reduced OCR in the maximal knock-down shACADS Huh7 cells.

The lower oxygen consumption capacity of the maximal knock-down shACADS Huh7 cells is in line with the observation that ACADS-deficiency clinically manifests most likely during periods of metabolic stress, when the mobilization and utilization of fatty acids fail to serve added needs (van Maldegem et al. 2006). Clinical experience substantiates a low tolerance to exercise (van Maldegem 2011) and mouse models showed cold intolerance with significant impact on survival (Schuler et al. 2004).

Etomoxir is a member of a family of substituted 2-oxirane-carboxylic acids that inhibit mitochondrial long-chain FAO. Once converted to its CoA ester, etomoxir irreversibly binds to the CPT I catalytic site and prevents long-chain fatty acids from entering the mitochondrion (Wolf 1992). Here, etomoxir was used to confirm that fuels from FAO are used for respiration. Interestingly, etomoxir decreases oxygen consumption even beneath the baseline value. This suggests that the cells already switched their metabolism to FAO before addition of palmitic acid, probably induced by the 1h starvation period. As a matter of fact, an alternative explanation could be the suggestion that etomoxir, in addition to blocking fatty acid transport into mitochondria, may partially inhibit the electron transport chain resulting in reduced oxygen consumption (Pike et al. 2010).

Efflux from intra- to extracellular milieu

Plasma acylcarnitines are the most important biomarkers currently used in the postnatal diagnosis and neonatal screening of mitochondrial fatty acid FAO disorders (Rinaldo et al. 2008; Sim et al. 2002). When acyl-CoA production exceeds consumption, these intermediates can be converted back to their acylcarnitine counterparts and exported from the mitochondria into the general circulation. The finding that carnitine supplementation improves glucose tolerance while increasing circulating acylcarnitines promotes the interpretation that production and efflux of these metabolites is beneficial rather than harmful (Noland et al. 2009). The positive correlation of intra- and extracellular short-, medium-, and long-chain acylcarnitines in the knock-down model suggests that the extracellular reflects the intracellular acylcarnitine pool. An exception was the opposed intra-

and extracellular C4:0-acylcarnitine levels in the maximal knock-down shACADS Huh7 cells. However, the true origin of acylcarnitines and their transport across the mitochondrial and plasmalemmal membranes into extracellular space remains elusive (Violante et al. 2013). Considering that, the cell line used and the experimental set up constitutes a possible model to study the conversion of accumulating acyl-CoA intermediates back to acylcarnitines and their exit from organelle and liver cells. This provides a supplementary model to the already used primary human skeletal myocytes (Noland et al. 2009) and fibroblasts (Violante et al. 2013).

1.6 Conclusion and outlook

The results from the *in situ* mitochondrial metabolite flux assay confirm the GWASs hypothesis stating that the association of rs2014355 with plasma C3/C4-acylcarnitine ratio implies a reduced ACADS activity. Gene- and protein expression analysis in EBV-LCLs, primary preadipocytes and adipocytes in combination with reporter-gene assays of bioinformatically predicted *cis*-regulatory variants in Huh7- and 3T3L1-cells suggested *cis*-regulatory functions of four SNPs in high linkage to the GWASs-associated variant, but not for the GWASs lead SNP rs2014355 itself.

Based on the literature the here observed genotype-dependent decreased ACADS activity associated with rs2014355 may be explained by the non-synonymous coding variant (rs1799958) that lies in perfect LD (r^2 = 1.0, European population, 1,000 Genome Phase 1) with rs2014355. In addition, repressing *cis*-regulatory variants that were found in Huh7- and 3T3L1-cells might contribute to the decreased ACADS activity by decreasing ACADS mRNA expression. However, also several activating *cis*-regulatory variants were found in Huh7- and 3T3L1-cells which support the finding that ACADS protein levels are up-regulated in primary human preadipocytes and mature adipocytes. The findings of this thesis, together with the reported increased ACADS mRNA levels in primary liver tissue (Mirkov et al. 2012) implies compensatory effects to cope with the impaired enzyme function by increasing gene and protein expression. Yet, fine-mapping of the *ACADS* locus in a GWAS that measured metabolic traits in human plasma is needed to reveal additional SNPs or other genetic variants that have not been included in the original genotyping platform. Thereby, association signals with metabolic traits could be specified and possibly haplotypes could be identified that might be of great interest to study activating or repressing *cis*-regulatory effects.

Moreover, the here inferred *cis*-regulatory activity provides fundamentals for experiments exploring differential binding of transcription factors depending on the SNP alleles. This is of special interest in situations of metabolic stress when differential transcription factor binding, resulting in subsequent increased ACADS gene expression, could compensate for impaired ACADS protein function. This could be explored in cell culture models simulating metabolic stress situations, e.g. prolonged fasting.

The knock-down of ACADS revealed a biochemical phenotype (C4:0-acylcarnitine accumulation) depending on the residual protein amount modelling the SNP associated reduced ACADS activity. Palmitic acid loading showed early, dynamic regulatory events which disrupt the usual FAO flux depending on the residual ACADS protein amounts. Further, the mitochondrial respiration was decelerated probably caused by a decreased amount of reducing equivalents due to the disrupted FAO flux or inhibitory effects of arising metabolites. This cell model could be used to shed light into the pathophysiology of ACADS deficiency during metabolic decompensation.

This is the first time that short-term effects of palmitic acid loading are studied in ACADS deficient cells. Evidence is provided that the alteration of one component of the complex interaction system of the FAO leads to regulation at multiple sites including mitochondrial respiration. The system could be of further use to gain deeper insights into so far undiscovered regulatory mechanisms of FAO and closely connected pathways.

Both, the *in situ* mitochondrial metabolite flux assay and the chemically inducible knock-down system provide valuable tools to investigate biological functions of associated GWASs SNPs. The partial regulatory knock-down system bypasses the often limited availability of relevant cell models to study functional SNPs and is useful to validate SNP-associated genes or to identify target genes.

2 Postprandial metabolic and inflammatory activation of human PBMC

2.1 Introduction

Numerous lines of evidence indicate that macronutrient intake activates peripheral mononuclear cells (PBMC) (van Oostrom et al. 2004; Gower et al. 2010) mediated by the NF-κB pathway (Dandona et al. 2010). Increasing plasma concentrations of endotoxin (lipopolysaccharide), lipopolysaccharide binding protein and the expression of its receptor (TLR4) induced by high-fat, high-carbohydrate meals contribute to this increased oxidative and inflammatory stress (Ghanim et al. 2009). However, the role of other signalling pathways in postprandial activation of PBMC remains largely elusive. In this context, insulin signalling is a prominent contender, in particular because numerous reports show an interrelationship of inflammatory and insulin signalling pathways (Ghanim et al. 2007; Ueki et al. 2004; Li et al. 2007; Rui et al. 2002; Kim et al. 2008; Houstis et al. 2006; Shoelson et al. 2003).

Two downstream targets of insulin signal transduction, the Akt and the mammalian target of rapamycin (mTOR) pathway, have been implicated in immune cell homeostasis (MacIver et al. 2008; Di Paolo et al. 2006); e.g. mTOR integrates growth factor signals relayed by insulin and insulin-like growth factors, nutrient signals generated by amino acids and energy signals acting through AMP-activated kinase in PBMC (Zoncu et al. 2011). Apart from their metabolic function, the importance of Akt and mTOR signalling in innate and adaptive immunity has been established during recent years. The regulation of both pathways by several intra- and extracellular stimuli including specific receptors, heat shock, oxidative stress and cytokines shows their involvement in a multitude of immunomodulatory processes (MacIver et al. 2008; Thomson et al. 2009; Pierau et al. 2012; Lee et al. 2011; Kim et al. 2012). Thus, both metabolic signalling pathways provide an important link between metabolism and immune cell function. However, up to now an activation of these pathways by defined meals has not been demonstrated, and moreover, the interaction of metabolic and inflammatory signalling in PBMC upon macronutrient intake remains poorly understood.

The present study was designed to investigate the effect of three different test meals on metabolic and inflammatory pathways in PBMC. Assessing the effects of test meals, the

study aimed to further unravel the link between inflammatory and metabolic signalling in PBMC. For this purpose, NF-κB binding activity, IκB-α protein degradation and phosphorylation of Akt and S6K as marker of mTOR activity (Beugnet et al. 2003) as well as gene expression of both NF-κB and Akt-FOXO target genes were measured. In addition, plasma insulin as a major regulator of Akt and S6K phosphorylation was determined. In this study, it was of particular interest to assess the dynamics of pathway activation as well as potential inter-individual differences.

2.2 Methods

2.2.1 Subjects

Six healthy, non-smoking, normal weight (body mass index (BMI) = 24.8 ± 2.5 kg/m^2) males aged 40-60 (44.3 ± 5.2) years were included in the study (clinical characteristics in Table 2.2-1). Each subject was subjected to three defined meal tests at the Human Study Centre of the Else Kröner-Fresenius-Centre for Nutritional Medicine (EKFZ) of the Technische Universität München between 8.00 and 9.00 am after a 12h overnight fast on three different days separated by at least three days.

Table 2.2-1: Baseline characteristics of the study participants

Variable	Mean SD	Range
Baseline characteristics	n = 6	
Age (years)	44.3 ± 5.2	40 - 53
Weight (kg)	83.0 ± 10.0	72.9 - 99.9
BMI (kg/m^2)	24.8 ± 2.5	22.3 - 28.6
WHR	0.95 ± 0.1	0.89 - 1.0
Lean mass BIA (kg)	69.6 ± 8.2	62.6 - 84.8
Fat mass BIA (kg)	13.4 ± 4.3	9.3 - 18.4
Body fat BIA (%)	16.1 ± 5.2	11.2 - 22.1
Blood pressure (mmHg)		
Systolic	125.5 ± 8.8	120 - 140
Diastolic	78.3 ± 4.1	70 - 80
Clinical chemical parameters		
Fasting blood glucose (mg/dl)	79.3 ± 6.7	70.8 - 90.8
Cholesterol (mg/dl)	193.2 ± 24.1	150 - 216
HDL (mg/dl)	60.7 ± 5.6	53 - 67
LDL (mg/dl)	122.2 ± 20.8	90 - 150
Triglycerides (mg/dl)	88.3 ± 16.9	60 - 112
GOT (U/l)	31.7 ± 9.7	26 - 49
GPT (U/l)	26.3 ± 7.4	20 - 40
Creatinine (mg/dl)	0.87 ± 0.05	0.79 - 0.94

BIA = bioelectrical impedance analysis, GOT = glutamic oxaloacetic transaminase, GPT = glutamic pyruvate transaminase, HDL = high-density lipoprotein, LDL= low-density lipoprotein, WHR = waist to hip ratio

At each day, fasting blood samples were obtained and subjects consumed one of the following meals: (1) a high-fat, high-carbohydrate (HFHC) meal containing 4630 KJ (48% carbohydrates, 11% protein, and 39% fat), (2) a standard oral lipid tolerance test (OLTT) consisting of three parts Fresubin Energy Drink (Fresenius Kabi, Bad Homburg, Germany) and one part Calogen (Nutricia, Zoetemeer, The Netherlands) (24% carbohydrate, 8% protein, and

67% fat) (the volume of the liquid meal was calculated for each volunteer to provide 35 g fat/m^2 body surface area), (3) a healthy breakfast (HB) containing 2710 KJ (55% carbohydrates, 19% protein, and 23% fat) (Nutrient composition of the meals in Table 2.2-2). Additional blood samples were obtained 1, 2, 3, 4 and 6h after the HB and additionally at 8h after the OLTT and HFHC meal. The study was conducted according to the guidelines of the Declaration of Helsinki and all procedures involving human subjects were approved by the ethics committee of the Technische Universität München. Written informed consent was obtained from all subjects. The study was registered as DRKS00004335 (www.germanctr.de).

Table 2.2-2: Nutrient composition of test meals per dose

Test meal	Big Mac Menu	Healthy breakfast	OLTT
composition	Big Mac, medium size fries, 0.5 l Fanta, ketchup (Mc Donalds, Germany)	100 g of whole grain bread , 35 g of cream cheese, 5 g margarine, 50 g boiled ham, 50 g tomato, 150 g yoghurt, 150 g apple, 200 g orange juice, 250 ml of herb tea	1:4 mixture of commercial available Calogen®neutral (Nutricia, Zoetemeer, Netherlands) and Fresubin® energy drink chocolate (Fresenius Kabi, Bad Homurg, Germany)
	per dose	per dose	per dose*
KJ	4630	2710	3987.8
kcal/KJ	1110	646	959.1
protein [g]	31.1	30.5	17.9
protein [%]	11	19	7.7
carbohydrates [g]	132	87.8	60.1
carbohydrates [%]	48	55	25.7
fat [g]	49.4	17.2	71.8
fat [%]	39	23	69.6
SFA [g]	19.8	8.3	7.2
MUFA [g]	11.8	5.8	44.2
PUFA [g]	12.5	2.6	20.4
cholesterol [g]	0.066	0.0554	≤12
fiber [g]	5.43	12.6	0
water [ml]	626	901	249.4
* on average 425 ml per dose			

2.2.2 Blood sampling and PBMC isolation

Venous blood samples were taken from subjects' forearm via a vein catheter (18 G 1 ¾ Vasofix Braunüle, Braun, Germany) and 4.9 ml EDTA K2-Gel tubes (Sarstedt, Nümbrecht, Germany) as well as 8 ml VACUTAINER® CPT™ (Cell Preparation Tube, BD, Franklin Lakes, NJ) containing sodium heparin as anti-coagulant. Plasma was obtained by immediate centrifugation (Centrifuge 5702 R, Eppendorf AF, Hamburg, Germany) at 3,000 g for 10 min at room temperature, immediately frozen on dry ice and subsequently stored at -80°C. The CPTs were processed according to the manufacturer's instructions by centrifugation at 1,750

g for 30 min at room temperature after which PBMC were collected and washed twice with PBS.

2.2.3 NF-κB electrophoretic mobility shift assay (EMSA)

For EMSA, nuclear proteins were harvested from PBMC. All procedures were performed at 4°C. Isolated PBMC were suspended in 400 µl buffer A (10 mM Hepes-KOH pH 8, 10 mM KCl, 0.1 mM EDTA, 0.1 mM EGTA, 1 mM DTT, 0.5 mM PMSF). After incubation for 15 min the cells were lysed by addition of 15 µl 10% Nonidet NP-40 and nuclei isolated by centrifugation for 3 min at 14,000 g. Supernatant was discarded, nuclei were resuspended in 50 µl buffer C (20 mM Hepes-KOH pH 8, 20% glycerol, 400 mM NaCl, 1.5 mM $MgCl_2$, 0.2 mM EDTA, 0.2 mM EGTA, 1 mM DTT, 1 mM PMSF), lysed by freezing in liquid nitrogen and subsequent shaking for 15 min. The nuclear protein fraction was collected as supernatant after centrifugation for 5 min at 21,000 g. Protein concentrations were determined according to Bradford using the Roti® Quant kit (Carl Roth GmbH, Karlsruhe, Germany). ^{32}P end-labelling of a NF-κB consensus oligonucleotide (5-AGTTGAGGGGACTTTCCCAGGC-3) using γ-^{32}P-ATP (Hartmann Analytic, Braunschweig, Germany) and T4 polynucleotide kinase (Promega, Madison, WI) was performed with a commercial kit according to the instructions of the manufacturer. Binding of NF-κB from 2 µg of nuclear extract to 1 ng of labelled oligonucleotides was performed in 10 mM Hepes pH 7.9, 0.5 mM EDTA, 25 mM KCl, 0.5 mM DTT, 2% Ficoll 400, 0.25 mg/ml BSA, and 50 µg/ml poly dI/dC in a total volume of 12 µl at room temperature for 20 min. Protein-DNA complexes were separated from the free DNA probe by electrophoresis on 6% native polyacrylamide gels at room temperature with 180 V for 2.5h. Gels were dried, exposed overnight to phosphor screen and subsequently read with a Typhoon 9400 imager (GE Healthcare, München, Germany). The intensity of the protein-DNA complexes was quantified using ImageJ Software (http://rsbweb.nih.gov/ij/).

2.2.4 Measurement of protein phosphorylation

1 x 10^6 PBMC were lysed in 30 µl 1x Milliplex MAP lysis buffer containing freshly prepared protease inhibitors according to the manufacturer's instructions. Protein concentration was determined using Pierce BCA Protein Assay Kit (Thermo Fisher Scientific Inc., Rockford, IL). Protein phosphorylation of Akt and S6K was measured by Luminex xMAP technology

(Millipore Corporation, Billerica, MA) in 20 µg protein according to the manufacturer's instructions using the Bio-Plex 100 system (Bio-Rad Laboratories, Hercules, CA).

2.2.5 Quantitative RT-PCR

Total RNA from PBMC was isolated using the NucleoSpin Kit (Macherey-Nagel, Dueren, Germany) according to the manufacturer's instructions, and 100 ng RNA was reverse transcribed into cDNA (high capacity cDNA reverse transcription kit, Applied Biosystems, Darmstadt, Germany). PCR amplification of the human transcripts at baseline and 4h after the test meal was performed using quantitative PCR Maxima SYBR-Green (Fermentas, Thermo Fisher Scientific Inc., Rockford, IL) in duplicates using the Roche LightCycler 482 (Mannheim, Germany) with an initial activation of 10 min at 95°C followed by 40 cycles of 15 sec at 95°C and 40 sec at 61°C. The results were corrected for phosphoglycerate kinase 1 (PGK1) expression as an internal control (Falkenberg et al. 2011). The following primers (MWG Biotech, München, Germany) were designed using NCBI primer blast software (http://www.ncbi.nlm.nih.gov/tools/primer-blast/): CCR5, 5'-CTGAACTTCTCCCCGACAAA-3' (forward), 5'-TCTCTTCTGGGCTCCCTACA-3' (reverse); ICAM-1, 5'-GGTAAGGTTCTTGCCCACTG-3' (forward), 5'-TAGAGACCCCGTTGCCTAAA-3' (reverse); MnSOD, 5'-TCTGTTGGTGTCCAAGGCTC-3' (forward), 5'-TAGTAAGCGTGCTCCCACAC-3' (reverse); PGK1, 5'-CAAGAAGTATGCTGAGGCTGTCA-3' (forward), 5'-CAAATACCCCCACAGGACCAT-3' (reverse).

2.2.6 Measurement of plasma insulin

Plasma insulin was measured using a commercially available insulin ELISA according to the manufacturer's instructions (Dako, Glostrup, Denmark).

2.2.7 Statistical analysis

All data are expressed as mean ± SEM. The phosphorylated S6K and Akt protein levels were normalized to the levels of total protein. All data on NF-κB, IκB-α, p-S6K and p-Akt were normalized to one for baseline and the following values were expressed as fold change of basal level. Statistical analysis was performed with one-way analysis of variance (ANOVA) for each test meal separately. Additionally, one sample t-tests were used to compare each value to baseline separately for each test meal. Pearson correlation was calculated between NF-κB

and p-Akt and Spearman correlation between NF-κB and IκB-α, as well as between p-S6K and insulin. Plasma insulin was analysed using two-way ANOVA to compare the effect of the three meals and one-way ANOVA was used for single meals with Bonferroni post test. Differences of gene expression at 4h after the test meals compared to baseline were assessed by Wilcoxon matched pairs test and Kruskal-Wallis ANOVA was used to compare 4h values after all three test meals with each other. Statistical analysis was performed using GraphPad Prism5 (GraphPad software, La Jola, USA).

2.3 Results

Time-dependent postprandial inflammatory activation of PBMC

To assess proinflammatory activation in PBMC after the test meals NF-κB DNA-binding activity by EMSA and IκB-α protein degradation by Luminex xMap technology were measured. EMSA gels revealed two specific bands that were confirmed to contain the p50 and p65 subunits, respectively, in supershift assays (Figure 2.3-1).

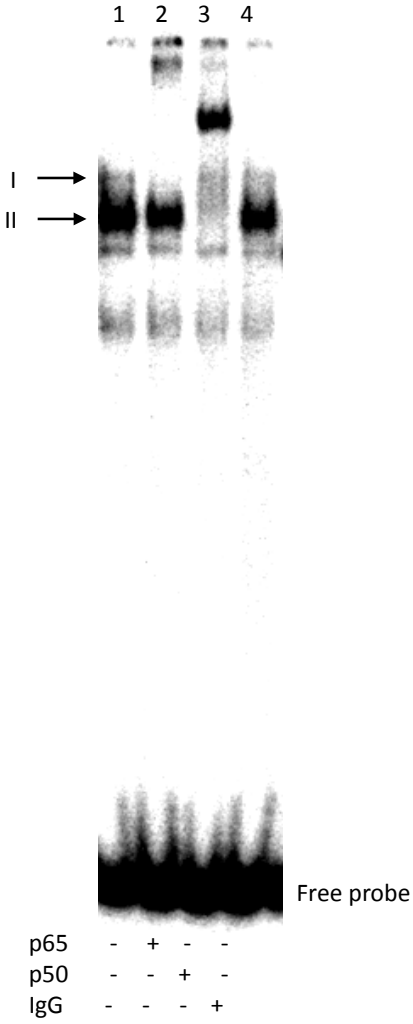

Figure 2.3-1: Representative electrophoretic mobility shift assay (EMSA)
EMSA is showing the relative NF-κB binding to the double stranded oligonucleotide containing the NF-κB DNA-binding site in a representative postprandial nuclear extract from PBMC. Two complexes were detected in the gels (I and II). The super shift assay showed that complex I contains the p65 subunit and complex II the p50 subunit of NF-κB. Lane 1: EMSA. Lane 2: Supershift assay with the use of an antibody against the p65 subunit. Lane 3: Supershift assay with the use of an antibody against the p50 subunit. Lane 4: Supershift assay with the use of an isotype control IgG showing no effect with the EMSA.

The postprandial time course of NF-κB binding activity was measured in PBMC nuclear extracts. Increased NF-κB binding activity following ingestion of the OLTT, the HFHC meal and interestingly to a similar extent of the HB (Figure 2.3-2a) was observed. Of note, baseline activity, maximal activation and in particular the time point of activation showed high inter-individual variation after the three test meals (Figure 2.3-2a-d) and did not reveal overall statistical significance for all meals (one-way ANOVA analysis Figure 2.3-2a). Both, the high

inter-individual differences and the low number of subjects may contribute to the fact that at most time points a significance of increased activity compared to baseline was not reached. NF-κB binding activity was significantly increased solely in response to OLTT after 4h, and to HB after 1h and 4h (Figure 2.3-2a). Corresponding to the increase in NF-κB binding activity a decrease in IκB-α total protein in response to OLTT, HFHC meal and HB was observed (Figure 2.3-2e) which did not reach overall statistical significance for each meal (one-way ANOVA analysis Figure 2.3-2e). A significant difference in mean IκB-α levels was observed in response to OLTT after 2h and 4h, to HFHC meal after 4h, 6h and 8h, and to HB after 1h (Figure 2.3-2e). Both, the significant increase of NF-κB binding activity and the parallel decrease of IκB-α level indicate a postprandial, inflammatory activation of PBMC. Of note, the activation of NF-κB binding activity and the corresponding decrease in IκB-α protein level appear to be delayed upon HFHC meal ingestion as compared to OLTT and HB (Figure 2.3-2a, e).

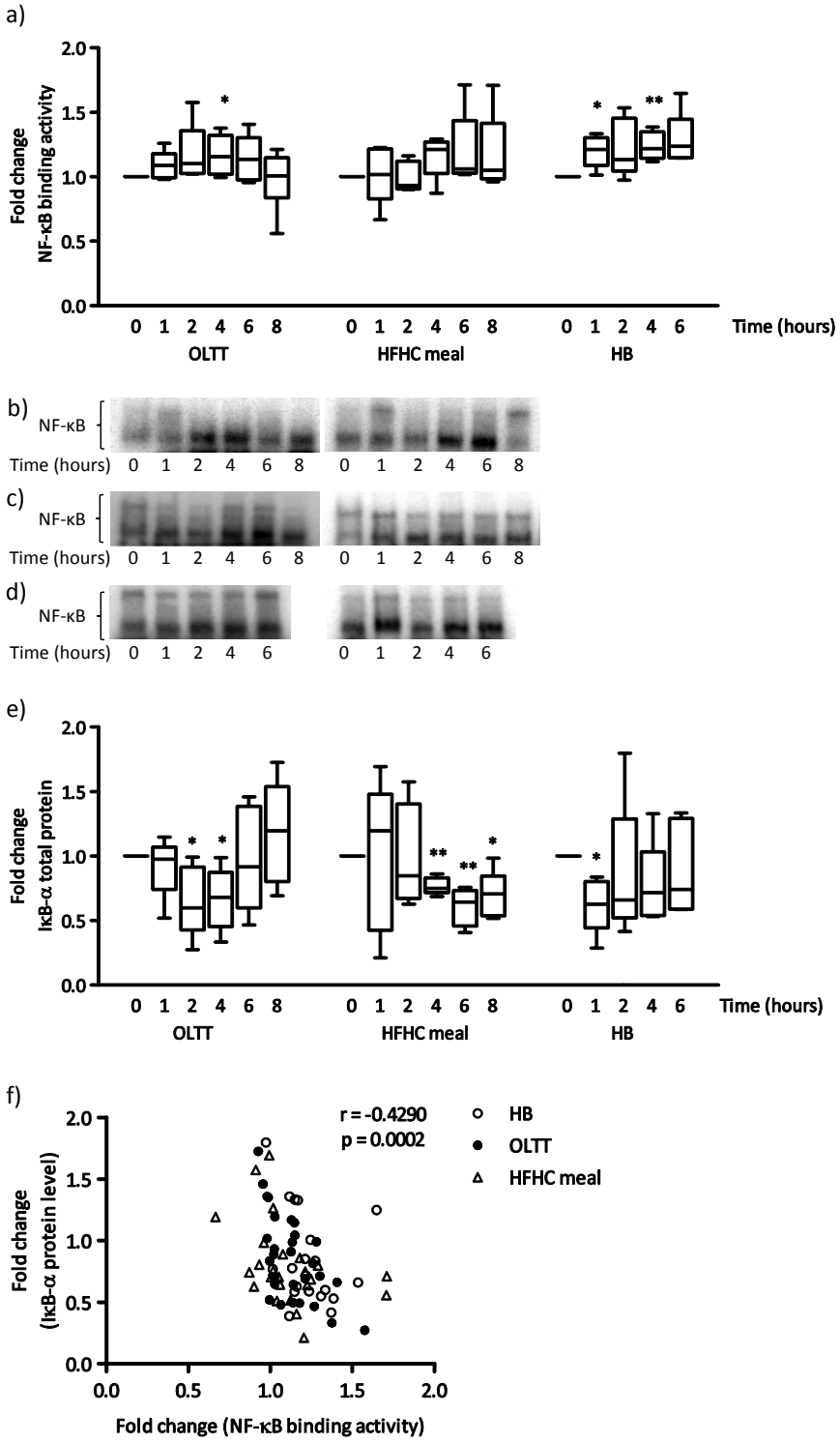

Figure 2.3-2: Postprandial activation of inflammatory signalling pathways in PBMC
a) Densitometric analysis of postprandial NF-κB binding activities in PBMC. b), c), d) Two representative electrophoretic mobility shift assay (EMSA) gels showing the NF-κB binding activity levels in PBMC nuclear protein extracts following b) OLTT, c) HFHC meal, d) HB, respectively. e) Analysis of postprandial IκB-α total protein levels. Both, NF-κB binding activities a) and IκB-α total protein levels e) were normalized to one for baseline time point and the following values were expressed as fold change of basal level (boxes extend from 1st quartile to 3rd quartile; median is indicated as a horizontal line; whiskers are drawn from minimum to maximum; n = 6 OLTT; n = 5 HFHC meal, n = 5 HB), * $p<0.05$; ** $p<0.01$ by one sample t-test. f) Fold changes of NF-κB binding activity and IκB-α total protein level are plotted against each other for each time point (OLTT - closed circles, HFHC meal – open triangles and HB - open circles) and each subject. Spearman correlation indicates a negative relationship ($r = -0.4290$, $p = 0.0002$).

To infer the known functional relation between NF-κB binding activity and IκB-α degradation from the here performed time course experiments Spearman correlation was calculated. A highly significant negative correlation between NF-κB binding activity and IκB-α degradation was found (Figure 2.3-2f). The NF-κB activation inferred from NF-κB / IκB-α correlations was significant for the OLTT meal as compared to the HFHC meal and the HB (Table 2.3-1). Overall, this finding reflects the well-established biological relationship of IκB-α degradation resulting in an increased DNA-binding activity of NF-κB. Thus, the assessment of time courses demonstrates a known biological relationship.

Table 2.3-1: Correlations of metabolic -, inflammatory signalling pathways and plasma insulin levels
Spearman correlation for fold change of indicated metabolic -, inflammatory markers, and plasma insulin at each time point of each meal separately (OLTT, HFHC meal and HB) and each subject was calculated.

Variables	OLT		HFHC meal		HB	
	r[#]	p[*]	r[#]	p[*]	r[#]	p[*]
NF-κB / IκB-α	-0.5828	0.0009	-0.3954	0.0558	-0.3023	0.1952
p-Akt / NF-κB	0.4262	0.0212	0.5256	0.007	0.5116	0.0211
p-Akt / IκB-α	-0.5734	0.0011	-0.4557	0.0252	-0.4752	0.0342
p-S6K / plasma insulin	0.5216	0.0044	0.499	0.0154	0.0872	0.7146

[#] Correlation coefficient; [*] approximate p value for non-parametric correlation

Time-dependent postprandial activation of the metabolic Akt and S6K pathways in PBMC

Phosphorylation of both Akt and S6K, two essential kinases for major metabolic signalling pathways, increased in PBMC total protein extracts following the ingestion of OLTT, HFHC meal and HB (Figure 2.3-3a, b). Similarly to NF-κB activity measures, a high inter-individual variation of S6K and Akt phosphorylation was observed and, thus, no overall statistical significance for all test meals was found (one-way ANOVA analysis Figure 2.3-3a, b). However, a significant increase of p-S6K protein in response to OLTT after 2h compared with baseline was found (Figure 2.3-3a). It has to be pointed out that due to inter-individual differences and limited power most comparisons to baseline were not significant. However, a rapid increase of S6K phosphorylation 1h after meal ingestion compared with baseline for all three test meals with a subsequent decrease was observed (Figure 2.3-3a). Moreover, a rapid increase of Akt phosphorylation after OLTT and HB in contrast to the HFHC meal was found. The Akt phosphorylation appeared to be delayed in response to the HFHC meal (Figure 2.3-3b).

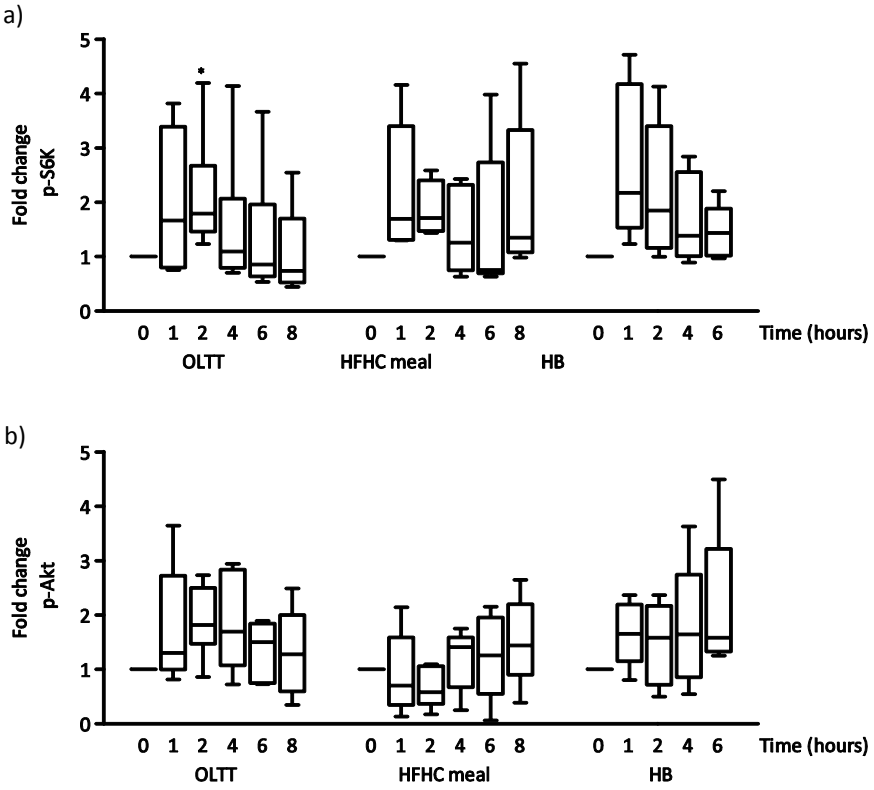

Figure 2.3-3: Postprandial activation of metabolic signalling pathways in PBMC
Changes in a) S6K and b) Akt phosphorylation in response to OLTT, HFHC meal, and HB quantified as ratio of phosphorylated - to total protein. All values were normalized to one for baseline time point and the following values were expressed as fold change of basal level. Results are presented as box whisker plots (boxes extend from 1st quartile to 3rd quartile; median is indicated as a horizontal line; whiskers are drawn from minimum to maximum); n = 6 OLTT; n = 5 HFHC meal; n = 5 HB. * $p \leq 0.05$ by one sample t-test.

Correlation of Akt phosphorylation with NF-κB activation

For NF-κB activation it was shown that correlation analysis of functionally related measures (here NF-κB binding activity and IκB-α degradation) in the time course experiment enables the assessment of temporal and functional-interactions in datasets with high inter-individual differences. Therefore, correlations for all measured metabolic and inflammatory signalling pathway were calculated (Table 2.3-2).

Table 2.3-2: Correlations of metabolic and inflammatory signalling pathway activation in PBMC
Correlation matrix (Pearson correlation for p-Akt and NF-κB; Spearman correlation for residual correlations): Overall correlation of fold change of each measured marker (OLTT, HFHC meal and HB), at each time point, and each subject was calculated.

Variable	IκB-α		NF-κB binding		p-Akt	
	r[#]	p[*]	r[#]	p[*]	r[#]	p[*]
p-S6K	0.1908	0.1084	-0.2266	0.0556	-0.1509	0.2058
p-Akt	-0.5257	<0.0001	0.3599	0.0016		
NF-κB binding	-0.429	0.0002				

[#] Spearman/Pearson correlation coefficient, * approximate p-value for parametric or non-parametric correlation

No significant correlations between any of the analysed parameters except a significant positive correlation between NF-κB binding activity and Akt phosphorylation were found (Figure 2.3-4). This interaction was reflected in a strongly significant negative correlation of Akt phosphorylation and IκB-α protein level (Table 2.3-2). Of note, the correlation of Akt phosphorylation with both measures of NF-κB activity was significant for each test meal (Table 2.3-1). The close correlation of both NF-κB activity measures with Akt phosphorylation implies a functional interference of postprandial Akt / NF-κB signalling in PBM.

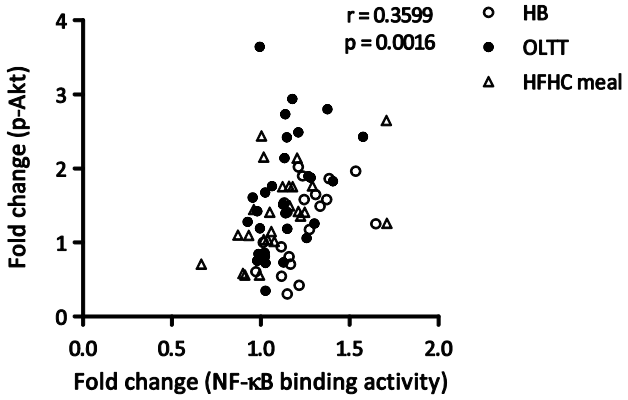

Figure 2.3-4: Correlation of postprandial activation of inflammatory and metabolic signalling pathways in PBMC. Fold change of NF-κB binding activity and Akt phosphorylation for each time point (OLTT - closed circles, HFHC meal – open triangles and HB - open circles) and each subject are plotted against each other. Pearson correlation indicates a positive relationship (r = 0.3599, p = 0.0016).

Correlation of S6K phosphorylation with insulin levels

Next, the relationship between the postprandial increase of plasma insulin and the measured intracellular parameters of metabolic and inflammatory activation, S6K/Akt phosphorylation and NF-κB binding activity/IκB-α degradation, respectively was investigated. A significant time dependent increase of plasma insulin levels after all meals that was not dependent on the meal type was found (two-way ANOVA Figure 2.3-5). Direct comparison of HB, OLTT, and HFHC induced insulin responses to baseline for specific time points revealed a significant increase from baseline to 1h for all meals, to 2h for the OLTT and the HFHC meal, but not for

the HB (one-way ANOVA, Figure 2.3-5). Thus, an extended insulin response was observed after the OLTT and HFHC meal compared to the HB (Figure 2.3-5).

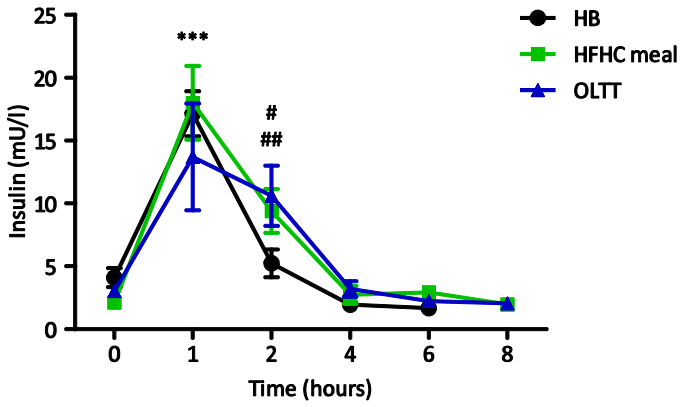

Figure 2.3-5: Postprandial plasma insulin levels. Plasma insulin levels (mU/l) at baseline and following the consumption of a HFHC meal, OLTT or HB are shown for the indicated time points. Data are mean ± SEM; n = 6. Time and meal effects calculated by two-way ANOVA with $p < 0.0001$, $p = 0.6365$, respectively. Direct comparison of meal-effects by one-way ANOVA, Bonferroni post test with *** $p < 0.0001$ for all three meals; # $p < 0.05$ for OLTT and ## $p < 0.01$ for HFHC meal compared to baseline.

Next, Spearman correlations were calculated for plasma insulin levels and all assessed intracellular signalling measures (Table 2.3-3).

Table 2.3-3: Correlations of intracellular signalling pathways in PBMC with plasma insulin levels.
Correlation matrix (Spearman correlation): overall correlation of fold change of each measured marker, at each time point (OLTT, HFHC meal and HB), and each subject was calculated.

Variable	Plasma insulin	
	r[#]	p[*]
p-S6K	0.3081	0.009
p-Akt	-0.0446	0.708
NF-κB binding	-0.0588	0.619
IκB-α	-0.0466	0.6973

[#] Spearman correlation coefficient,
[*] approximate p-value for non-parametric correlation

A significantly positive relationship between plasma insulin and S6K phosphorylation was found (Figure 2.3-6). Of note, the correlation of S6K phosphorylation with plasma insulin levels was significant for the OLTT and HFHC, but not for the HB (Table 2.3-1). Moreover, no significant correlation was observed for p-Akt, IκB-α, NF-κB and plasma insulin (Table 2.3-3).

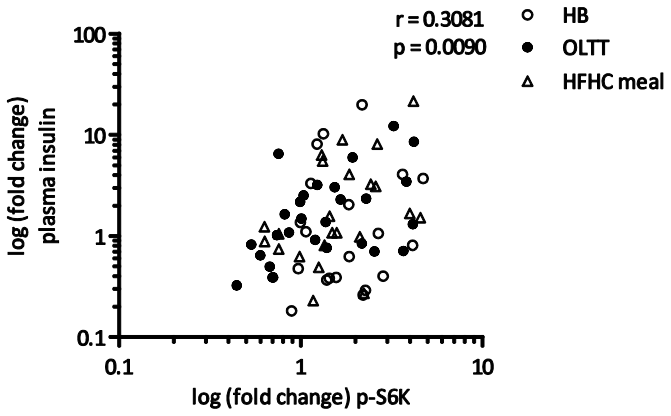

Figure 2.3-6: Correlation of postprandial plasma insulin levels and S6K activation. Log transformed fold change of plasma insulin and p-S6K, for each time point (OLTT - closed circles, HFHC meal – open triangles and HB - open circles), and each subject are plotted against each other (r = 0.3081, p = 0.0090 by Spearman correlation).

Postprandial changes in gene expression

To assess the consequences of the diet-induced inflammatory (NF-κB) and metabolic (Akt) activation on gene expression, mRNA levels for known target genes of NF-κB and of FOXO (a transcription factor inhibited by Akt kinase) were studied using qRT-PCR. Expression of the FOXO target gene MnSOD was significantly down-regulated after 4h compared to baseline after ingestion of both the OLTT and the HFHC meal, but not after the HB (Figure 2.3-7a). Comparing the expression levels of the NF-κB target gene CCR5 at baseline to the levels 4h after ingestion of the test meals, none of the meals induced a significant change of mRNA levels. However, when comparing the induction of expression after ingestion of OLTT versus HB a significant difference of CCR5 mRNA levels was found. Notably, OLTT resulted in an up-regulation of CCR5 mRNA levels, whereas HB in a down-regulation of gene expression (Figure 2.3-7b). mRNA expression levels of the NF-κB target gene ICAM-1 did not change significantly after ingestion of any of the analysed test meals (Figure 2.3-7c). Mean PAI-1, also an NF-κB target gene, expression level was reduced in response to all three test meals, reaching significance solely for the OLTT (Figure 2.3-7d).

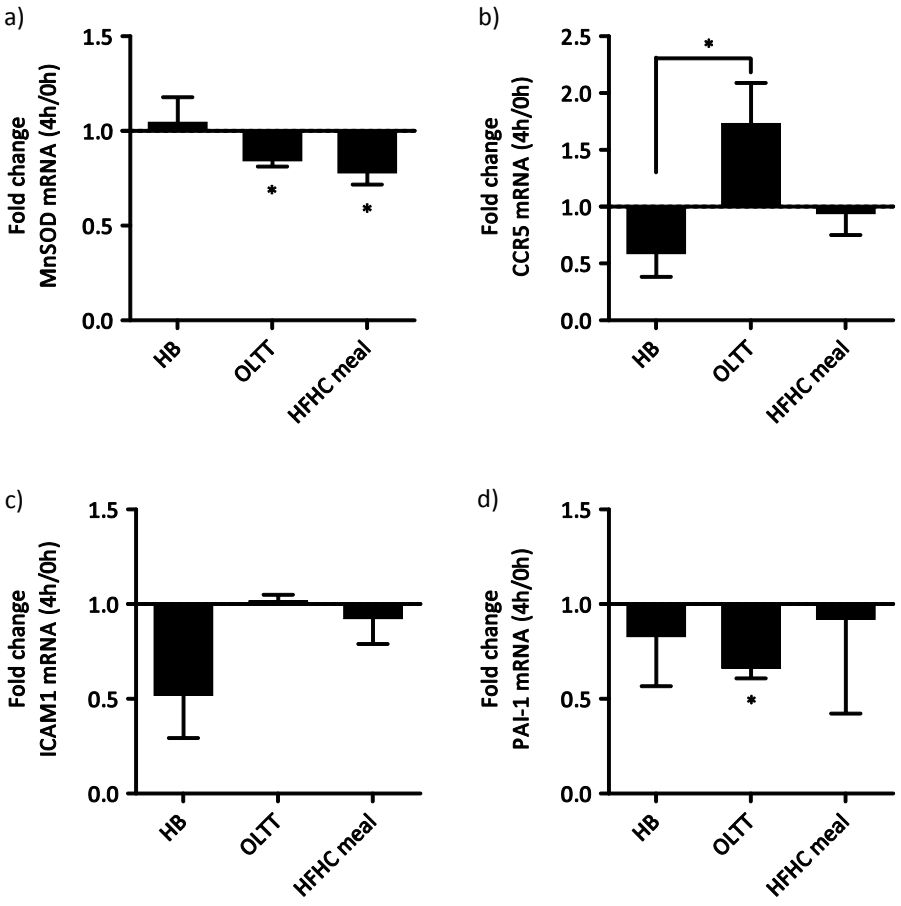

Figure 2.3-7: Gene expression analysis of selected target genes
Mean and SEM effects of test meals on gene expression of selected target genes of NF-κB and FOXO after 4h compared to baseline. a) Manganese superoxid dismutase (MnSOD). b) CC-chemokine-receptor 5 (CCR5). c) Intercellular adhesion molecule 1 (ICAM-1). d) Plasminogen activator inhibitor-1 (PAI-1). Differences were assessed by using Wilcoxon matched pairs test and Kruskal-Wallis ANOVA. * indicate value difference from baseline (0h) or a difference between test meals at a given time ($p < 0.05$).

2.4 Discussion

The results of this study show the well-established postprandial inflammatory activation of PBMC at the level of NF-κB binding activity and IκB-α degradation. Moreover, the interaction of postprandial NF-κB activation with other metabolic signalling pathways in a defined time course of up to 8h was analysed. A correlation of NF-κB signalling with Akt phosphorylation, but not with mTOR-pS6K activation was found. Moreover, a correlation of insulin levels with mTOR-S6K activation, but not with Akt or NF- κB activation was observed.

Here, for the first time an increase of Akt and S6K phosphorylation by three different test meals was described. To date, altered Akt phosphorylation in PBMC was described in insulin resistant conditions, e.g. low p-Akt levels in PBMC of insulin resistant rheumatoid arthritis patients (Stagakis et al. 2012). Similarly, impaired insulin signalling was reported for PBMC from patients with metabolic syndrome (Pasini et al. 2010) and reduced insulin receptor phosphorylation in PBMC from obese subjects (Ghanim et al. 2007). Here, participants were selected with normal body weight, normal glucose metabolism and without a family history of diabetes, and thereby excluding a state of insulin resistance. It is known that the activation of the mTOR downstream target S6K by nutrients or insulin inhibits insulin-receptor signalling, in case of insulin by triggering a negative feedback loop involving Akt mediated activation of S6K1 (Manning 2003). In mice an excess of nutrient supply and hyperinsulinaemia associated with the obese state was attributed to a constitutive activation of mTOR/S6K1 in adipose tissue, muscle and liver and consequently desensitization of insulin signalling (Um et al. 2004). This mechanisms may be partially triggered by the here observed postprandial activation of S6K phosphorylation. Future studies are needed to elucidate a possible postprandial activation of S6K in other tissues and the role of postprandial S6K phosphorylation in PBMC both under physiological and pathophysiological conditions such as insulin resistance. Moreover, it remains elusive if S6K activation is induced directly by insulin or other mediators which are increased postprandial, i.e. incretin hormones (Kwon et al. 2004) or metabolites (Krug et al. 2012).

In contrast to p-S6K, no correlation of insulin levels with p-Akt was found. Moreover, no correlation of S6K and Akt phosphorylation was observed, despite their well-established interaction at the molecular level (Inoki et al. 2002; Vander Haar et al. 2007; Sarbassov et al.

2005). These findings may be attributed to the well-established complex interrelationship of both pathways, e.g. postprandial activated p-S6K may decrease Akt phosphorylation by negative feedback (Zhang et al. 2008) and in turn modulate the expression of NF-κB target genes. Such interactions in PBMC require further analysis. Furthermore, it is well established that Akt is activated by several other stimuli besides insulin or growth factors (Li et al. 2007) like T- and B-cell receptor activation (Cheng et al. 2011; So et al. 2013) and integrins (Kim et al. 2009).

The observed findings imply a functional relation of postprandial inflammatory NF-κB and metabolic Akt signalling in PBMC. In fact, Akt was shown to induce NF-κB activation by both, phosphorylation of IKK2 (Nidai Ozes et al. 1999) and IKK1/2-independent phosphorylation of the p65 subunit (Madrid 2001; Sizemore 2001). Moreover, Akt-signalling was implied in T-cell activation by interfering with NF-κB activation, however Akt dampens but does not impair NF-κB activity (Cheng et al. 2011). Moreover, several mouse studies implicate a contribution of PBMC in the development of systemic insulin resistance, e.g. mice with a myeloid lineage specific deletion of insulin-receptor (IR) or inhibitor NF-κB kinase 2 (IKK2) are protected from the development of diet-induced insulin resistance, and both lineages exhibit a dramatic reduction of chronic and systemic low-grade inflammation associated with obesity (Mauer et al. 2010; Arkan et al. 2005). Overall, these data support a combined mode of action of inflammatory activation and impaired insulin action in PBMC, a mechanism to which the here proposed postprandial inference of NF-κB and Akt signalling may contribute. However, it has to be noted that, even if it was shown that there is no difference in the temporal pattern of activation of both pathways, future studies are needed to elucidate the precise molecular mechanisms underlying postprandial inference of both pathways and moreover, factors responsible for activation, i.e. endocrine pathways or metabolites.

The expression of the FOXO target gene MnSOD was down-regulated after ingestion of OLTT and HFHC meal, but not HB, reflecting the known PI3K / Akt signalling mediated decrease of FOXO activity and FOXO target genes expression (Kops et al. 2002). Regulation of the major mitochondrial antioxidant enzyme MnSOD suggests that postprandial Akt phosphorylation may be involved in the modulation of cellular ROS levels. In fact, intake of HFHC meals was shown to increase MnSOD protein levels (Lim et al. 2011) and, compared to a meal rich in fibre and fruit, to induce oxidative stress (Ghanim et al. 2009). Furthermore, it could be

shown that expression levels of the NF-κB target gene CCR5 was significantly increased 4h after OLTT as compared to HB, implying that consumption of a meal enriched with lipids compared to a well-balanced meal may contribute to PBMC migration into adipose tissue. In humans, an enhanced CCR5 expression was found in adipose tissue (Huber et al. 2008) and the CCR5 ligand CCL5 was shown to trigger adhesion and transmigration of blood monocytes through endothelial cells of human white adipose tissue (Keophiphath et al. 2009). Unexpectedly, as the expression of the NF-κB target gene PAI-1 is increased in adipose tissue and macrophages in obesity and diabetes (Jankun 2011), it was found that PAI-1 gene expression levels in PBMC were reduced in response to all three test meals.

PBMC could serve as a valuable tool to improve diagnostics of diseases, as they remain the most accessible human tissue and represent a practical, minimally invasive surrogate biopsy material. Transcript signatures of patient PBMC have recently been proposed as a disease-specific and predictive inflammatory biomarker for type 1 diabetes (Levy et al. 2012). It was shown that inflammatory mediators were related to reduced insulin receptor phosphorylation in PBMC from obese subjects (Ghanim et al. 2007). Therefore, well established measurements of inflammatory and metabolic markers in PBMC might be useful for prediction of insulin resistance.

In summary, for the first time an increase of Akt and S6K phosphorylation in PBMC after three defined test meals was demonstrated. The possible postprandial interaction of Akt and NF-κB contributes to a better understanding of the postprandial immune system and metabolism interaction.

Appendix

Table A.1: Simultaneously measured acylcarnitine panel by ESI-MS/MS in EBV-LCLs
Simultaneous measured acylcarnitine panel in EBV-LCL extracts and supernatants by ESI-MS/MS (Laboratory Becker, Olgemöller and Colleagues, München, Germany).

C2:0	Acetyl-L-carnitine
C3:0	Propionyl-L-carnitine
C4:0	Butyryl-L-carnitine
C5:1	Tiglyl-L-carnitine
C5:0	Valeryl-L-carnitine
C6:0 (C4:1-DC)	Hexanoyl-L-carnitine/Fumaryl-L-carnitine
C5:0-OH (C3-DC-M)	Hydroxyvaleryl-L-carnitine/Methylmalonyl-L-carnitine
C8:0	Octanoyl-L-carnitine
C10:2	Decadienyl-L-carnitine
C10:1	Decenoyl-L-carnitine
C10:0	Decanoyl-L-carnitine
C4:0-DC	Methylmalonyl-L-carnitine
C5:0-DC (C6-OH)	Glutaryl-L-carnitine/ Hydroxyhexanoyl-L-carnitine
C12:0	Dodecanoyl-L-carnitine
C6:0-DC	Methylglutaryl-L-carnitine
C14:2	Tetradecadienyl-L-carnitine
C14:1	Tetradecenoyl-L-carnitine
C14:0	Tetradecanoyl-L-carnitine
C14:0-OH	Hydroxytetradecanoyl-L-carnitine
C16:1	Hexadecenoyl-L-carnitine
C16:0	Hexadecanoyl-L-carnitine
C16:0-1-OH	Hydroxyhexdecenoyl-L-carnitine
C16:0-OH	Hydroxyhexadecanoyl-L-carnitine
C18:2	Octadecadienyl-L-carnitine
C18:1	Octadecenoyl-L-carnitine
C18:0	Octadecanoyl-L-carnitine
C12:0-DC	Dodecanedioyl-L-canitine
C18:1-OH	Hydroxyoctadecenoyl-L-carnitine
C3:0-DC (C4-OH)	Malonyl-L-carnitine/Hydroxybutyryl-L-carnitine
C4:0-OH	Hydroxybutyryl-L-carnitine
C5:0-DC (C6-OH)	Glutaryl-L-carnitine/ Hydroxyhexanoyl-L-carnitine
C8:1	Octenoyl-L-carnitine
C12:1	Dodecenoyl-L-carnitine
C12:2	Dodecadienyl-L-carnitine
C16:2	Hexadecadienyl-L-carnitine
C18:2-OH	Hydroxyoctadecadienyl-L-carnitine
C18-OH	Hydroxyoctadecenoyl-L-carnitine
C16:2-DC	Dicarboxyhexadecadienyl-L-carnitine
C18:2-DC	Dicarboxyoctadecadienyl-L-carnitine
C16:1-DC	Dicarboxyhexadecenoyl-L-carnitine
C16:0-DC	Dicarboxypalmitoyl-L-carnitine
C18:1-DC	Dicarboxyoctadecenoyl-L-carnitine
C18:0-DC	Dicarboxyoctadecanoyl-L-carnitine

Table A.2: Simultaneous measured acylcarnitine panel by HPLC-MS/MS in Huh7 cells
Simultaneous measured acylcarnitine panel in shACADS and shNTC knock-down Huh7 cell extracts and supernatants by HPLC-MS/MS (Prof. H. Daniel, Lehrstuhl für Ernährungsphysiologie, TU München)

C2:0	Acetyl-L-carnitine
C3:1	Propenyl-L-carnitine
C3:0	Propionyl-L-carnitine
C4:1	Butenyl-L-carnitine
C4:0	Butyryl-L-carnitine
C3-OH	Hydroxypropionyl-L-carnitine
C5:1	Tiglyl-L-carnitine
C5:0	Valeryl-L-carnitine
C3:0-DC (C4-OH)	Malonyl-L-carnitine/Hydroxybutyryl-L-carnitine
C6:1	Hexenoyl-L-carnitine
C6:0 (C4:1-DC)	Hexanoyl-L-carnitine/Fumaryl-L-carnitine
C5:0-OH (C3-DC-M)	Hydroxyvaleryl-L-carnitine/Methylmalonyl-L-carnitine
C5:1-DC	Glutaconyl-L-carnitine
C5:0-DC (C6-OH)	Glutaryl-L-carnitine/ Hydroxyhexanoyl-L-carnitine
C8:0	Octanoyl-L-carnitine
C9:0	Nonacyl-L-carnitine
C7:0-DC	Pimelyl-L-carnitine
C10:2	Decadienyl-L-carnitine
C10:1	Decenoyl-L-carnitine
C10:0	Decanoyl-L-carnitine
C12:1	Dodecenoyl-L-carnitine
C12:0	Dodecanoyl-L-carnitine
C14:2	Tetradecadienyl-L-carnitine
C14:1	Tetradecenoyl-L-carnitine
C14:0	Tetradecanoyl-L-carnitine
C12:0-DC	Dodecanedioyl-L-canitine
C14:2-OH	Hydroxytetradecadienyl-L-carnitine
C14:1-OH	Hydroxytetradecenoyl-L-carnitine
C16:2	Hexadecadienyl-L-carnitine
C16:1	Hexadecenoyl-L-carnitine
C16:0	Hexadecanoyl-L-carnitine
C16:2-OH	Hydroxyhexadecadienyl-L-carnitine
C16:1-OH	Hydroxyhexdecenoyl-L-carnitine
C16:0-OH	Hydroxyhexadecanoyl-L-carnitine
C18:2	Octadecadienyl-L-carnitine
C18:1	Octadecenoyl-L-carnitine
C18:0	Octadecanoyl-L-carnitine
C18:1-OH	Hydroxyoctadecenoyl-L-carnitine
C5:0-M-DC	Methylglutaryl-L-carnitine

References

Abecasis GR, Altshuler D, Auton A et al. (2010): A map of human genome variation from population-scale sequencing. *Nature* 467 (7319), 1061–1073.

Adams SH, Hoppel CL, Lok KH et al. (2009): Plasma acylcarnitine profiles suggest incomplete long-chain fatty acid beta-oxidation and altered tricarboxylic acid cycle activity in type 2 diabetic African-American women. *J. Nutr.* 139 (6), 1073–1081.

Amaral AU, Cecatto C, Busanello ENB et al. (2012): Ethylmalonic acid impairs brain mitochondrial succinate and malate transport. *Mol. Genet. Metab.* 105 (1), 84–90.

Amoli MM, Carthy D, Platt H et al. (2008): EBV Immortalization of human B lymphocytes separated from small volumes of cryo-preserved whole blood. *Int J Epidemiol* 37 Suppl 1, i41-5.

Arkan MC, Hevener AL, Greten FR et al. (2005): IKK-β links inflammation to obesity-induced insulin resistance. *Nat Med* 11 (2), 191–198.

Baillet L, Mullur RS, Esser V et al. (2000): Elucidation of the mechanism by which (+)-acylcarnitines inhibit mitochondrial fatty acid transport. *J. Biol. Chem.* 275 (47), 36766–36768.

Bell FP (1980): Inhibition of adenine nucleotide translocase by oleoylcarnitine, oleoylcoa and oleate in isolated arterial mitochondria. *Atherosclerosis* 37 (1), 21–32.

Bene J, Márton M, Mohás M et al. (2013): Similarities in serum acylcarnitine patterns in type 1 and type 2 diabetes mellitus and in metabolic syndrome. *Ann. Nutr. Metab.* 62 (1), 80–85.

Beugnet A, Tee AR, Taylor PM et al. (2003): Regulation of targets of mTOR (mammalian target of rapamycin) signalling by intracellular amino acid availability. *Biochem. J.* 372 (2), 555.

Birkebaek NH, Simonsen H, Gregersen N (2002): Hypoglycaemia and elevated urine ethylmalonic acid in a child homozygous for the short-chain acyl-CoA dehydrogenase 625G A gene variation. *Acta Paediatr.* 91 (4), 480–482.

Birney E, Stamatoyannopoulos JA, Dutta A et al. (2007): Identification and analysis of functional elements in 1% of the human genome by the ENCODE pilot project. *Nature* 447 (7146), 799–816.

Bremer J and Wojtczak AB (1972): Factors controlling the rate of fatty acid -oxidation in rat liver mitochondria. *Biochim. Biophys. Acta* 280 (4), 515–530.

Buxton DB, Barron LL, Taylor MK et al. (1984): Regulatory effects of fatty acids on decarboxylation of leucine and 4-methyl-2-oxopentanoate in the perfused rat heart. *Biochem. J.* 221 (3), 593–599.

Califano A, Butte AJ, Friend S et al. (2012): Leveraging models of cell regulation and GWAS data in integrative network-based association studies. *Nat. Genet.* 44 (8), 841–847.

Caliskan M, Cusanovich DA, Ober C et al. (2011): The effects of EBV transformation on gene expression levels and methylation profiles. *Hum. Mol. Genet.* 20 (8), 1643–1652.

Caron M, Imam-Sghiouar N, Poirier F et al. (2002): Proteomic map and database of lymphoblastoid proteins. *J. Chromatogr. B Analyt. Technol. Biomed. Life Sci.* 771 (1-2), 197–209.

Carter KL, Cahir-McFarland E, Kieff E (2002): Epstein-barr virus-induced changes in B-lymphocyte gene expression. *J. Virol.* 76 (20), 10427–10436.

Cheng J, Phong B, Wilson DC et al. (2011): Akt Fine-tunes NF- B-dependent Gene Expression during T Cell Activation. *Journal of Biological Chemistry* 286 (41), 36076–36085.

Corydon MJ, Andresen BS, Bross P et al. (1997): Structural organization of the human short-chain acyl-CoA dehydrogenase gene. *Mamm. Genome* 8 (12), 922–926.

Corydon MJ, Gregersen N, Lehnert W et al. (1996): Ethylmalonic aciduria is associated with an amino acid variant of short chain acyl-coenzyme A dehydrogenase. *Pediatr. Res.* 39 (6), 1059–1066.

Corydon MJ, Vockley J, Rinaldo P et al. (2001): Role of common gene variations in the molecular pathogenesis of short-chain acyl-CoA dehydrogenase deficiency. *Pediatr. Res.* 49 (1), 18–23.

Craddock N, Hurles ME, Cardin N et al. (2010): Genome-wide association study of CNVs in 16,000 cases of eight common diseases and 3,000 shared controls. *Nature* 464 (7289), 713–720.

Dandona P, Ghanim H, Chaudhuri A et al. (2010): Macronutrient intake induces oxidative and inflammatory stress: potential relevance to atherosclerosis and insulin resistance. *Exp Mol Med* 42 (4), 245.

Davidson B and Schulz H (1982): Separation, properties, and regulation of acyl coenzyme A dehydrogenases from bovine heat and liver. *Arch. Biochem. Biophys.* 213 (1), 155–162.

Deberardinis RJ, Sayed N, Ditsworth D et al. (2008): Brick by brick: metabolism and tumor cell growth. *Curr. Opin. Genet. Dev.* 18 (1), 54–61.

Di Paolo S, Teutonico A, Leogrande D et al. (2006): Chronic inhibition of mammalian target of rapamycin signaling downregulates insulin receptor substrates 1 and 2 and AKT activation: A crossroad between cancer and diabetes? *J Am Soc Nephrol* 17 (8), 2236–2244.

Dimas AS, Deutsch S, Stranger BE et al. (2009): Common regulatory variation impacts gene expression in a cell type-dependent manner. *Science* 325 (5945), 1246–1250.

Dokoupil K and Ensenauer R: Disorders of Mitochondrial Beta-Oxidation of Fatty Acids: A Growing Challenge For Pediatric Dietetics. *Aktuelle Ernährungsmedizin* 33, 195–200.

Dunham I, Kundaje A, Aldred SF et al. (2012): An integrated encyclopedia of DNA elements in the human genome. *Nature* 489 (7414), 57–74.

Dupuis J, Langenberg C, Prokopenko I et al. (2010): New genetic loci implicated in fasting glucose homeostasis and their impact on type 2 diabetes risk. *Nat. Genet.* 42 (2), 105–116.

Eaton S (2002): Control of mitochondrial beta-oxidation flux. *Prog. Lipid Res.* 41 (3), 197–239.

Eaton S, Bartlett K, Pourfarzam M (1996): Mammalian mitochondrial beta-oxidation. *Biochem. J.* 320 (Pt 2), 345–357.

Ensenauer R, Fingerhut R, Schriever SC et al. (2012): *In situ* assay of fatty acid β-oxidation by metabolite profiling following permeabilization of cell membranes. *J. Lipid Res.* 53 (5), 1012–1020.

Falkenberg VR, Whistler T, Murray JR et al. (2011): Identification of Phosphoglycerate Kinase 1 (PGK1) as a reference gene for quantitative gene expression measurements in human blood RNA. *BMC Res Notes* 4 (1), 324.

Fould B, Garlatti V, Neumann E et al. (2010): Structural and functional characterization of the recombinant human mitochondrial trifunctional protein. *Biochemistry* 49 (39), 8608–8617.

Frerman FE and Goodman SI (1985): Fluorometric assay of acyl-CoA dehydrogenases in normal and mutant human fibroblasts. *Biochem Med* 33 (1), 38–44.

Gallant NM, Leydiker K, Tang H et al. (2012): Biochemical, molecular, and clinical characteristics of children with short chain acyl-CoA dehydrogenase deficiency detected by newborn screening in California. *Mol. Genet. Metab.* 106 (1), 55–61.

Ghanim H, Abuaysheh S, Sia CL et al. (2009): Increase in Plasma Endotoxin Concentrations and the Expression of Toll-Like Receptors and Suppressor of Cytokine Signaling-3 in Mononuclear Cells After a High-Fat, High-Carbohydrate Meal: Implications for insulin resistance. *Diabetes Care* 32 (12), 2281–2287.

Ghanim H, Aljada A, Daoud N et al. (2007): Role of inflammatory mediators in the suppression of insulin receptor phosphorylation in circulating mononuclear cells of obese subjects. *Diabetologia* 50 (2), 278–285.

Ghisla S and Thorpe C (2004): Acyl-CoA dehydrogenases. A mechanistic overview. *Eur. J. Biochem.* 271 (3), 494–508.

Gieger C, Geistlinger L, Altmaier E et al. (2008): Genetics meets metabolomics: a genome-wide association study of metabolite profiles in human serum. *PLoS Genet.* 4 (11), e1000282.

Gower RM, Wu H, Foster GA et al. (2010): CD11c/CD18 Expression Is Upregulated on Blood Monocytes During Hypertriglyceridemia and Enhances Adhesion to Vascular Cell Adhesion Molecule-1. *Arteriosclerosis, Thrombosis, and Vascular Biology* 31 (1), 160–166.

Green H and Meuth M (1974): An established pre-adipose cell line and its differentiation in culture. *Cell* 3 (2), 127–133.

Gregersen N, Hansen J, Palmfeldt J (2012): Mitochondrial proteomics--a tool for the study of metabolic disorders. *J. Inherit. Metab. Dis.* 35 (4), 715–726.

Gregersen N, Winter VS, Corydon MJ et al. (1998): Identification of four new mutations in the short-chain acyl-CoA dehydrogenase (SCAD) gene in two patients: one of the variant alleles, 511C--T, is present at an unexpectedly high frequency in the general population, as was the case for 625G--A, together conferring susceptibility to ethylmalonic aciduria. *Hum. Mol. Genet.* 7 (4), 619–627.

He XY, Yang SY, Schulz H (1989): Assay of L-3-hydroxyacyl-coenzyme A dehydrogenase with substrates of different chain lengths. *Anal. Biochem.* 180 (1), 105–109.

Hindorff LA, Sethupathy P, Junkins HA et al. (2009): Potential etiologic and functional implications of genome-wide association loci for human diseases and traits. *Proc. Natl. Acad. Sci. U.S.A.* 106 (23), 9362–9367.

Hong M, Karlsson R, Magnusson PKE et al. (2013): A genome-wide assessment of variability in human serum metabolism. *Hum. Mutat.* 34 (3), 515–524.

Hornbak M, Banasik K, Justesen JM et al. (2011): The minor C-allele of rs2014355 in ACADS is associated with reduced insulin release following an oral glucose load. *BMC Med. Genet.* 12, 4.

Houstis N, Rosen ED, Lander ES (2006): Reactive oxygen species have a causal role in multiple forms of insulin resistance. *Nature* 440 (7086), 944–948.

Houten SM and Wanders RJA (2010): A general introduction to the biochemistry of mitochondrial fatty acid β-oxidation. *J. Inherit. Metab. Dis.* 33 (5), 469–477.

Huber J, Kiefer FW, Zeyda M et al. (2008): CC Chemokine and CC Chemokine Receptor Profiles in Visceral and Subcutaneous Adipose Tissue Are Altered in Human Obesity. *Journal of Clinical Endocrinology & Metabolism* 93 (8), 3215–3221.

Hue L, Maisin L, Rider MH (1988): Palmitate inhibits liver glycolysis. Involvement of fructose 2,6-bisphosphate in the glucose/fatty acid cycle. *Biochem. J.* 251 (2), 541–545.

Illig T, Gieger C, Zhai G et al. (2010): A genome-wide perspective of genetic variation in human metabolism. *Nat. Genet* 42 (2), 137–141.

Inoki K, Li Y, Zhu T et al. (2002): TSC2 is phosphorylated and inhibited by Akt and suppresses mTOR signalling. *Nat. Cell Biol.* 4 (9), 648–657.

Ishikawa M, Tsuchiya D, Oyama T et al. (2004): Structural basis for channelling mechanism of a fatty acid beta-oxidation multienzyme complex. *EMBO J.* 23 (14), 2745–2754.

Jankun J (2011): Can inactivators of plasminogen activator inhibitor alleviate the burden of obesity and diabetes? (Review). *Int J Mol Med*. 29 (1), 3-11.

Johnson AD, Handsaker RE, Pulit SL et al. (2008): SNAP: a web-based tool for identification and annotation of proxy SNPs using HapMap. *Bioinformatics* 24 (24), 2938–2939.

Johnson DT, Harris RA, French S et al. (2009): Proteomic changes associated with diabetes in the BB-DP rat. *Am. J. Physiol. Endocrinol. Metab.* 296 (3), E422-32.

Kastenmüller G, Römisch-Margl W, Wägele B et al. (2011): metaP-server: a web-based metabolomics data analysis tool. *J. Biomed. Biotechnol.* 2011: 839862.

Keophiphath M, Rouault C, Divoux A et al. (2009): CCL5 Promotes Macrophage Recruitment and Survival in Human Adipose Tissue. *Arteriosclerosis, Thrombosis, and Vascular Biology* 30 (1), 39–45.

Kim GW, Kim H, Cho K et al. (2009): The role of MMP-9 in integrin-mediated hippocampal cell death after pilocarpine-induced status epilepticus. *Neurobiol. Dis.* 36 (1), 169–180.

Kim J, Kim JE, Liu H et al. (2008): Regulation of interleukin-6-induced hepatic insulin resistance by mammalian target of rapamycin through the STAT3-SOCS3 pathway. *J. Biol. Chem.* 283 (2), 708–715.

Kim SY, Jeong E, Joung SM et al. (2012): PI3K/Akt contributes to increased expression of Toll-like receptor 4 in macrophages exposed to hypoxic stress. *Biochem. Biophys. Res. Commun.* 419 (3), 466–471.

Kops GJPL, Dansen TB, Polderman PE et al. (2002): Forkhead transcription factor FOXO3a protects quiescent cells from oxidative stress. *Nature* 419 (6904), 316–321.

Krug S, Kastenmüller G, Stückler F et al. (2012): The dynamic range of the human metabolome revealed by challenges. *FASEB J.* 26 (6), 2607–2619.

Kwon G, Marshall CA, Pappan KL et al. (2004): Signaling elements involved in the metabolic regulation of mTOR by nutrients, incretins, and growth factors in islets. *Diabetes* 53 Suppl 3, S225-32.

Latipää PM, Kärki TT, Hiltunen JK et al. (1986): Regulation of palmitoylcarnitine oxidation in isolated rat liver mitochondria. Role of the redox state of NAD(H). *Biochim. Biophys. Acta* 875 (2), 293–300.

Laumen H, Saningong AD, Heid IM et al. (2009): Functional characterization of promoter variants of the adiponectin gene complemented by epidemiological data. *Diabetes* 58 (4), 984–991.

Law L, Tang NL, Hui J et al. (2007): A novel functional assay for simultaneous determination of total fatty acid beta-oxidation flux and acylcarnitine profiling in human skin fibroblasts using (2)H(31)-palmitate by isotope ratio mass spectrometry and electrospray tandem mass spectrometry. *Clin. Chim. Acta* 382 (1-2), 25–30.

Lee YG, Lee J, Byeon SE et al. (2011): Functional role of Akt in macrophage-mediated innate immunity. *Front Biosci* 16, 517–530.

Leipnitz G, Schuck PF, Ribeiro CAJ et al. (2003): Ethylmalonic acid inhibits mitochondrial creatine kinase activity from cerebral cortex of young rats *in vitro*. *Neurochem. Res.* 28 (5), 771–777.

Levy H, Wang X, Kaldunski M et al. (2012): Transcriptional signatures as a disease-specific and predictive inflammatory biomarker for type 1 diabetes. *Genes Immun.* 13 (8), 593–604.

Lewis CM (2002): Genetic association studies: design, analysis and interpretation. *Brief. Bioinformatics* 3 (2), 146–153.

Li L, Naples M, Song H et al. (2007): LCAT-null mice develop improved hepatic insulin sensitivity through altered regulation of transcription factors and suppressors of cytokine signaling. *Am. J. Physiol. Endocrinol. Metab.* 293 (2), E587-94.

Lim S, Won H, Kim Y et al. (2011): Antioxidant enzymes induced by repeated intake of excess energy in the form of high-fat, high-carbohydrate meals are not sufficient to block oxidative stress in healthy lean individuals. *Br J Nutr* 106 (10), 1544–1551.

MacIver NJ, Jacobs SR, Wieman HL et al. (2008): Glucose metabolism in lymphocytes is a regulated process with significant effects on immune cell function and survival. *Journal of Leukocyte Biology* 84 (4), 949–957.

Madrid LV (2001): Akt Stimulates the Transactivation Potential of the RelA/p65 Subunit of NF-kappa B through Utilization of the Ikappa B Kinase and Activation of the Mitogen-activated Protein Kinase p38. *Journal of Biological Chemistry* 276 (22), 18934–18940.

Manning AK, Hivert M, Scott RA et al. (2012): A genome-wide approach accounting for body mass index identifies genetic variants influencing fasting glycemic traits and insulin resistance. *Nat. Genet.* 44 (6), 659–669.

Manning B (2003): Rheb fills a GAP between TSC and TOR. *Trends in Biochemical Sciences* 28 (11), 573–576.

Mauer J, Chaurasia B, Plum L et al. (2010): Myeloid Cell-Restricted Insulin Receptor Deficiency Protects Against Obesity-Induced Inflammation and Systemic Insulin Resistance. *PLoS Genet* 6 (5), e1000938.

Maurano MT, Humbert R, Rynes E et al. (2012): Systematic localization of common disease-associated variation in regulatory DNA. *Science* 337 (6099), 1190–1195.

McCarroll SA, Kuruvilla FG, Korn JM et al. (2008): Integrated detection and population-genetic analysis of SNPs and copy number variation. *Nat. Genet.* 40 (10), 1166–1174.

McHugh DMS, Cameron CA, Abdenur JE et al. (2011): Clinical validation of cutoff target ranges in newborn screening of metabolic disorders by tandem mass spectrometry: a worldwide collaborative project. *Genet. Med.* 13 (3), 230–254.

Mihalik SJ, Goodpaster BH, Kelley DE et al. (2010): Increased levels of plasma acylcarnitines in obesity and type 2 diabetes and identification of a marker of glucolipotoxicity. *Obesity (Silver Spring)* 18 (9), 1695–1700.

Mirkov S, Myers JL, Ramírez J et al. (2012): SNPs affecting serum metabolomic traits may regulate gene transcription and lipid accumulation in the liver. *Metab. Clin. Exp.* 61 (11), 1523–1527.

Modre-Osprian R, Osprian I, Tilg B et al. (2009): Dynamic simulations on the mitochondrial fatty acid beta-oxidation network. *BMC Syst Biol* 3, 2.

Montoliu I, Genick U, Ledda M et al. (2013): Current status on genome-metabolome-wide associations: an opportunity in nutrition research. *Genes Nutr* 8 (1), 19–27.

Morris AP, Voight BF, Teslovich TM et al. (2012): Large-scale association analysis provides insights into the genetic architecture and pathophysiology of type 2 diabetes. *Nat Genet* 44 (9), 981–990.

Nagan N, Kruckeberg KE, Tauscher AL et al. (2003): The frequency of short-chain acyl-CoA dehydrogenase gene variants in the US population and correlation with the C(4)-acylcarnitine concentration in newborn blood spots. *Mol. Genet. Metab.* 78 (4), 239–246.

Nakabayashi H, Taketa K, Yamane T et al. (1984): Phenotypical stability of a human hepatoma cell line, HuH-7, in long-term culture with chemically defined medium. *Gann* 75 (2), 151–158.

Nelson, David L.; Cox, Michael M.; Lehninger, Albert L. (2008): Lehninger principles of biochemistry. 5th edition New York: W.H. Freeman.

Neph S, Vierstra J, Stergachis AB et al. (2012): An expansive human regulatory lexicon encoded in transcription factor footprints. *Nature* 489 (7414), 83–90.

Newgard CB (2012): Interplay between lipids and branched-chain amino acids in development of insulin resistance. *Cell Metab.* 15 (5), 606–614.

Nica AC, Parts L, Glass D et al. (2011): The architecture of gene regulatory variation across multiple human tissues: the MuTHER study. *PLoS Genet.* 7 (2), e1002003.

Nicholson G, Rantalainen M, Li JV et al. (2011): A genome-wide metabolic QTL analysis in Europeans implicates two loci shaped by recent positive selection. *PLoS Genet.* 7 (9), e1002270.

Nicolae DL, Gamazon E, Zhang W et al. (2010): Trait-associated SNPs are more likely to be eQTLs: annotation to enhance discovery from GWAS. *PLoS Genet.* 6 (4), e1000888.

Nidai Ozes O, Mayo LD, Gustin JA et al. (1999): NF-κB activation by tumour necrosis factor requires the Akt serine- threonine kinase. *Nature* 401 (6748), 82–85.

Noland RC, Koves TR, Seiler SE et al. (2009): Carnitine insufficiency caused by aging and overnutrition compromises mitochondrial performance and metabolic control. *J. Biol. Chem.* 284 (34), 22840–22852.

Oh JH, Kim YJ, Moon S et al. (2013): Genotype instability during long-term subculture of lymphoblastoid cell lines. *J. Hum. Genet.* 58 (1), 16–20.

Okun JG, Kölker S, Schulze A et al. (2002): A method for quantitative acylcarnitine profiling in human skin fibroblasts using unlabelled palmitic acid: diagnosis of fatty acid oxidation disorders and differentiation between biochemical phenotypes of MCAD deficiency. *Biochim. Biophys. Acta* 1584 (2-3), 91–98.

Olowe Y and Schulz H (1980): Regulation of thiolases from pig heart. Control of fatty acid oxidation in heart. *Eur. J. Biochem.* 109 (2), 425–429.

Pasini E, Flati V, Paiardi S et al. (2010): Intracellular molecular effects of insulin resistance in patients with metabolic syndrome. *Cardiovasc Diabetol* 9, 46.

Patti M and Corvera S (2010): The role of mitochondria in the pathogenesis of type 2 diabetes. *Endocr. Rev.* 31 (3), 364–395.

Paul DS, Nisbet JP, Yang T et al. (2011): Maps of open chromatin guide the functional follow-up of genome-wide association signals: application to hematological traits. *PLoS Genet.* 7 (6), e1002139.

Pedersen CB, Bross P, Winter VS et al. (2003): Misfolding, degradation, and aggregation of variant proteins. The molecular pathogenesis of short chain acyl-CoA dehydrogenase (SCAD) deficiency. *J. Biol. Chem.* 278 (48), 47449–47458.

Pedersen CB, Kølvraa S, Kølvraa A et al. (2008): The ACADS gene variation spectrum in 114 patients with short-chain acyl-CoA dehydrogenase (SCAD) deficiency is dominated by missense variations leading to protein misfolding at the cellular level. *Hum. Genet.* 124 (1), 43–56.

Pierau M, Na S, Simma N et al. (2012): Constitutive Akt1 signals attenuate B-cell receptor signaling and proliferation, but enhance B-cell migration and effector function. *Eur. J. Immunol.* 42 (12), 3381-93.

Pike LS, Smift AL, Croteau NJ et al. (2011): Inhibition of fatty acid oxidation by etomoxir impairs NADPH production and increases reactive oxygen species resulting in ATP depletion and cell death in human glioblastoma cells. *Biochim. Biophys. Acta*. 1807 (6), 726-34.

Portius D (2012): Metabolic profiling during adipocyte differentiation and analysis of metabolic pathways in hepatoma cells. Diploma thesis. Martin-Luther-Universität, Halle-Wittenberg. Naturwissenschaftliche Fakutät III; Institut für Agrar- und Ernährungswissenschaften.

Powell PJ, Lau SM, Killian D et al. (1987): Interaction of acyl coenzyme A substrates and analogues with pig kidney medium-chain acyl-coA dehydrogenase. *Biochemistry* 26 (12), 3704–3710.

Prip-Buus C, Bouthillier-Voisin AC, Kohl C et al. (1992): Evidence for an impaired long-chain fatty acid oxidation and ketogenesis in Fao hepatoma cells. *Eur. J. Biochem.* 209 (1), 291–298.

Ribes A, Riudor E, Garavaglia B et al. (1998): Mild or absent clinical signs in twin sisters with short-chain acyl-CoA dehydrogenase deficiency. *Eur. J. Pediatr.* 157 (4), 317–320.

Rinaldo P, Cowan TM, Matern D (2008): Acylcarnitine profile analysis. *Genet. Med.* 10 (2), 151–156.

Rodrigues JV and Gomes CM (2012): Mechanism of superoxide and hydrogen peroxide generation by human electron-transfer flavoprotein and pathological variants. *Free Radic. Biol. Med.* 53 (1), 12–19.

Roe CR, Millington DS, Maltby DA (1986): Identification of 3-methylglutarylcarnitine. A new diagnostic metabolite of 3-hydroxy-3-methylglutaryl-coenzyme A lyase deficiency. *J. Clin. Invest.* 77 (4), 1391–1394.

Rui L, Yuan M, Frantz D et al. (2002): SOCS-1 and SOCS-3 block insulin signaling by ubiquitin-mediated degradation of IRS1 and IRS2. *J. Biol. Chem.* 277 (44), 42394–42398.

Sarbassov DD, Guertin DA, Ali SM et al. (2005): Phosphorylation and regulation of Akt/PKB by the rictor-mTOR complex. *Science* 307 (5712), 1098–1101.

Sauer SW, Okun JG, Hoffmann GF et al. (2008): Impact of short- and medium-chain organic acids, acylcarnitines, and acyl-CoAs on mitochondrial energy metabolism. *Biochim. Biophys. Acta* 1777 (10), 1276–1282.

Saxena R, Hivert M, Langenberg C et al. (2010): Genetic variation in GIPR influences the glucose and insulin responses to an oral glucose challenge. *Nat. Genet.* 42 (2), 142–148.

Schmidt SP, Corydon TJ, Pedersen CB et al. (2010): Misfolding of short-chain acyl-CoA dehydrogenase leads to mitochondrial fission and oxidative stress. *Mol. Genet. Metab.* 100 (2), 155–162.

Schopfer LM, Massey V, Ghisla S et al. (1988): Oxidation-reduction of general acyl-CoA dehydrogenase by the butyryl-CoA/crotonyl-CoA couple. A new investigation of the rapid reaction kinetics. *Biochemistry* 27 (17), 6599–6611.

Schuler AM, Gower BA, Matern D et al. (2004): Influence of dietary fatty acid chain-length on metabolic tolerance in mouse models of inherited defects in mitochondrial fatty acid beta-oxidation. *Mol. Genet. Metab.* 83 (4), 322–329.

Schulze-Bergkamen A, Okun JG, Spiekerkötter U et al. (2005): Quantitative acylcarnitine profiling in peripheral blood mononuclear cells using *in vitro* loading with palmitic and

2-oxoadipic acids: biochemical confirmation of fatty acid oxidation and organic acid disorders. *Pediatr. Res.* 58 (5), 873–880.

Scott RA, Lagou V, Welch RP et al. (2012): Large-scale association analyses identify new loci influencing glycemic traits and provide insight into the underlying biological pathways. *Nat. Genet.* 44 (9), 991–1005.

Seahorse Bioscience Inc: Conducting a Fatty Acid Oxidation Assay on the XF Analyzer. http://seahorsebio.com/resources/tech-writing/protocol-fatty-acid-oxidation.pdf: June 21, 2013.

Shoelson SE, Lee J, Yuan M (2003): Inflammation and the IKK beta/I kappa B/NF-kappa B axis in obesity- and diet-induced insulin resistance. *Int. J. Obes. Relat. Metab. Disord.* 27 Suppl 3, S49-52.

Siess EA and Wieland OH (1976): Phosphorylation state of cytosolic and mitochondrial adenine nucleotides and of pyruvate dehydrogenase in isolated rat liver cells. *Biochem. J.* 156 (1), 91–102.

Sim KG, Hammond J, Wilcken B (2002): Strategies for the diagnosis of mitochondrial fatty acid beta-oxidation disorders. *Clin. Chim. Acta* 323 (1-2), 37–58.

Simon-Sanchez J, Scholz S, Fung H et al. (2007): Genome-wide SNP assay reveals structural genomic variation, extended homozygosity and cell-line induced alterations in normal individuals. *Hum. Mol. Genet.* 16 (1), 1–14.

Sizemore N (2001): Distinct Roles of the Ikappa B Kinase alpha and beta Subunits in Liberating Nuclear Factor kappa B (NF-kappa B) from Ikappa B and in Phosphorylating the p65 Subunit of NF-kappa B. *Journal of Biological Chemistry* 277 (6), 3863–3869.

Solaini G, Sgarbi G, Baracca A (2011): Oxidative phosphorylation in cancer cells. *Biochim. Biophys. Acta* 1807 (6), 534–542.

So L, Yea SS, Oak JS et al. (2013): Selective inhibition of phosphoinositide 3-kinase p110α preserves lymphocyte function. *J. Biol. Chem.* 288 (8), 5718–5731.

Stagakis I, Bertsias G, Karvounaris S et al. (2012): Anti-tumor necrosis factor therapy improves insulin resistance, beta cell function and insulin signaling in active rheumatoid arthritis patients with high insulin resistance. *Arthritis Res Ther* 14 (3), R141.

Tein I, Haslam RH, Rhead WJ et al. (1999): Short-chain acyl-CoA dehydrogenase deficiency: a cause of ophthalmoplegia and multicore myopathy. *Neurology* 52 (2), 366–372.

ter Veld F, Primassin S, Hoffmann L et al. (2009): Corresponding increase in long-chain acyl-CoA and acylcarnitine after exercise in muscle from VLCAD mice. *J. Lipid Res.* 50 (8), 1556–1562.

The International HapMap Consortium (2005): A haplotype map of the human genome. *Nature* 437 (7063), 1299–1320.

Thomson AW, Turnquist HR, Raimondi G (2009): Immunoregulatory functions of mTOR inhibition. *Nat Rev Immunol* 9 (5), 324–337.

Thurman RE, Rynes E, Humbert R et al. (2012): The accessible chromatin landscape of the human genome. *Nature* 489 (7414), 75–82.

Ueki K, Kondo T, Kahn CR (2004): Suppressor of cytokine signaling 1 (SOCS-1) and SOCS-3 cause insulin resistance through inhibition of tyrosine phosphorylation of insulin receptor substrate proteins by discrete mechanisms. *Mol. Cell. Biol.* 24 (12), 5434–5446.

Um SH, Frigerio F, Watanabe M et al. (2004): Absence of S6K1 protects against age- and diet-induced obesity while enhancing insulin sensitivity. *Nature* 431 (7005), 200–205.

van Maldegem BT (2011): Short-chain acyl-CoA dehydrogenase deficiency. University of Amsterdam (UvA); Faculty of Medicine. http://dare.uva.nl/document/201713: June 21, 2013.

van Maldegem BT, Duran M, Wanders RJA et al. (2006): Clinical, biochemical, and genetic heterogeneity in short-chain acyl-coenzyme A dehydrogenase deficiency. *JAMA* 296 (8), 943–952.

van Maldegem BT, Wanders RJA, Wijburg FA (2010): Clinical aspects of short-chain acyl-CoA dehydrogenase deficiency. *J. Inherit. Metab. Dis.* 33 (5), 507–511.

van Oostrom A, Rabelink T, Verseyden C et al. (2004): Activation of leukocytes by postprandial lipemia in healthy volunteers. *Atherosclerosis* 177 (1), 175–182.

Vander Haar E, Lee S, Bandhakavi S et al. (2007): Insulin signalling to mTOR mediated by the Akt/PKB substrate PRAS40. *Nat. Cell Biol.* 9 (3), 316–323.

Ventura FV, Costa CG, Struys EA et al. (1999): Quantitative acylcarnitine profiling in fibroblasts using [U-13C] palmitic acid: an improved tool for the diagnosis of fatty acid oxidation defects. *Clin. Chim. Acta* 281 (1-2), 1–17.

Ventura FV, Tavares de Almeida I, Wanders RJA (2007): Inhibition of adenine nucleotide transport in rat liver mitochondria by long-chain acyl-coenzyme A beta-oxidation intermediates. *Biochem. Biophys. Res. Commun.* 352 (4), 873–878.

Violante S, Ijlst L, Te Brinke H et al. (2013): Carnitine palmitoyltransferase 2 and carnitine/acylcarnitine translocase are involved in the mitochondrial synthesis and export of acylcarnitines. *FASEB J.* 27 (5), 2039–2044.

Wanders RJ, Vreken P, den Boer ME et al. (1999): Disorders of mitochondrial fatty acyl-CoA beta-oxidation. *J. Inherit. Metab. Dis.* 22 (4), 442–487.

Wang Y, Mohsen A, Mihalik SJ et al. (2010): Evidence for physical association of mitochondrial fatty acid oxidation and oxidative phosphorylation complexes. *J. Biol. Chem.* 285 (39), 29834–29841.

Ward LD and Kellis M (2011): HaploReg: a resource for exploring chromatin states, conservation, and regulatory motif alterations within sets of genetically linked variants. *Nucleic Acids Research* 40 (D1), D930.

Waterson RM and Hill RL (1972): Enoyl coenzyme A hydratase (crotonase). Catalytic properties of crotonase and its possible regulatory role in fatty acid oxidation. *J. Biol. Chem.* 247 (16), 5258–5265.

Wichmann HE, Gieger C, Illig, T (2005): KORA-gen--resource for population genetics, controls and a broad spectrum of disease phenotypes. *Gesundheitswesen*. 67 Suppl 1, 26-30.

Wolf HP (1992): Possible new therapeutic approach in diabetes mellitus by inhibition of carnitine palmitoyltransferase 1 (CPT1). *Horm. Metab. Res.* Suppl 26, 62–67.

Yao KW and Schulz H (1996): Intermediate channeling on the trifunctional beta-oxidation complex from pig heart mitochondria. *J. Biol. Chem.* 271 (30), 17816–17820.

Yaqoob P, Newsholme EA, Calder PC (1994): Fatty acid oxidation by lymphocytes. *Biochem. Soc. Trans.* 22 (2), 116S.

Yenamandra SP, Lundin A, Arulampalam V et al. (2009): Expression profile of nuclear receptors upon Epstein -- Barr virus induced B cell transformation. *Exp. Oncol.* 31 (2), 92–96.

Young SP, Matern D, Gregersen N et al. (2003): A comparison of *in vitro* acylcarnitine profiling methods for the diagnosis of classical and variant short chain acyl-CoA dehydrogenase deficiency. *Clin. Chim. Acta* 337 (1-2), 103–113.

Zamule SM, Strom SC, Omiecinski CJ (2008): Preservation of hepatic phenotype in lentiviral-transduced primary human hepatocytes. *Chem. Biol. Interact.* 173 (3), 179–186.

Zeggini E, Scott LJ, Saxena R et al. (2008): Meta-analysis of genome-wide association data and large-scale replication identifies additional susceptibility loci for type 2 diabetes. *Nat. Genet.* 40 (5), 638–645.

Zhang J, Gao Z, Yin J et al. (2008): S6K directly phosphorylates IRS-1 on Ser-270 to promote insulin resistance in response to TNF-(alpha) signaling through IKK2. *J. Biol. Chem.* 283 (51), 35375–35382.

Zhou W, Choi M, Margineantu D et al. (2012): HIF1α induced switch from bivalent to exclusively glycolytic metabolism during ESC-to-EpiSC/hESC transition. *EMBO J.* 31 (9), 2103–2116.

Zolkipli Z, Pedersen CB, Lamhonwah A et al. (2011): Vulnerability to oxidative stress *in vitro* in pathophysiology of mitochondrial short-chain acyl-CoA dehydrogenase deficiency: response to antioxidants. *PLoS ONE* 6 (4), e17534.

Zoncu R, Efeyan A, Sabatini DM (2011): mTOR: from growth signal integration to cancer, diabetes and ageing. *Nat. Rev. Mol. Cell Biol.* 12 (1), 21–35.

Publications and Presentations

Ehlers K, Brand T, Bangert A, Hauner H, Laumen H. Postprandial activation of metabolic and inflammatory pathways in peripheral mononuclear cells. Br J Nutr (in review).

Claussnitzer M, Klocke B, Dankel SN, Grallert H, Berulava T, Lee H, Hansson O, Glunk V, Ehlers K, Wahl S, Hoffmann C, Bretschneider N, Rönn T, Skurk T, Horsthemke B, Sim X, Daniel NPK, Tai ES, DIAGRAM+ Consortium, Spieler D, Klingenspor M, Mellgren G, Kern MJ, Groop L, Hauck SM, Illig T, Seifert M, Hauner H, Laumen H. Leveraging cross-species transcription factor binding site patterns: from diabetes risk loci to disease mechanisms (in review).

Krinninger P, Ensenauer R, Ehlers K, Rauh K, Krauss-Etschmann S, Hauner H, Laumen H. Peripheral monocytes of obese women exhibit increased chemokine receptor expression and migration capacity (submitted).

Ehlers K, Stückler F, Ensenauer R, Daniel H, Hauner H, Laumen H. *In vitro* modelling of an mQTL (metabolic quantitative trait locus) indicates novel features of ACADS function in β-oxidation (in preparation).

Kirschner A, Schriever SC, Rauh K, Ehlers K, Pagel P, Ensenauer R. Meta-Analysis of Whole Blood Gene Expression Experiments reveals new genetic Markers for early Detection of metabolic Dysregulation in Obesity (in preparation).

Update in the Field of Metabolic Syndrome, Obesity, Diabetes and Atherosclerosis; School of Medicine; University of Banja Luka; Bosnien and Herzegovina, 3rd June 2011
Talk on "Functional characterization of gene variants in lipid metabolism."

Systems Biology of Metabotypes (SysMBo) Abschlußkolloquium 12th December, 2012
Talk on "Gene variants – functional human studies."

Phenotypic Flexibility Symposium, Madrid Spain, 6th February 2013
Talk on "Postprandial inflammatory and metabolic activation of PBMC: a subject of inter-individual differences."

Wahl S, Krug S, Then C, Brand T, Ehlers K, Claussnitzer M, Skurk T, Lechner A, Wichmann H, Huth C, Meisinger C, Prehn C, Stückler F, Kastenmüller G, Adamski J, Suhre K, Illig T, Grallert H, Laumen H, Seissler J, Hauner H. Metabolic characterization of common variants of the *FTO* and *TCF7L2* loci by nutritional challenge tests. Abstract/Poster P13.09. European Human Genetics Conference, Nürnberg, 23-26 June 2012.

Ehlers K, Brand T, Hastreiter L, Bangert A, Hauner H, Laumen H. Inflammatory and metabolic activation of PBMC: a subject of inter-individual differences. Abstract/Poster P30. 28. Jahrestagung der Deutschen Adipositas-Gesellschaft, Stuttgart, 4.-6. October 2012.

Wahl S, Then C, Krug S, Brand T, Ehlers K, Claussnitzer M, Skurk T, Lechner A, Wichmann H.-E., Heier M, Huth C, Thorand B, Meisinger C, Prehn C, Stückler F, Kasternmüller G, Adamski J, Suhre K, Illig T, Grallert H, Laumen H, Hauner H, Seissler J. *TCF7L2* and *FTO*-What can we learn from metabolic challenge tests. Abstract/Poster P93. 28. Jahrestagung der Deutschen Adipositas-Gesellschaft, Stuttgart, 4.-6. October 2012.

Ehlers K, Brand T, Bangert A, Hastreiter L, Skurk T, Adamski J, Halama A, Möller G, Suhre K, Römisch-Margl W, Kastenmüller G, Hauner H, Laumen H. Postprandial inflammatory and metabolic activation of PBMC: a subject of inter-individual differences. Abstract/Poster 87. EMBO/EMBL Symposium Diabetes and Obesity, Heidelberg, 13-16. September 2012.